Mario-Franz Martin, BSc

Recognition of stress markers through biofeedback

MASTER'S THESIS

to achieve the university degree of

Diplom-Ingenieur

Master's degree programme: Biomedical Engineering

submitted to

Graz University of Technology

Supervisor

Univ.-Prof. Dipl.-Ing. Dr. techn. Christian Baumgartner

Ing. Robert Neubauer

Institut für Health Care Engineering mit Europaprüfstelle für Medizinprodukte

Graz, 04.11.2020

EIDESSTATTLICHE ERKLÄRUNG

Ich erkläre an Eides statt, dass ich die vorliegende Arbeit selbstständig verfasst, andere als die angegebenen Quellen/Hilfsmittel nicht benutzt, und die den benutzten Quellen wörtlich und inhaltlich entnommenen Stellen als solche kenntlich gemacht habe.

<table>
<tr><td>Graz, 04.11.2020</td><td></td></tr>
<tr><td>……………………………………………</td><td>……………………………………………</td></tr>
<tr><td>(Ort, Datum)</td><td>(Unterschrift)</td></tr>
</table>

STATUTORY DECLARATION

I declare that I have authored this thesis independently, that I have not used other than the declared sources / resources, and that I have explicitly marked all material which has been quoted either literally or by content from the used sources.

<table>
<tr><td>Graz, 04.11.2020</td><td></td></tr>
<tr><td>……………………………………………</td><td>……………………………………………</td></tr>
<tr><td>(Place, Date)</td><td>(Signature)</td></tr>
</table>

Content

Table of figures

Table of Abbreviations

Abbreviation	Full Description
ABF	Automatic Band Filter
ABLC	Automatic Black-Level Calibration
ADC	Analog Digital Converter
AEC	Automatic Exposure Control
AGC	Automatic Gain Control
AWB	Automatic White Balance
CMOS	Complementary Metal-Oxide Semiconductor
CS	Chip Select
DAC	Digital Analog Converter
DC	Direct Current
ECG	Electrocardiography
EDA	Electrodermal Activity
FAT	File Allocation Table
FFC	Flexible Flat Cable
FTDI	Future Technology Devices International
GND	Ground
GSR	Galvanic Skin Response
GUI	Graphical User Interface
HTTP	HyperText Transfer Protocol
I^{2}C	I-Squared-C Bus
IC	Integrated Circuit
IP	Internet Protocol
LED	Light-Emitting Diode
MicroSD	Micro Secure Digital Memory Card
MISO	Master Input Slave Output
MOSI	Master Output Slave Input
O$_2$	Oxygen
PC	Personal Computer
PCB	Printed Circuit Board
PLA	Polyactide
PPG	Photoplethysmography
PWM	Pulse Width Modulation
QQVGA	Quarter Quarter Video Graphics Array
RAM	Random Access Memory
RGB	Red Green Blue
RTC	Real Time Clock
SCCB	Serial Camera Control Bus
SCL	Serial Clock Line
SDA	Serial Data Line
SPI	Serial Peripheral Interface
SSID	Service Set Identifier
STL	Standard Triangulation Board
TPU	Thermoplastic Polyurethane
UART	Universal Asynchronous Receiver Transmitter
USB	Universal Serial Bus
UXGA	Ultra Extended Graphics Array
VCC	Voltage at the Common Collector
VLC	Video Lan Client
WLAN	Wireless Local Area Network

Zusammenfassung / Abstract

Deutsche/German Version:

Das Ziel der vorliegenden Masterarbeit war es, einen wissenschaftlichen Beweis für die These zu finden, ob Stress wesentlich durch ein oder mehrere Biosignale ermittelt werden kann und ob zwischen Eustress (positivem Stress) und Distress (negativem Stress) unterschieden werden kann. Der Fokus lag dabei auf der Unterscheidung von verschiedenen Stresssituationen, die im Laufe des Tages bei unterschiedlichen Personen auftreten können. Die bisherigen Systeme, die auf dem Markt sind, können nur die physischen Belastungen des Körpers ermitteln, jedoch nicht bestimmen, ob es sich dabei um Eustress oder Distress handelt.

Aus diesem Grunde bestand die Hauptaufgabe der Arbeit darin, ein mobiles Stressmessgerät zu entwickeln, das in der Lage ist, verschiedene Biosignale sowie Augen- bzw. Pupillenbewegungen der ProbandInnen aufzuzeichnen, um einen Rückschluss auf ihre Stresssituationen über den Tag hinweg schließen zu können. Überdies wurde auf eine komfortable Handhabung und Bedienbarkeit des mobilen Gerätes Wert gelegt, um Einschränkungen möglichst gering zu halten und Messverfälschungen zu verhindern. Als Messstelle der biologischen Daten wurde der Kopfbereich gewählt, wodurch das Design des mobilen Gerätes an die Form einer Brille erinnert. Die gesammelten Daten sollten anschließend sowohl über einen Mikrocontroller verarbeitet und abgespeichert werden als auch in Echtzeit für andere Systeme (z. B. Automobil oder Smartphone) zur weiteren Verarbeitung verfügbar sein. Um den Tragekomfort des Aufzeichnungsgerätes zu erhöhen, wurden mehrere Einstellungsmöglichkeiten im Design berücksichtigt. Die Umsetzung erfolgte durch Prototypenerstellung mit einem 3D-Druck-Verfahren.

Des Weiteren beinhaltet die Arbeit den Entwurf des elektronischen Schaltungsdesigns und dessen hardwaretechnische Realisierung. Darauf aufbauend wurde ein dreidimensionaler Prototyp in einem CAD-Programm entworfen, der auch für weitere Probandenversuche verwendet werden kann. Die Arbeit inkludiert auch die softwaretechnische Verarbeitung der Daten und deren Bereitstellung auf einem Webserver (siehe Kapitel 4.6.2 und 4.6.4).

Mithilfe eines Auswertungsverfahrens konnten Änderungen der Biosignale durch physische Stresssituationen festgestellt werden. Die Feststellung und Analyse von Stressmarker werden somit in einer weiterführenden Arbeit behandelt. Dies ermöglicht einem Probanden bestmögliche Unterstützung im Umgang mit dem vorhandenen Stress.

English version:

The aim of the present master thesis was to find a scientific proof for the thesis whether stress can be essentially determined by one or more biosignals and whether it is possible to distinguish between eustress (positive stress) and distress (negative stress). Emphasis was put on identifying stress situations that were recorded by different people during the day. The currently available systems on the market can only determine the physical strain on the body, but cannot distinguish between eustress and distress.

For this reason, the main part of the work was to develop a mobile device capable of recording various biosignals as well as eye and pupil movements of the test persons in order to draw conclusions about their stress situations throughout the day. Furthermore, great importance was attributed to a comfortable handling and operability of the mobile device in order to keep restrictions to a minimum and prevent measurement falsifications. The head area was selected as the measuring region for the biological data, which makes the design of the mobile device look like a pair of glasses. The collected data were then processed by and stored on a microcontroller and made available in real time to other systems (e.g. automobile or smartphone) for further processing. In order to increase the wearing comfort of the recording device, several adjustment options were considered in the design. The implementation was achieved by prototyping using a 3D printing process.

Furthermore, the work includes the draft of the electronic circuit design and its hardware implementation. Based on this, a three-dimensional prototype was designed in a CAD, which can also be used for further test person trails. The work also included the software processing of the data and their provision on a web server (see chapter 4.6.2 and 4.6.4).

The developed evaluation procedure ensures the detection of changes in biosignals caused by physical stress situations. The detection and analysis of stress markers will be treated in a further work. This enables a test person to receive the best possible support in dealing with the existing stress.

1   Introduction

The identification and description of stress factors has become an important topic in today's society, as stress and strains in work and private life are constantly increasing [1]. Stress factors are most pronounced in people who have a larger area of responsibility in their professional or private environment (e.g. project managers and executives). These factors cause a release of stress hormones in the body, which in turn can have a negative effect on the body and/or psyche of the individual person. In extreme cases, this can lead to burnout and depression [2,3]. However, stress can also have positive effects on the body, for example when doing sports. The body also shows stress as a positive side effect by producing sweat. When working out we focus on physical activity and can simultaneously clear our minds.

The fact that stress is related to physical conditions of the human body is well known and has already been discussed in multiple scientific publications with respect to changes in the ECG[1], the heart rate variability. This is also the basis for most mobile sports measuring devices (like heart rate monitors and running trackers), which use physical biosignals (e.g. the pulse beat) and inform the user about his or her physical condition either via device itself or smartphone app. However, all these devices have one thing in common: They are designed for a certain activity and hence, assume a certain physical condition of their users.

1.1   Motivation

In both today's private and business life, performance and progress are one of the highest ranked priorities, which results in a large number of people making sacrifices regarding their physical and mental health. This leads to an increase in illnesses, such as depression or burnout, which require either medical intervention and/or psychotherapy.

The question is: What does physical stress do and why do we need it? The answer is that stress is a physical reaction to make the body alert and raise performance. Stress hormones trigger the fight-or-flight reaction of a person's body. The heart starts to beat faster, the breath rate goes up and the muscles tense. This reaction is made to protect the body in a case of emergency and to react quickly.

Everyone rates stress differently. This is the reason why everyone must find their own work-life-balance, that is the individual ratio between work and relaxation. The aim is to bring one's private interests in line with the requirements of the business world, thus, achieving a healthy balance. Generally, one should avoid distress as much as possible. For this reason, the motivation behind this master's thesis was to create a device that helps people recognize negative stress and be able to take appropriate stress prevention measures.

---

[1] [4], Medizintechnik Kramme R., Medizintechnik EKG - Kapitel 8 (S. 86-96)

1.2 Idea behind this thesis

The main idea behind this thesis is to create a device that identifies stress factors in work and private life so that the person wearing it can take appropriate stress prevention measures. This raises the question whether stress can be measured general. The best example is exam stress when students get clammy hands before an exam and their hearts start to beat faster.

The first question is: What are stress parameters? Body reactions can be determined through galvanic skin response (GSR), body temperature, electrocardiogram (ECG) or pulse oximetry (PPG). This brings up a second question: How many sensors are necessary and can be put onto a mobile device to measure these parameters? Most body reactions to stress include increased sweat production, dilated pupils, increased heart rate and temperature. All these parameters shall be monitored and logged onto a mobile device.

The purposes of this device are manifold for employees of different business areas, for example conveyor belt workers, test drivers or surgeons. Each of these areas requires the highest level of attention and concentration to avoid any kind of negative stressors.

Figure 1: Conveyor belt workers [5]   *Figure 2: Test driver [6]*   *Figure 3: Surgeons [7]*

The aim of this thesis is to investigate the possibility of using biofeedback to determine a stress marker that can distinguish between negative (= distress) and positive (= eustress) stress situations. It is intended to measure and evaluate these stress situations by means of ECG signals (= electrocardiography), pulse, body temperature, skin conductance and eye or pupil movement. Based on these parameters, a healthcare practitioner should be able to implement appropriate prevention methods and therefore improve the mental and physical condition of the test person.

1.3 Main tasks of this master's thesis

- **Task 1:** Mechanical design of a portable device
  This includes a wearable eyeglass frame by creating a 3D model of the frame that is easy to attach to the user and causes minimal disruption in everyday life. The production of the three-dimensional eyeglass model shall be effected by a 3D printer so that modifications can easily be implemented and spare parts can be reproduced at any time (see chapters 2.2, 3, 5.2, 6.1, 6.2, Appendix D).

- **Task 2:** Electrical and software design of a portable device
  This task deals with the development of the electrical circuitry of the individual processors as well as the sensors on the eyeglass frame and the control unit (see chapters 4, Appendix A, Appendix B). It also includes the layout and assembly of the resulting circuit boards. Furthermore, the processors are programmed so that the individual components (sensors, modules etc.) communicate with each other (see chapter Appendix C).

- **Task 3:** Determining biosignal data in real time
  This task includes the application of an ECG, the measurement of blood pressure, heart rate, body temperature and skin impedance as well as the recording of eye-pupil movements. For more information, see chapter 6.3.

- **Task 4:** Pre-processing of the recorded data
  The focus in task 4 is on filtering, visualizing and storing the recorded data. This information is provided in chapters 2.1.4 and 4.6.

- **Task 5:** Suitable wireless transmission of biosignal data
  A suitable transmission method will be determined and implemented. Furthermore, a transmitting and receiving station is to be set up. Chapters 3.2 and 4.6 will explain these processes in more detail.

2 Related work

This chapter briefly states the relevant medical and technological background knowledge needed for this thesis. It provides the general definitions of stress and its causes, the methods used to measure biosignals and existing examples of recording eye movement.

2.1 Background knowledge – Medical and technical information

2.1.1 Stress

Evolution has given human beings the genetic emergency program "stress" to be able to react quickly to dangerous situations and ensure survival, using either the fight or flight mode. The physical reactions to stress are still the same today as they were in the past. However, in our modern society, they are not so much triggered by hunger, cold, attacks or hard work, but rather by stimulus satiation, time and performance pressure, conflicts and fatalities. On the one hand, stress can be perceived as something positive and trigger positive feelings of satisfaction (eustress), with some people even needing it to work effectively. On the other hand, negative stress (distress) can cause long-term damage to the body, especially if the person in question is unable to recover sufficiently between two periods of tension [8].

Stress factors can have a major influence on people's bodies because these factors influence overall health and well-being, which has been confirmed [9–11]. For example, stress reactions and their effects on the body are clearly described [10]. It is also becoming increasingly clear that young, healthy people can successfully process stress reactions without causing health problems. However, if the stressors are continuous, especially in older or unhealthy people, they can cause long-term damage to health. Constant or continuous exposition to acute stressors can further lead to chronic cardiovascular diseases, which can cause an increase in blood pressure. As a result, blood vessels constrict and the resting blood pressure increases. Chronically high blood pressure forces the heart to work harder, leading to hypertrophy of the left ventricle. When high blood pressure persists over a longer period, it can damage the arteries and cause plaque to form in the artery. This is just one of many examples that require medical and/or psychological treatment [12].

Permanent stress can harm the following areas of the body:

- **Immune system**
  Increased cortisol levels slow down the cytokine synthesis. Normally, cytokines activate the B-lymphocytes that contribute to the development of helper and killer cells. If this cycle is slowed down, the body loses immune power. This results in the respiratory tract to be more sensitive to infectious diseases such as a cold or cough. Herpes is also a reaction to the strain on the immune system.

- **Stomach**
  The hormone norepinephrine constricts the blood vessels of the digestive organs so that the poor blood circulation allows pathogens to multiply unhindered. Furthermore, the stomach reacts sensitively to acid under stress.

- **Muscles**
  Hardening of the neck muscles caused by constant psychological stress impede the blood flow to the brain. As a consequence, tension headaches and migraines can arise. Muscle pain and tension occur because of constantly increased adrenaline and cortisol levels.

- **Nerves and brain**

  Increased cortisol levels can influence the function of the hippocampus and subsequently, the memory. The consequences are lack of concentration or a weak memory.

- **Blood vessels**

  Chronically increased blood pressure leads to a damage of the vessel walls. Blood clots and fat accumulate and can cause arteriosclerosis and heart attacks.

2.1.2 Electrocardiography

Electrocardiography (ECG) is the process of recording and diagnostically evaluating electrocardiograms that show the temporal and local course of electrical excitation processes in the form of waves, spikes and stretches of the heart muscle. Every impulse transmission through fibres of the heart is the source of an electrical voltage [13].

In this thesis, voltage is measured by a non-invasive derivation, which is generated by an electric field on the body surface. This voltage represents the voltage generated in a fraction of the heart. The derivation method corresponds to the bipolar extremity derivation according to Einthoven. However, the measurement points have been changed from the extremities to the left and right side of the head. Furthermore, the reference electrode was attached to the forehead.
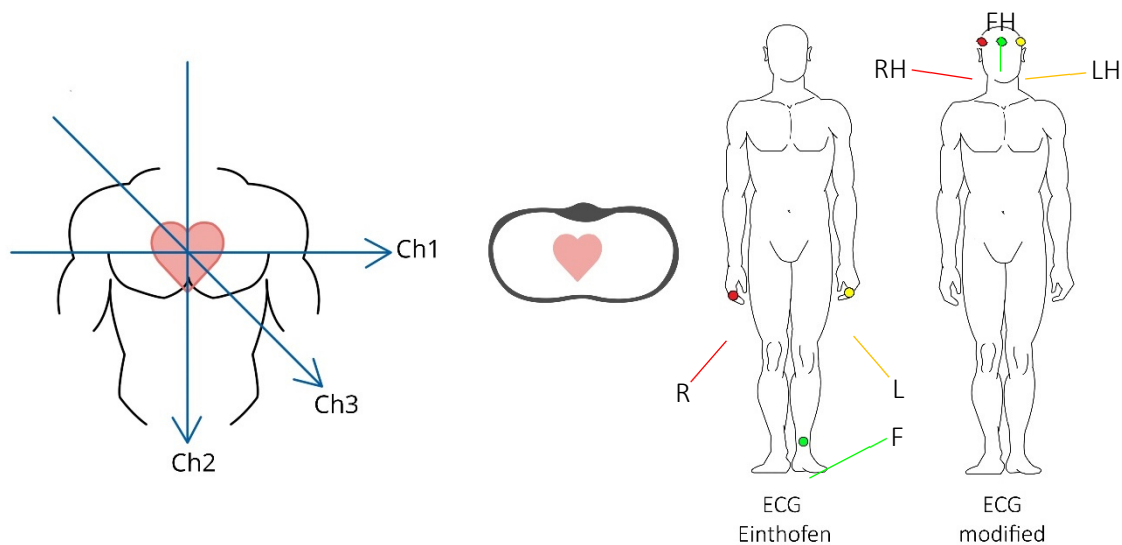
Figure 4: 3-Channel ECG derivation system according to Einthoven [13]

In extremity conduction according to Einthoven, the potential difference between two electrodes is measured. The same derivations are deduced from the same principle, but with the measuring points on the head.

R:	Right arm	= red dot	RH: Right head side	= red dot
L:	Left arm	= yellow dot	LH: Left head side	= yellow dot
F:	Left foot	= green dot	FH: Forehead	= green dot

A 3-channel ECG measurement is a common method for the diagnosis of excitation spread disorders and is also used in this work a long-term measurement.

2.1.3 Photoplethysmography

Photoplethysmography (PPG) is a non-invasive method for recording the constantly changing blood volume measured in the capillaries. When the heart pumps blood into the body (systole), the volume is larger than when blood flows back to the heart (diastole). During systole, the blood is transported into the body. It is highly enriched with oxygen, which is bound to the protein hemoglobin (oxygen-rich hemoglobin) and then transported within the body. During diastole, this protein is free of oxygen (deoxygenated haemoglobin). Depending on the oxygen content of the haemoglobin there is a change of a light absorption. The heart rate can be derived from the rhythm of systole and diastole and the changing blood volume using the measurement method photoplethysmography. [14]

A pulse oximeter consists of two parts: a light source and a light sensor. The light sensors can be grouped into two different types of light detectors: transmission and reflection pulse oximeters. The first measures the light absorption and the other one the light reflection. Since the reflection sensor is used in this thesis, all further explanations refer to this sensor.

The light source emits infrared light waves that transmit or reflect light through the artery. The reflecting light components are then detected by the light sensor (see Figure 5).
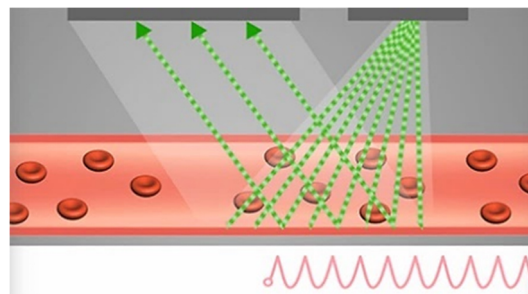
Figure 5: Principle of the pulse oximeter [15] with light reflection sensor

The light absorption in the blood depends on the haemoglobin concentration and the saturation of haemoglobin (part of the red blood cells) with oxygen (O_2). Oxygenated (HbO_2) and deoxygenated haemoglobin (RHB) absorb light in a characteristic way. During a pulse wave, two values are determined. The absorbance is measured at 640 nm (red light) and approximately 920 nm (infrared light). The determination of the arterial oxygen saturation of haemoglobin is calculated from the relative amounts of light using Lambert-Beer's law [4].

Lambert-Beer's law:

A ray of light loses intensity when it passes through matter. In general, it is necessary to enclose the absorbing medium in a cuvette that is also transmitted by light. This is where loss through absorption, reflection or scattering occurs.
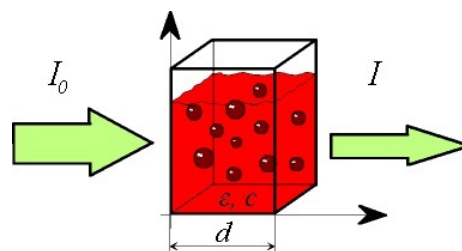
Figure 6: The derivation of Lambert-Beer's law [16]

The absorbance of material for light of the wavelength λ, also known as extinction, is determined by Lambert-Beer's law.

$$E = \log\left(\frac{I_0}{I}\right) = \varepsilon \cdot c \cdot d \tag{1}$$

$E \ldots Extinction\ (= Absorption)$
$I_0 \ldots Intensity\ of\ the\ rays\ before\ the\ sample$
$I \ldots Intensity\ of\ the\ ray\ after\ the\ sample$
$\varepsilon \ldots Molar\ extinction\ coefficient\ [l/mol]$
$c \ldots Concentration\ of\ the\ light\ absorbing\ substance\ [mol/l]$
$d \ldots Layer\ thickness\ of\ the\ sample\ [m]$

The law describes the relationship between the intensity of the transmitted light I and the intensity of the incident light I_0. The variable c corresponds to the concentration of the absorbing substance in the liquid, d is the path length of the light in the material and ε is the decadic extinction coefficient at the wavelength λ.

2.1.4 Electrodermal activity

Electrodermal activity (EDA) or galvanic skin response (= GSR) is a method that detects short-term changes in the skin conduction resistance. Such changes are caused by emotional-affective reactions that result in increased sweat production. The electrodermal phenomena are both spontaneous and induced changes in a complex system with elements of different electrophysical properties. All electrodermal models include variable resistors and capacitors. Some of these models also take voltage sources into consideration because sweat glands in the skin represent polarized membranes and are physically charged capacitors [17]. There are three basic methods for recording GSR:

- **Endosomatic measurements**
  This method measures active changes from the body itself. The electrical energy is taken from the polarized membrane in the skin.

- **Exosomatic measurements with direct current**
  Electrical energy is supplied from outside. The voltage or current is kept constant.

- **Exosomatic measurements with alternating current**
  This method analyzes system responses to periodically changing excitations. Furthermore, it attempts to obtain more information about the time response of the system during oscillation processes.

For the realization of this thesis, exosomatic measurement with direct current voltage (DC) is used by applying 3.3 V to the skin and determining the voltage drop at another point on the skin. A 32-bit microprocessor (see chapter 4.2.2.2) records the GSR signal and applies 3.3 V to the skin with electrode 1 and measures the voltage drop with electrode 2. The analog/digital input GPIO39 of the ESP32 microprocessor is used as signal line. The measured voltage is assigned a value between 0 and 4095. The value 0 V corresponds to the digital value 0 and 3.3 V corresponds to the digital value 4095. The measured signal is hardware-filtered by a capacitive low-pass filter to avoid possible interference signals (see Figure 7). The impedance of the capacitor decreases with increasing frequency. Low impedance in parallel with

the load resistor tends to short-circuit high-frequency signals, which causes a drop in most of the voltage across resistor R_{TP}.
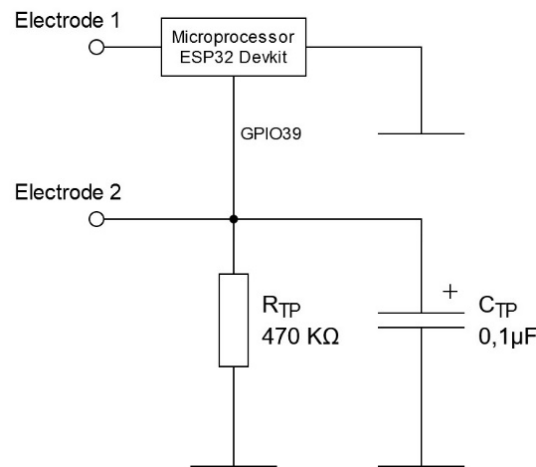
Figure 7: Circuit for GSR measurement

For the calculation of a GSR value, the recorded digital value (V_{mes}) must be converted into voltage (V_{GSR}).

$$V_{GSR} = \frac{V_{mes} \cdot 3,3V}{4095}$$

(2)

The skin resistance must be determined beforehand in order to determine the skin conductance value. The resistance of the capacitive low-pass filter is also considered.

$$R_{Skin} = \frac{V_{GSR} \cdot R_{TP}}{3,3V - V_{GSR}}$$

(3)

The inverse value of the skin resistance results in the required conductance with the unit *siemens*.

$$G_{Skin} = \frac{1}{R_{Skin}}$$

(4)

2.2 Existing examples of eye-tracking glasses

In this thesis, also eye or pupil movements are recorded in order to detect any symptoms of fatigue. For this reason, the market was searched for existing systems which fulfil the required functions. It should be noted that this study was conducted in 2020 and therefore includes state-of-the-art technology. The aim of this search is to integrate the possibilities and feasibility of an eye-tracking system into the device so that eye or pupil movements can be included into the biosignals.

2.2.1 Tobii Pro Glasses 2

The Tobii Pro Glasses 2 from the company Tobii Pro are a portable eye-tracking system that obtains objective data on the human visual gaze by showing exactly what a person observes while moving freely in any real environment. The glasses consist of a wide-angle camera capable of recording 1080p HD at 25fps with a 90° view angle, a microphone, a gyroscope and an accelerometer. On the inside of the lenses, there are a series of IR sensors, IR illuminators and eye-tracking cameras.

Figure 8: Tobii Pro Glasses 2 [18]

The basic principle of these glasses is that an infrared light source illuminates the eye and small high-speed cameras take 100 images of the eye every second. Inside the frame, sensors track the gaze of the person wearing the glasses. This gaze is recorded by the camera and the recorded images or the real-time video can then be displayed on a laptop or tablet.

2.2.2 Pupil Core

The Pupil Core is a portable, mobile eye-tracking headset with a camera and an infrared spectrum eye camera to detect dark pupils. Both cameras are connected via USB 2.0 to a laptop, desktop or mobile computing platform. The camera's video streams are read out with the Pupil Capture Software to enable pupil recognition, gaze mapping, recording and other functions in real time. The device includes a cable clip attachment that allows the user to move their head more freely.

Figure 9: Pupil Core [19]

Another difference to other eye-tracking systems is the variable use of the components. The system can be equipped in different ways depending on the requirements.
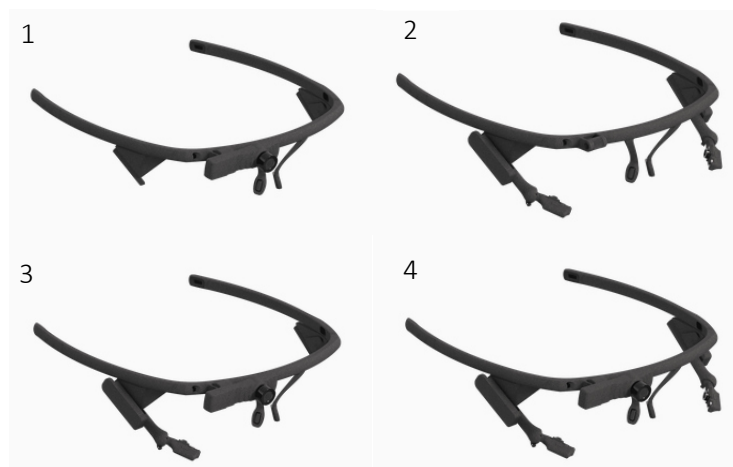
Figure 10: Pupil Core – Packages [20]
1 – Egocentric vision research | 2 – Eye movement research | 3 – Monocular Package | 4 – Binocular Package

The egocentric vision package (Figure 10 - 1) is the basic model and contains an eye camera to track the test person's vision. The monocular package (Figure 10 - 2) contains another monocular system for recording gaze and gathering pupil data. It can be upgraded to a binocular system (Figure 10 - 3) at any time by adding an additional eye camera. For pure eye movement research, it is also possible to equip the eyeglasses with a binocular system to obtain only binocular pupil data in real time or for post-hoc analysis.

2.2.3 Dikablis Glasses 3

The model Dikablis Glasses 3 by Ergoneers consists of two parts, the eye-tracking glasses and a control unit. Eye movement is recorded by cameras at the frame side of the glasses and the data is further processed and analyzed in the control unit. This design is also suitable for eyeglass wearers since they can wear their regular glasses under the frame. The eye cameras can be adjusted individually so that the eye movement can be ideally recorded. Furthermore, the data is stored in the control unit, which enables real-time transmission via WLAN.

Figure 11: Dikablis Glasses 3 [21]

3 Technical design concepts

3.1 Measuring points of the eyeglasses

To determine a suitable measuring point, the course of the arteries of the head has to be examined first. The position of a normal eyeglass is simulated in order to select the possible arteries, as is shown in the following figure. Figure 12 shows very clearly that principally, only three arteries are to be considered for the measurement, namely the arteria auricularis posterior, the arteria angularis and the arteria temporalis superficialis, which are highlighted in yellow. These three arteries derive from the external carotid artery, which supplies arterial blood to most of the head, soft tissues of the neck and parts of the bony skull. These three minor arteries are suitable for obtaining precise signals such as PPG and ECG. Body temperature and pulse are recorded at measuring point (MP) MP1 and ECG at MP1, MP2 and MP3. The ECG signal is generated by a two-point derivation, where MP1 and MP3 represent the derivation electrodes and MP2 the reference electrode. The skin conductance is recorded at measuring points MP4 and MP5. A voltage of 5 V is applied to the head at MP4 and the resulting voltage drop is measured at MP5, which is needed to determine the skin impedance.

Measurement point	Marker	Position
MP1	ECG_INP PPG Temperature	Behind the ear (left)
MP2	ECG_REF	Forehead
MP3	ECG_INN	Behind the ear (right)
MP4	GSR_IN	Input-Signal (5V)
MP5	GSR_SIG	Measurement signal
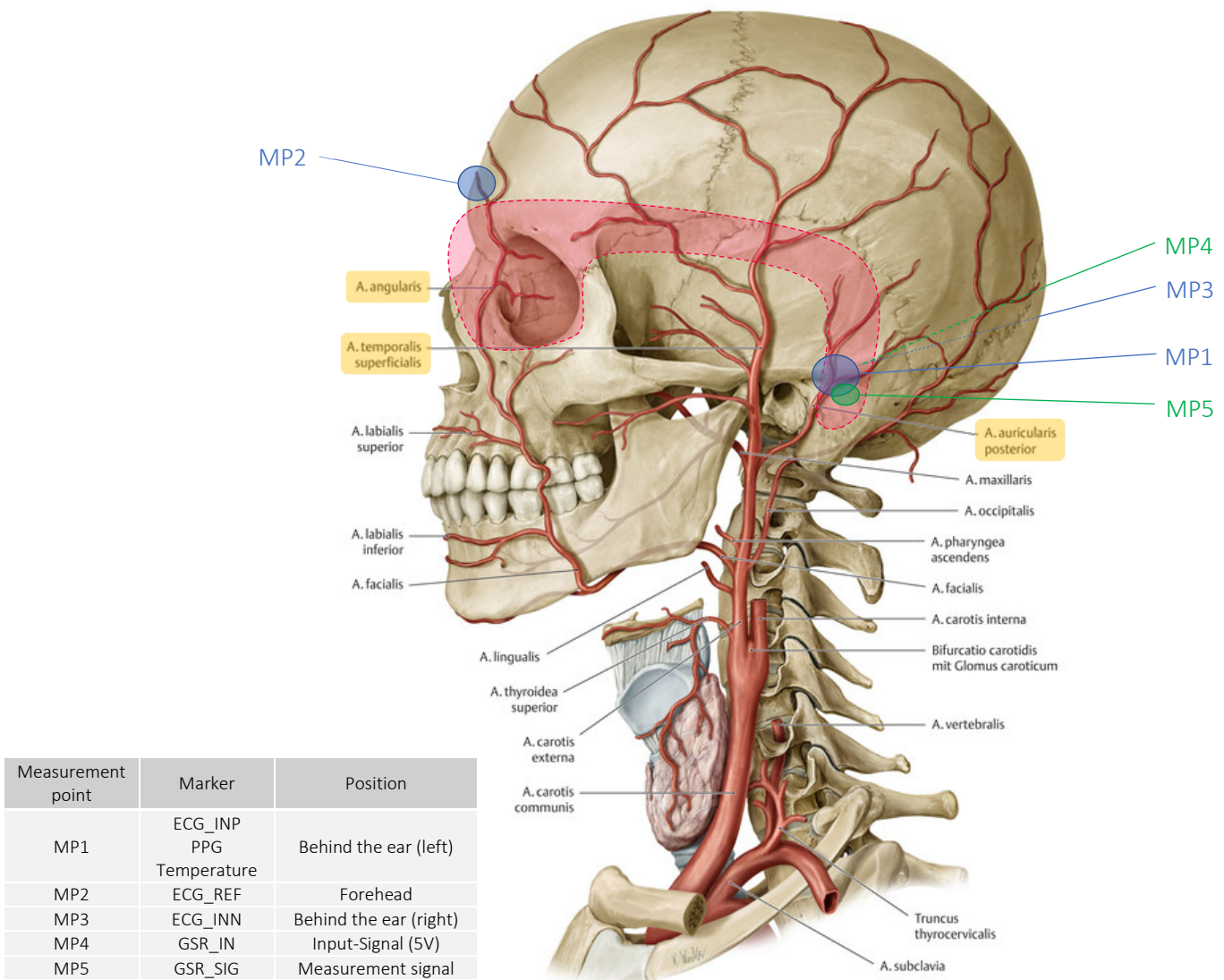
Figure 12: Head arteries with measurement points [22]

3.2   Schematic structure of the eyeglass design

When planning this project, it was decided to divide the first prototype into two units. This separation was created by the processor performance during the processing of the data from the biosignals and the camera recordings. Figure 13 shows the schematic structure of developed mobile device in this master's thesis.
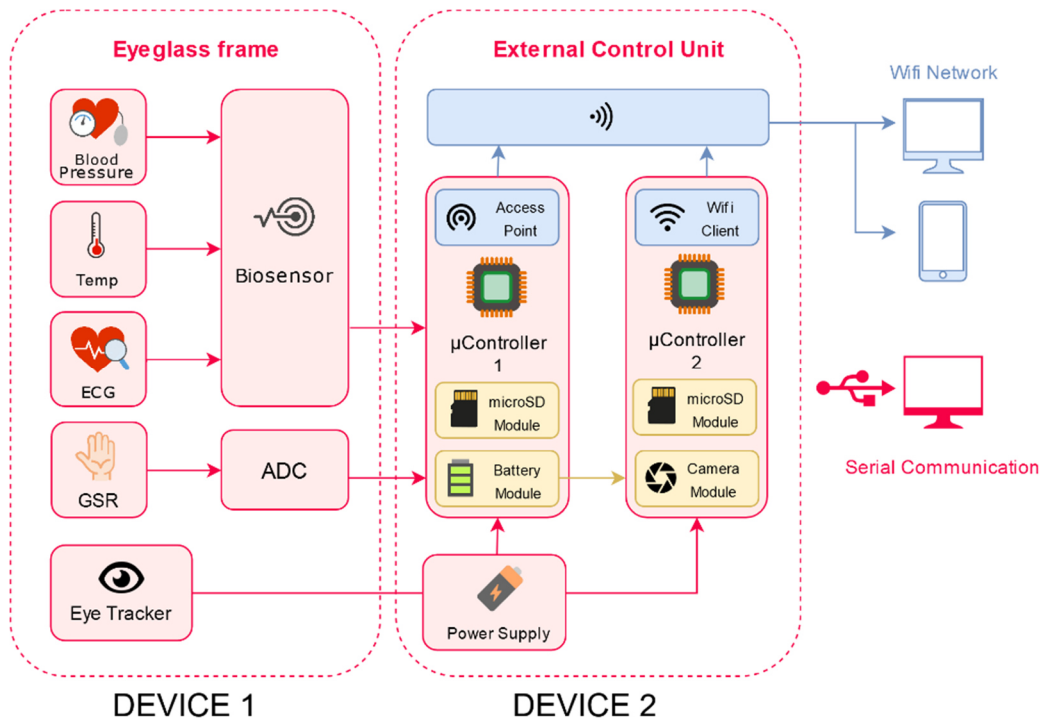
Figure 13: Schematic structure

Device 1 represents the eyeglass frame in which all sensors are positioned. A biosensor which records the biosignal data is used to record blood pressure, body temperature and ECG. The skin conductance value (GSR) is determined using an analog-to-digital converter that is integrated in microcontroller 1 to convert the analog signals into digital signals. The eye movement is recorded by a CMOS camera which is also built into the eyeglass frame.

In the second unit, device 2, the recorded data is processed and stored onto a storage medium. Two microcontrollers are used for data processing; one is responsible for processing the biosignals (blood pressure, body temperature, ECG and GSR) and the other one for the eye movement. The power source are accumulators which supply both units with voltage. The second unit is also used to transfer data to external devices such as computers, tablets or mobile phones. For this purpose, a microprocessor is set up as access point to provide access to the outside world via WLAN. The second microprocessor connects to the access point as a WLAN client, which allows both signal data (biosignal and eye movements) to be retrieved simultaneously from a WLAN network.

3.2.1   Eyeglass frame

The basic design idea of the eyeglass frame was taken from existing eyeglass designs with eye-tracking functions (see chapter 2.2). The concept was adapted to the corresponding measurement requirements, resulting in a new eyeglass frame (Figure 14). The final design was created in a 3D program (Autodesk Fusion 360) and produced with a 3D printer. For the first test print PLA (= polylactide) was used as printing material, which was replaced by TPU (= thermoplastic polyurethane) in the final version. For more detailed information about these materials, see chapter 5.1.

Figure 14: Designed eyeglass frame

The temples are slightly bent inwards to ensure a better fit of the frame and the sensors. All sensors are covered to prevent direct contact and to avoid measurement errors. The camera acts as an eye tracker and offers two manual adjustment options through a ball-and-socket, and hinge joint which allow for the camera to be aligned at will. The ball-and-socket joint is additionally equipped with a twist lock to hold the camera part in the desired position. With the hinge function, the camera can be positioned vertically. The ends of the temples have additional hinges that allow for optimal contact of the sensors to the skin. Another adjustment option can be found on the nose wings, which can also be adjusted to suit the shape of the face and therefore ensure an optimum eyeglass fit.

3.2.2 Controller board

The controller board enables the complete processing of all sensor and camera data as well as their forwarding via WLAN or serial connection (USB). Several components had to be considered for the design of the case. The cover is fixed horizontally with several screws on all sides. In the housing, the battery has to be placed on one side and several processors and modules on the other side (Figure 15 and Figure 16). The user-friendliness is also incorporated into the design of the housing. Several functions are integrated into the front area of the housing. A push-button on the right side allows for checking the battery status, which is represented by four indication diodes.

Figure 15: Designed control unit housing

Figure 16: Control unit housing - inside view

Furthermore, two mini slide switches are positioned on the front cover and function as on/off switch and recording switch. The status of the two switches is indicated by two LEDs – red to signal recording and green for the status (on/off) of the device. The USB ports of the voltage module for charging the battery are located on the left and lower side. The serial port can be found on the right side, which directly enables the serial communication between the device and the PC (via MATLAB).

One of the most important aspects was the attachment to the user without restricting their freedom of movement. As can be seen in Figure 17 – mark 1, a clip that can either be attached to the belt or directly to the trousers was chosen. The same concept is used for the connection point on the frame of the glasses (Figure 17 – mark 2). This clip is smaller than the belt clip and therefore easy to attach to the collar. The two conducted FFC foil cables are supported by 3D-printed cable drag chains to prevent damage.

Figure 17: Control unit - bottom view

3.2.3 Carried eyeglass frame and controller board

Figure 18 shows the use of the eyeglass frame and the control unit. An elastic connecting band with a closure at both ends of the temple ensures optimal contact between the sensors and the electrodes. The communication between the sensors on the eyeglass frame and the microprocessor on the control unit is realized with several FFC flat ribbon cables.

Figure 18: Carried eyeglass frame and controller board

The microprocessor ESP32-Cam had to be moved from the control unit to the eyeglass frame because of the too long data line, as can be seen in the previous figure. The data line between the control unit and the eyeglass frame is secured by a clip on the test person's collar.

4 Technical implementation

In this chapter, the choice of the individual components is explained separately. In addition to the components, the power supply and data storage of the biosignals also play a major role in this project and are therefore described as well. At the end of this chapter, the software realization as well as the characteristics of the used printing materials for the case and eyeglass frame are explained in detail.

4.1 Sensor feasibility studies

Before the actual hardware could be chosen, sensor-side test measurements had to be carried out to ensure feasibility. The first tests were conducted with an evaluation board from the company *ams AG*. This board contains a vital signs sensor (AS7024), a temperature sensor (AS6200), an accelerometer (LIS2DH12) and three discharge electrodes located on the breakout board, as shown in Figure 19.
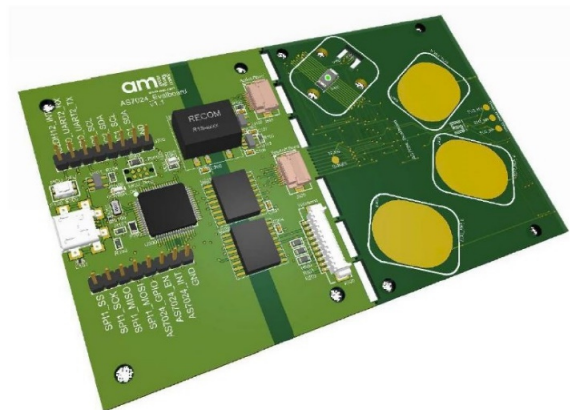
Figure 19: ams - AS7024 Evaluation Board v1.2 [23]

The measured data from the individual sensors are transmitted via an I²C bus to the mainboard, where the data are processed, for example by low-pass filtering. The board is supplied with power via a USB micro interface, which also serves as communication interface to the PC. The mainboard contains a DC/DC converter and several isolation ICs for all signals to avoid a direct connection from the electrodes to the power supply. Figure 20 shows the current and communication flow between the PC and the evaluation board or to the AS7024 Evaluation Kit.
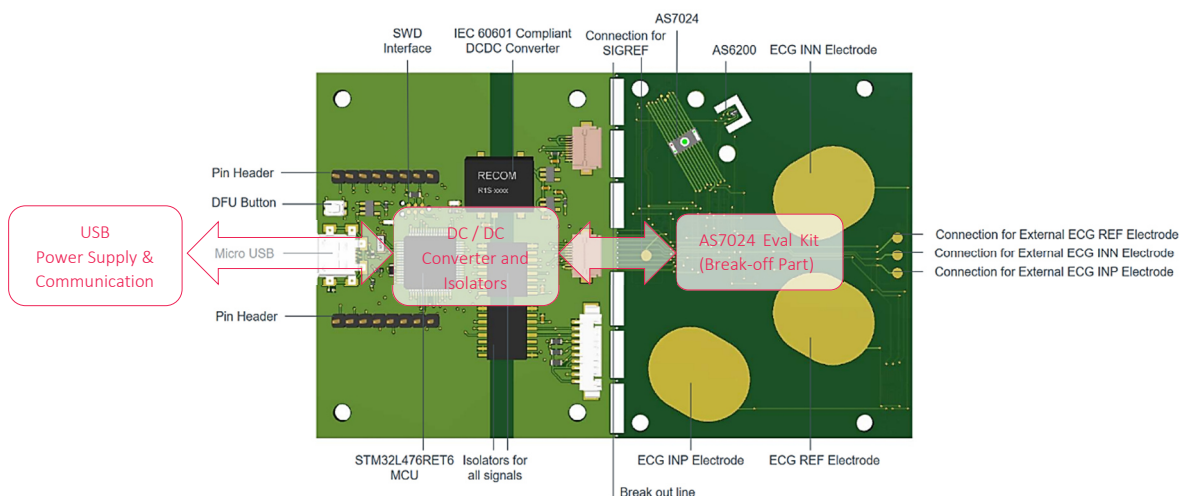
Figure 20: Evaluation board with power supply & communication [24]

A special feature of this board is that the mainboard can be separated from the sensor board so that a FPC cable can connect external sensors which are compatible with the mainboard. This allows to use the AS7024 Add-On Board from the same company. Figure 21 shows the conversion of the evaluation board with the AS7024 Add-On Board. The 10-pin FPC connector on top is used as an interface. In this case, it is important that the other two FPC connectors on the mainboard are free because the communication of the middle FPC connector is always considered first by the mainboard.
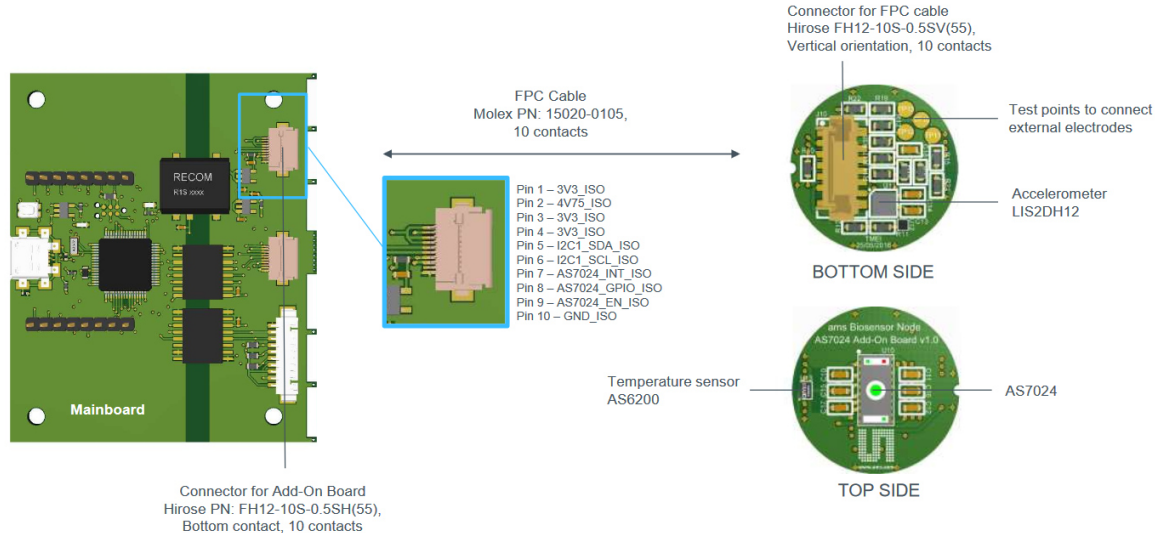
Figure 21: AS7024 Add-On Board [25]

The add-on board enables a local measurement at the desired measuring point from chapter 3.1. This allowed to check prior to the start of the project whether the biosignals could be measured at the desired locations. To determine the biosignals, the manufacturing company provides software which can display all signals from the different sensors. An example of how to use the software is shown in Figure 22, where a measurement is performed simultaneously on the AS7024 sensor and the local ECG pads on the break-off board. Mark 1 shows the PPG signal and mark 2 the ECG signal.
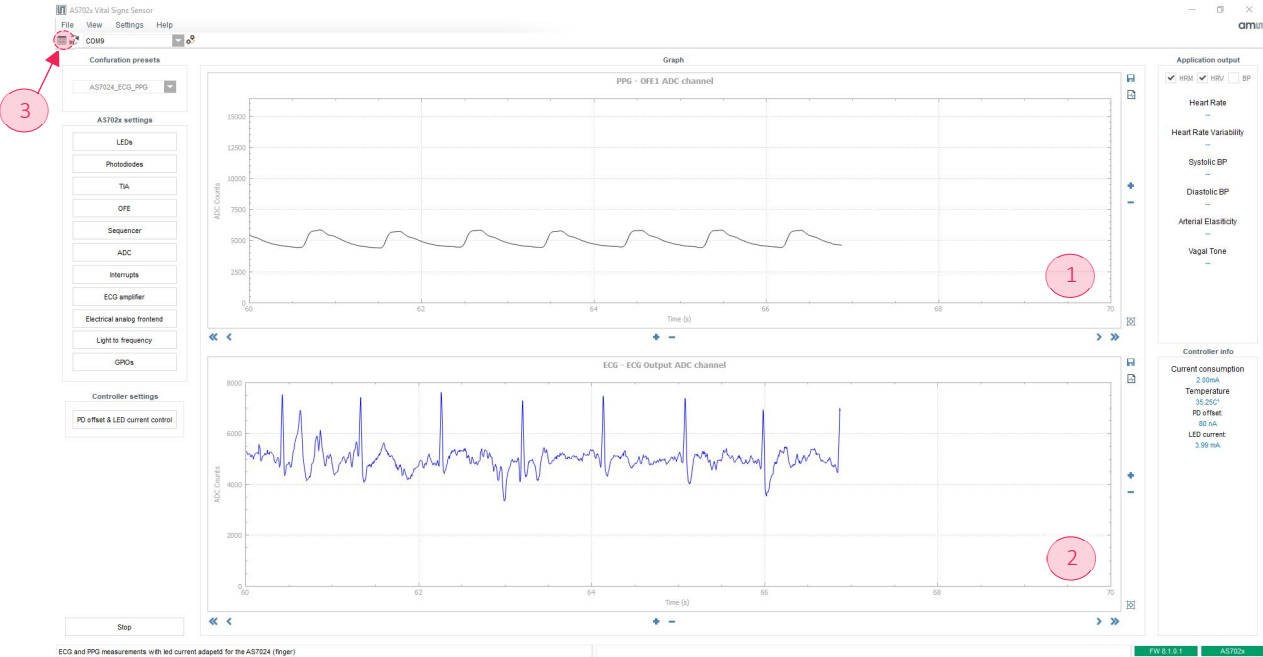
Figure 22: The ams AG software of AS7024 vital signs sensor (1 = PPG, 2 = ECG)

A particularly important setting option is the "Register Map" function (Figure 22 – Point 3), which plays a crucial role in the software implementation of the project. This map is used to set the individual functions of the AS7024 Add-On Board, such as the sampling frequency, switching on the LEDs on the AS7024 and many other functions, which are described in more detail in chapter 4.2.2.1.

4.2 Hardware

When choosing the hardware, several factors and requirements that are listed in this section had to be considered. For the realization of the project, the selection was made on the basis of available modules that can be integrated as individual components in the future. Another important factor that had a major influence in the selection was the cost of these modules.

4.2.1 Requirements

Four requirements were essential in this project: mobility, user-friendliness, data transmission and user security. Mobility refers to the portability of the device so that measurements can be taken almost anywhere. User-friendliness refers to the operation of the device and the fit of the eyeglass frame so that the device can be operated and worn by anyone.

Another focus was on selecting components that allow for low power consumption, the smallest possible component size and wireless data transmission. All components should be able to record data for at least half a day up to a full day.

Finally, the availability of the recorded biosignals was an important criterion as well. This means that it should be possible to both follow the data live on any platform and to process the data via a serial interface using a PC.

4.2.2 Chosen components

When selecting the hardware, the requirements listed in section 4.2.1 had to be fulfilled to the greatest extent. Another key point was on choosing modules that could already combine several required functions to save space. This meant that compromises had to be made, which are explained in more detail in the following list of components: sensors, microcontroller, camera and electrodes.

4.2.2.1   Sensors

One of the most important sensor units in this master's thesis is the AS7024 Add-On Board for vital signs from the company *ams AG*. This board was briefly described in chapter 4.1.
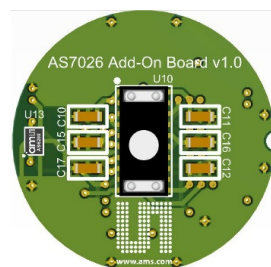
Figure 23:
AS7024-Add-On Board [26]
(top view)
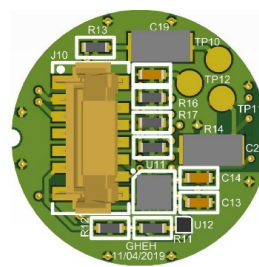
Figure 24:
AS7024 Add-On Board [27]
(bottom view)

The only problem was that the recorded data is further processed and that the manufacturer only offers the use of the evaluation board. This led to additional work for the project since this project focuses on the possibility to read and process the data in another microprocessor. Still, the decision was made to use this add-on board because it is relatively small and already combines some sensor units that are essential for the project. Another major advantage of this board is that all sensor data are provided by an I^2C bus.

The core of the add-on board is the AS7024 sensor (Figure 24 – Labelling U10), which can record the pulse (PPG) as well as the electrical activity of the heart (ECG). Both measurements are based on the principles of chapters 2.1.2 and 2.1.3. For pulse measurement, the AS7024 chip contains three controllable LEDs at the edge and a detector in the middle that detects the reflected light from the blood vessels. During PPG measurements, it is important to ensure that the sensor is not pressed too hard on the measurement point, otherwise the blood flow in the vessels will be restricted and incorrect measurements occur. The ECG measurement is a two-point derivation with a reference point. Therefore, three SMD pads are provided on the board to make it possible to attach external electrodes to the system (Figure 24 – Labelling TP10, TP11, TP12). The ECG amplifier is a high-impedance, low-noise instrumentation amplifier with an analog circuit for bandpass filtering of the signal and amplification before conversion by the AD converter. The full control of the sensor is handled by the register map, which is controlled by setting binary values at the corresponding address. The following table shows the complete register map of the AS7024 sensor. All setting options can be determined in the datasheet of the sensor.

Table 1: Register map of the AS7024 sensor

	Addr.	7	6	5	4	3	2	1	0	Value
CONTROL	0x00	1		0				1	1	0x83
GPIO_A	0x08					1	1	1	1	0x0F
GPIO_E	0x09					0	0	0	0	0x00
GPIO_O	0x0A					0	0	0	0	0x00
GPIO_I	0x0B					0	0	0	0	0x00
GPIO_P	0x0C	0	0	0	0	0	0	0	0	0x00
GPIO_SR	0x0D					0	0	0	0	0x00
GPIO_T	0x0E					0	0	0	0	0x00
LED_CFG	0x10		1	0	0	0	0	1	1	0x43
LED1_CURRL	0x12	0	1							0x40
LED1_CURRH	0x13	0	0	0	0	1	0	0	0	0x08
LED2_CURRL	0x14	0	1							0x40
LED2_CURRH	0x15	0	0	0	0	1	0	0	0	0x08
LED3_CURRL	0x16	0	1							0x40
LED3_CURRH	0x17	0	0	0	0	1	0	0	0	0x08
LED4_CURRL	0x18	0	1							0x40
LED4_CURRH	0x19	0	0	0	0	1	0	0	0	0x08
PD_CFG	0x1A			1	1	1	1	0	0	0x3C
PDOFFX_LEDOFF	0x1B	0	0	0	0	0	0	0	0	0x00
PDOFFX_LEDON	0x1C	0	0	0	0	0	0	0	0	0x00
PD_AMPRCCFG	0x1D	1	0	1	0	0	0	1	0	0xA2
PD_AMPCFG	0x1E	1	0	1	1	1	1	0	0	0xBC
PD_THRESHCFG	0x1F	1	0	1	0	0	1	0	0	0xA4
LTFDATA0_L	0x20	0	0	0	0	0	0	0	0	0x00
LTFDATA0_H	0x21	0	0	0	0	0	0	0	0	0x00
LTFDATA1_L	0x22	0	0	0	0	0	0	0	0	0x00
LTFDATA1_H	0x23	0	0	0	0	0	0	0	0	0x00
ITIME	0x24	0	0	0	0	0	0	0	0	0x00
LTF_CONFIG	0x25	0	0	0	1			0	0	0x10

	Addr.	7	6	5	4	3	2	1	0	Value
LTF_CONFIG	0x25	0	0	0	1			0	0	0x10
LTF_SEL	0x26		0	0	0		0	0	0	0x00
LTF_GAIN	0x27			0	0	0	0	0	0	0x00
LTF_CONTROL	0x28							0		0x00
AZ_CONTROL	0x29							0	0	0x00
OFFSET0	0x2A	0	0	0	0	0	0	0	0	0x00
OFFSET1	0x2B	0	0	0	0	0	0	0	0	0x00
LED12_MODE	0x2C	0	0	1	0	0	0	1	0	0x22
LED34_MODE	0x2D	0	0	0	0	0	0	0	0	0x00
MAN_SEQ_CFG	0x2E	0	0	0	0	0	0	0	1	0x01
SEQ_CNT	0x30	0	0	0	0	0	0	0	0	0x00
SEQ_DIV	0x31	0	0	0	0	1	0	0	1	0x09
SEQ_START	0x32							0	0	0x00
SEQ_PER	0x33	1	0	1	0	0	1	1	0	0xA6
SEQ_LED_STA	0x34	0	1	0	1	0	0	1	1	0x53
SEQ_LED_STO	0x35	0	1	1	0	1	0	0	0	0x68
SEQ_SECLED_STA	0x36	0	0	0	0	0	0	0	0	0x00
SEQ_SECLED_STO	0x37	0	0	0	0	0	0	0	0	0x00
SEQ_ITG_STA	0x38	0	0	0	0	0	0	0	1	0x01
SEQ_ITG_STO	0x39	0	0	0	0	0	0	0	0	0x00
SEQ_SDP1_STA	0x3A	0	1	0	1	0	1	0	0	0x54
SEQ_SDP1_STO	0x3B	0	1	1	0	1	0	0	0	0x68
SEQ_SDP2_STA	0x3C	0	0	0	0	0	0	0	0	0x00
SEQ_SDP2_STO	0x3D	0	0	0	0	0	0	0	0	0x00
SEQ_SDM1_STA	0x3E	0	0	0	0	0	0	0	1	0x01
SEQ_SDM1_STO	0x3F	0	0	0	1	0	1	0	0	0x14
SEQ_SDM2_STA	0x40	0	0	0	0	0	0	0	0	0x00
SEQ_SDM2_STO	0x41	0	0	0	0	0	0	0	0	0x00
SEQ_ADC	0x42	0	0	0	0	0	0	0	1	0x01

Name	Addr.	7	6	5	4	3	2	1	0	Value
SEQ_ADC2TIA	0x43	0	1	0	1	0	1	0	0	0x54
SEQ_ADC3TIA	0x44	0	0	0	0	0	0	0	0	0x00
SD_SUBS	0x45	0	0	0	0	0	0	0	0	0x00
SEQ_CFG	0x46								0	0x00
SEQ_ERR	0x47	0								0x00
OFE_CFGA	0x50	0	1	1	1	1	0	0	0	0x78
OFE_CFGB	0x51	1	0	1	0	0	0	0	0	0xA0
OFE_CFGC	0x52		0	0	0	0	1	1	1	0x07
OFE_CFGD	0x53							0	1	0x01
OFE1_CFGA	0x54	1	1	1	1	0	0	0	1	0xF1
OFE1_CFGB	0x55		0	1	1	1	1	0	0	0x3C
OFE2_CFGA	0x58	1	0	0	0	0	0	0	1	0x81
OFE2_CFGB	0x59		0	0	0	0	0	0	0	0x00
ECG_CFGA	0x5C	1		1	1	1	0	0	0	0xB8
ECG_CFGB	0x5D	0	1	1	0	0	1	1	0	0x66
ECG_CFGC	0x5E							1	1	0x03
ECG_CFGD	0x5F			0	0	0	0	0		0x00
CYC_COUNTER	0x60	0	0	0	0	0	0	0	0	0x00
SEQ_COUNTER	0x61	0	0	0	0	0	0	0	0	0x00
SUBS_COUNTER	0x62	0	0	0	0	0	0	0	0	0x00
ADC_THRESHOLD	0x68	1	1	1	1	1	1	1	1	0xFF
ADC_THRESHOLD_CFG	0x69							0	0	0x00
AFE_CFG	0x70					0	0	1	0	0x02
FIFO_CFG	0x78	0	1	0	0	0	0	1	1	0x43
FIFO_CNTRL	0x79								0	0x00
EAF_GST	0x80	1	1	1	0	0	1	1	0	0xE6
EAF_BIAS	0x81	0	0	0						0x00
EAF_DAC	0x82			0	0	0	0	0	0	0x00
EAF_DAC1_L	0x83	0	0							0x00

Name	Addr.	7	6	5	4	3	2	1	0	Value
EAF_DAC1_H	0x84	0	0	0	0	0	0	0	0	0x00
EAF_DAC2_L	0x85	0	0							0x00
EAF_DAC2_H	0x86	0	0	0	0	0	0	0	0	0x00
EAF_DAC_CFG	0x87							0	0	0x00
ADC_CFGA	0x88						0	0	0	0x00
ADC_CFGB	0x89	0	0	0	0	1	0	0	1	0x09
ADC_CFGC	0x8A				1	1	1	0	1	0x1D
ADC_CHANNEL_MASK_L	0x8B	0	0	0	0	0	0	1	1	0x03
ADC_CHANNEL_MASK_H	0x8C	0	0	0	0	0	0	0	1	0x01
ADC_READCALIBCLOCK	0x8D								0	0x00
ADC_DATA_L	0x8E	0	0	0	0	1	0	0	0	0x08
ADC_DATA_H	0x8F		0	0	0	0	0	0	0	0x00
SUBID	0x91	1	0	0	0	0	0	1	0	0x82
ID	0x92	1	1	0	0	1	1	0	0	0xCC
STATUS	0xA0	0	1	0	0	0	0	1	1	0x43
CLIPSTATUS	0xA1					1	0	0	0	0x08
LEDSTATUS	0xA2				0	0	0	0	0	0x00
FIFOSTATUS	0xA3	0	0	0	0	0	0	0	0	0x00
LTFSTATUS	0xA4							0	0	0x00
INTENAB	0xA8	0	0	0	1	0	0	0	0	0x10
INTR	0xA9	0	0	0	0	0	0	0	0	0x00
TEST1	0xC0	0	0	0	0	0	0	0	0	0x00
TEST2	0xC1	1	1	0	0	0	0	0	0	0xC0
TMUX1	0xC2			0	0	1	1	0	0	0x0C
TMUX2	0xC3			0	0	1	1	0	0	0x0C
TMUX3	0xC4			0	0	0	0	0	0	0x00
DIGTMUX	0xC5	0	0	0	0	0	0	0	0	0x00
FIFOL	0xFE	0	0	0	1	1	1	1	0	0x1E
FIFOH	0xFF	0	0	1	0	1	1	1	0	0x2E

One example for using the register map would be to activate or deactivate the set measurement on the sensor. The measurement is started by setting the sequencer address 0x32 to the value 0x01 and stopping the measurement at 0x00. The I²C slave address of the AS7024 sensor is 0x30 and allows a data bus speed of up to 400 kbps.

The same add-on board also includes an AS6200 temperature sensor (Figure 23 – Labelling U13) which measures body temperature to detect temperature fluctuations under stress. The sensor addressed by the I²C slave address is 0x48 and has a data bus speed of 400 kbps up to 3.4 Mbps.

Although the add-on board has an acceleration sensor as well, it was not used in this project.

The add-on board could also determine the skin impedance (GSR), but this was solved directly by the following microprocessor. One line injects 5 V into the skin and the other line measures the voltage drop through the analog input of the microprocessor. It was necessary to insert a hardware-based low-pass filter before the ADC input of the microprocessor to avoid interference signals.

4.2.2.2 Microcontroller

In this project, the ESP32-WROOM-32 is used. It is an ESP32-based module that integrates several key components, including a crystal oscillator and an antenna adjustment circuit. The module represents a ready-to-use solution for integration into end products. In combination with some additional components, such as a programming interface, bootstrap resistors and a pin header, the full ESP32 functionality can be used. For this reason, the ESP32-DevKit V2 was chosen for the project, since it combines the previously discussed functions of the ESP32 module.
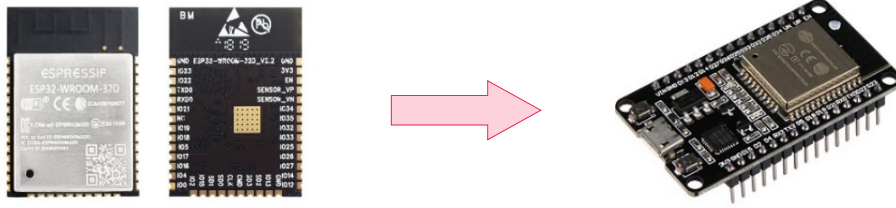
Figure 25: ESP32-WROOM-32D (left side) [28] and ESP32-DevKit (right side) [29]

The pins of the ESP32 Development Board are labelled on the upper side of the board which makes them easy to identify. ESP32 is equipped with an on-board reset (EN) and boot buttons. Moreover, it comes with an USB-to-UART interface to be able to program it with ProgramIO, Arduino IDE or other development environments and also has a voltage regulator circuit. The board can be powered via a micro USB connector and it is not supplied with a battery connector.

The specifications of the ESP32-DevKit:

- The ESP32 has two processors (dual-core) and can execute 32-bit programs.
- Another special feature is built-in WLAN and Bluetooth (BLE and Bluetooth Classic).
- The clock frequency can reach up to 240 MHz and it offers a 512 kB RAM.
- It also has a variety of peripherals available, such as capacitive touch, ADCs, DACs, UART, SPI, I^2C and more.
- It comes with a built-in hall effect sensor and a built-in temperature sensor.

Furthermore, this work requires an eye-tracking system, which is why a second ESP32 processor is placed on another development board called ESP32-CAM because of the required image processing. The ESP32-CAM is a very small camera module with an ESP32-S chip, which has a microSD card slot in addition to the OV2640 Camera and several GPIOs for connecting peripheral devices. This memory slot can be used to back up images or data previously captured by the camera.
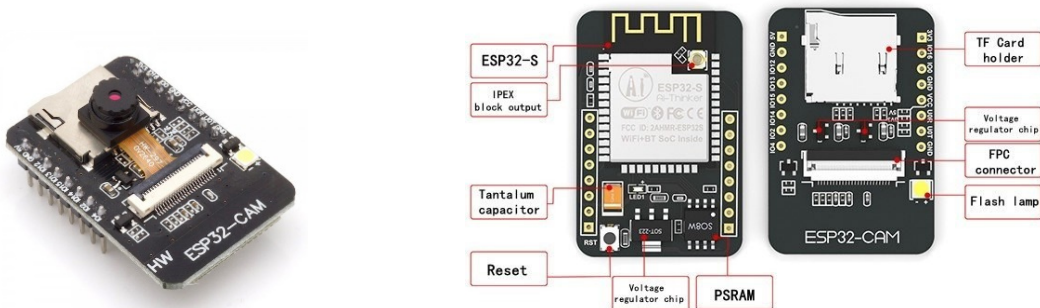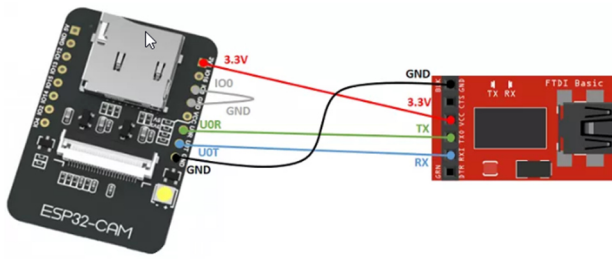

Figure 26: ESP32-CAM [30]

Figure 27: ESP32-CAM components

The ESP32-CAM is not supplied with a USB port, so an FTDI programmer is needed to upload code via the serial pins (U0R and U0T). It should be noted that some FTDI programmers have a jumper that allows to choose between 3.3 V or 5 V. The jumper should be set to 5 V for programming. Figure 28 shows the schematic diagram for programming the ESP32-CAM board. It is important that pin GPIO0 is connected to GND so that the programmed code can be uploaded.

ESP32-CAM	FTDI Programmer
GND	GND
5V	VCC (5V)
U0R	TX
U0T	RX
GPIO0	GND

Figure 28: ESP32-CAM programming schematic

Features of the ESP32-CAM:

- the smallest 802.11 b/g/n Wi-Fi BT SoC module,
- low-power 32-bit CPU,
- up to 160 MHz clock speed,
- built-in 520 kB SRAM and external 4 MB PSRAM,
- supports UART/SPI/I^{2}C/PWM/ADC/DAC,
- supports OV2640 and OV7670 cameras, built-in flash lamp,
- supports image Wi-Fi upload,
- supports TF card,
- supports STA/AP/STA+AP operation mode.

4.2.2.3   Camera

The OV2640 Camera used is a low-voltage CMOS image sensor, that offers the full functionality of a single-chip UXGA camera (1632x1232) and an image processor in a small package (see Figure 29). The OV2640 produces 8-bit/10-bit images in a variety of formats controlled via Serial Camera Control Bus (SCCB) interface. The camera has an image field that can operate at up to 15 frames per second (fps) in UXGA resolution. All necessary image processing functions, including lighting control, gamma, white balance, color saturation, hue control, white pixel suppression, noise reduction and more, are also programmable via the SCCB interface. The OV2640 also features a compression engine to increase processing power.
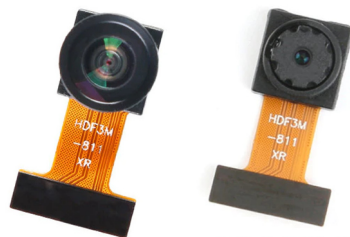

Figure 29: OV2640 – Wide-angle lens (left side) and normal-angle lens (right side) [31]

In addition, the camera chip uses proprietary sensor technology to improve image quality by reducing or eliminating DC/electric sources of image pollution, such as fixed-pattern noise, to produce a clean, completely stable color image. The CMOS sensor camera is available in two versions with a normal- and a wide-angle lens. Currently, the normal version is used because it was delivered with the ESP32-CAM board.

Important specifications of the CMOS camera for the project:

- high sensitivity for low light operation,
- low operating voltage for embedded portable apps,
- standard SCCB interface,
- output support for RAW RGB, RGB (RGB565/555), GRB422, YUV (422/420) and YCbCr (4:2:2) formats,
- supports image sizes UXGA, SXGA, SVGA and other resolutions,
- automatic image control functions including automatic exposure control (AEC), automatic gain control (AGC), automatic white balance (AWB), automatic band filter (ABF) and automatic black-level calibration (ABLC),
- image quality controls including color saturation, gamma, sharpness, lens correction, white pixel suppression, noise reduction and 50/60 Hz luminance detection,
- optical black level output capability,
- video or snapshot operation,
- variable frame rate control,
- embedded microcontroller.

4.2.2.4   Electrodes

The electrodes required for recording the biosignals shall be easily attachable and removable. Another important consideration is that the electrodes may be used several times and can easily be incorporated into an eyeglass frame. From the characteristics described, it is evident that normal silver-silver chloride electrodes cannot be used for the project. After several tests, the decision was made to use spring contacts from the company Preci-Dip since they are a suitable alternative to conventional connection solutions. These low-resistance modular connectors feature spring-loaded contacts with SMD pads and gold-plated contacts (see Figure 30).

Figure 30: Preci-Dip surface mount spring contacts [32]
(male straight, grid 2.54 mm)

The multi-point electrical connection between the mobile plunger and the camp guarantees low, stable electrical resistance values without micro-interruptions, even if the plunger moves or vibrates, ensuring maximum reliability.

4.3   Power supply

The power supply for the project is provided by two 18650 batteries which are mounted on a finished module with several functions (see Figure 31 and Figure 32). The decision for using the 18650 batteries as power supply was a deliberate one. These batteries have two advantages: first the high current capacity with a fixed power supply, in this case 5.2 Ah at 3.7 V, second , the easy change as well as the replacement of defective battery cells.
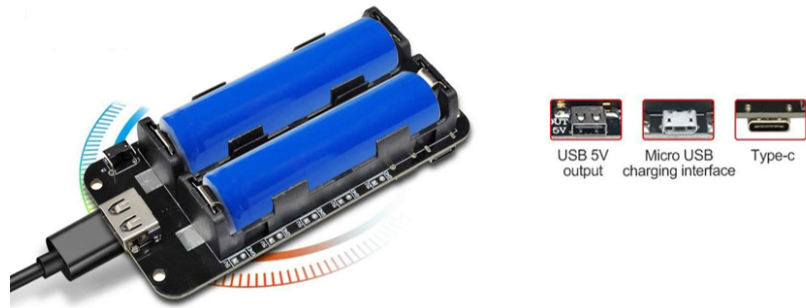
Figure 31: 18650 battery shield [33]

One of these functions mentioned above is a portable mobile power supply that supports two voltage outputs with 3 V/1 A and 5 V/2,2 A, which are needed in this project. Another function is the charging function via several USB interfaces, such as USB Type-A, micro-B USB and USB Type-C. A voltage indicator with four LEDs (LED1, LED2, LED3 and LED4) is also integrated into this module and can be used to check the battery status of the 18650 batteries by pressing the button on the module. Battery protection against overcharging and overdischarging is also integrated into the module.

Figure 32: 18650 module in detail [34]

4.4   Data storage

The recorded biosignals must be stored for 24 hours for processing and evaluation. Furthermore, these data must be marked with a timestamp. For this reason, a data logger module is used in this project. The data logger module can store data on any formatted FAT16 or FAT32 MicroSD card and the included RTC (real-time clock) adds the current timestamp to the data (see Figure 33 and Figure 34). The RTC keeps the time even when the power is off by using a coin cell battery as buffer supply.
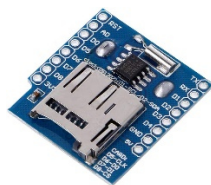

Figure 33:
Mini data logger (MicroSD + RTC) [35] -
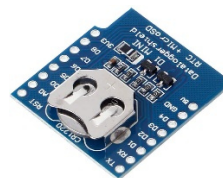*Top view*

Figure 34:
Mini data logger (MicroSD + RTC) [36] -
Bottom view

The DS1307 RTC Module is controlled by I^{2}C bus (pin SCL and SDA) through the address 0x68 and the memory card via an SPI connection to the ESP32 microcontroller.

The following list describes the individual pins in more detail:

CS	Pin for SD card acquisition
SCK	Pin for synchronization of the data transfer through the master pins
MOSI	Pin for data transfer (Master Out Slave In)
MISO	Pin for data transfer (Master In Slave Out)
VCC	Pin for power supply
GND	Pin for the ground pin

4.5 Software tools

The software realization of this project was executed in different programs, for instance for programming the microprocessors or creating the 3D models. These programs are explained in more detail in this chapter to provide a comprehensive insight into the decision to use them.

4.5.1 MegunoLink

In the first test phase, determining biological data was carried out using the MegunoLink software. With the help of this software, the data can quickly be displayed visually via the serial interface. MegunoLink is a companion application for ESP32. The software receives the raw data via the serial interface and plots it in several graphs. This connection setup is illustrated in Figure 35 and is ensured by a serial USB micro cable.
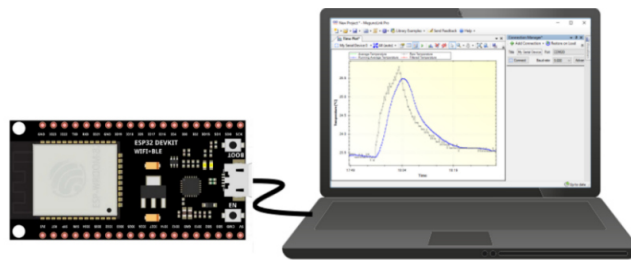

Figure 35: MegunoLink – first communication link to an ESP32 [37,38]

An important factor in the decision whether to use this program was a quick and easy evaluation of the first test measurements to determine if the planned measuring points would provide the desired measurement results. These measurements were important for the further course of the project and will be explained in detail in chapter 6.3.

4.5.2   Microsoft Visual Studio Code / PlatformIO IDE

The programming of the ESP32 microcontroller was performed in Microsoft Visual Studio Code with the extension PlatformIO IDE. This software is a free source code editor from Microsoft. Visual Studio Code is available cross-platform for the operating systems Windows, macOS and Linux. The framework used is Electron and offers syntax highlighting, code-following, debugging, auto-completion, version management and much more. Unlike Visual Studio, Visual Studio Code does not work with project files, but based on the source code files and folders. For this reason, Visual Studio Code works with workspaces that store an editing state, the order of open files and their line position.

The decision to use this software was made because the software offers two major advantages over other programs. Firstly, it would allow for easy integration of different libraries, which would make the integration of the individual components much easier, and secondly, the software is freeware and runs on all current operating systems.

4.5.3   Autodesk Eagle

The program Eagle is a PCB layout and schematic editing tool from the company Autodesk. This software has several features that are useful for creating a printed circuit board. Two of these features are, for example, the reusable design blocks which can be used by drag-and-drop into the project and the complete synchronisation of the schematic and PCB circuits. An additional feature is the electronic control check so that one can immediately identify any circuit errors (e.g. incorrect switching connections). Furthermore, this software facilitates the creation of PCB layouts where components can be linked to 3D parts to create a true-to-scale model of the PCB in other programs such as Autodesk Fusion 360.

This product was chosen because it enables the simple drawing of circuits and their layout realization. Another crucial factor was the integration of the layout into Autodesk Fusion 360 to equip the virtually created circuit board with visual components that provide the most detailed picture of the finished board.

4.5.4   Autodesk Fusion 360

Fusion 360 provides all the tools needed to create a new product. This means that all steps from design to production are combined in this program. The integrated functions allow design ideas to be evaluated quickly and directly. The Autodesk cloud-computing platform lets users view these design ideas in a web browser or on a mobile device. Recently, a slicer for 3D printing has been added, eliminating the need for an external slicer to convert the 3D model into machine code.

The major advantage of this program is its great user-friendliness, which simplifies the creation of 3D models. Another important aspect in choosing this software was the saving of the 3D model in an STL (= Standard Triangulation Language) format. This format provides geometric information of three-dimensional data models, which is necessary for 3D printing. The slicer function in this program was not used in this software program because it is still in the test phase; therefore, an external slicer was used.

4.5.5 Simplify3D

Simplify3D translates 3D models into introductions that the printer can then implement. This software can easily import digital models, select from pre-configured settings and generate G-code commands within seconds. Different slicing settings can be used within a component to achieve optimum print quality. Other settings such as layer thickness, speed and temperature can also be varied. The interactive and animated preview allows the user to view the printing process. At the same time, the software provides information about the printing sequence to keep material costs as low as possible even before printing starts.

The slicer was chosen for Simplify3D because this program allows you to add manual support structures, which is not possible with other programs. This function is very useful for complicated models because you can adjust them yourself. Another advantage is the interactive and animated print preview, which allows for a virtual animation of the model print. In addition, a precise print preview is also available and facilitates layer-by-layer or line-by-line checking.

4.6 Implementation software

4.6.1 Access point

In this project, microcontroller 1 acts as a WLAN access point so that microcontroller 2 can connect to the network as a client. This enables a complete communication of all data (biosignals and video) with only one network interface. The connection is established in several steps. In the first step, the access point is set up by microcontroller 1 at start-up. Next, microcontroller 2 connects to the network as a WLAN client. At this point, all data can be accessed via the access point. A simple WLAN connection through a PC or mobile device then allows access to these data. Access is granted via the SSID (Service Set Identifier) `HCE_Eyeglasses` with the password `hceStress`.

4.6.2 Data access

Data access to the recorded biosignal data is obtained via the internal file server, which is set up via the access point. The file server can be reached via the IP address `192.168.4.1` if the connection at the access point was successful. When this IP address is accessed, an HTTP page is automatically loaded. "Home", "Live-Chart", "Download", "Upload", "Delete", "Directory" and "Camera" can then be selected in the tab menu. The "Home" tab provides an overview of the status of individual components installed in the system, for example whether an SD card is present or whether biosignals are received. The "Live-Chart" tab shows the received signals and displays them in corresponding diagrams. In the "Download" menu, it is possible to download the individual data record files from the SD card. This enables offline analysis of data records so that statistics can be created or further filter functions (e.g. low-pass filter) can be applied to the data. With the tabs "Upload" and "Delete", data can be saved on or deleted directly from the microSD card without removing the memory card from the control unit. The tab "Camera" allows for a live switching of the camera from the second microcontroller (ESP32-CAM) where the test person's eye is visible. It should be noted that this function is only possible if microprocessor 2 (ESP32-CAM) has successfully connected to the access point from microprocessor 1. Microprocessor 1 has been programmed to connect to the network with the static IP address `192.168.4.2`. A detailed description of the video function will be given in the following chapter 4.6.3.

Figure 36: WLAN connection via access point

4.6.3 Live video

The video stream of the eye pupil is provided via the internal port 81 of microcontroller 2 (ESP32-CAM). The format is MJPEG, which is established via the URL `192.168.4.2`. After successful access, the web interface shown in Figure 37 can be accessed in any internet browser. When the "Start Stream" button (top left) is pressed, the microcontroller starts the live video recording, however, without saving it. On the left side of the web interface, some setting options are listed that allow for easy control of the camera.
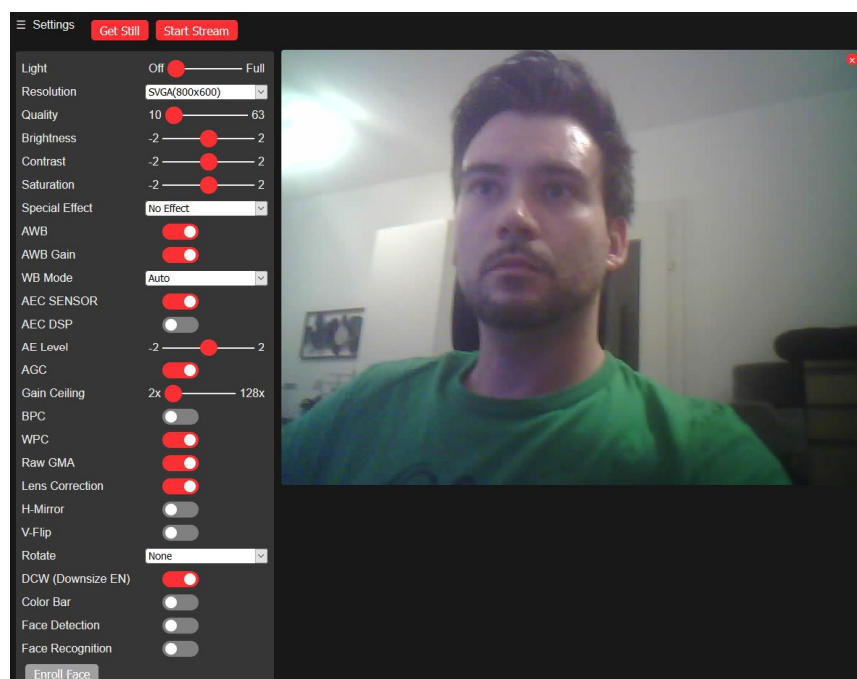

Figure 37: Web interface of ESP32-Cam

The first point "Light" activates the LED, which is located directly on the ESP32-CAM board and was not needed for this project. The setting "Resolution" lets the user change the camera resolution in the range of QQVGA (160x120) and UXGA (1600x1200). It should be noted that the lower the resolution, the smoother the video runs. A good compromise would be CIF (400x296), because face recognition even up to this resolution works, which will be reprogrammed to an eye-tracking system in further projects. The next four adjustment points ("Quality", "Brightness", "Contrast" and "Saturation") refer to the image quality, which can be adjusted by individual sliders. An important setting would be the item "Special Effects." For example, one could display the captured image as a negative or in grayscale (see Figure 38

and Figure 39). This could possibly eliminate dark image conditions and simplify the determination of the pupil position.

Figure 38:
Special effect "Negative"

Figure 39:
Special effect "Grayscale"

The other settings refer to other image settings such as white balance or orientation. The last three options "Face Detection", "Face Recognition" and "Enroll Face" are responsible for face recognition, which was not needed for this project, still, the function can be used for pupil tracking. A more detailed explanation of eye tracking is given in chapter 6.3.5. It is possible to stream the video directly via the VLC player. This player is a free and open source multimedia player that runs on different operating systems and supports different streaming protocols, such as in this thesis.

4.6.4   Live sensor data

The sensor data can be evaluated via the USB interface using MATLAB. For this purpose, a GUI interface was developed, in which all four signals are displayed individually in the window. The graphic visualization of the programmed GUI is shown in Figure 40. For navigation, a start, stop and exit button were set up to control the MATLAB GUI. The process for using the MATLAB GUI is achieved by a serial connection between the control unit and a computer, on which MATLAB is installed. The connection is then established via the GUI by pressing the start button. If the connection is successful, all signals should be displayed directly on the GUI. The stop button is used to stop the live display and the exit button is used to exit the GUI.
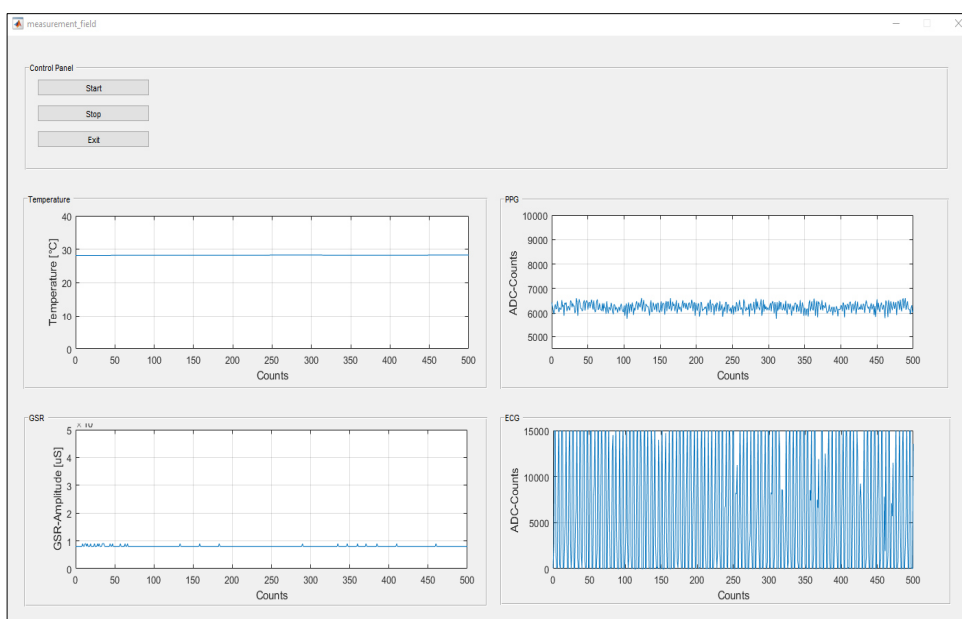

Figure 40: Serial data interface (USB) and created MATLAB GUI

Another option is to access the microcontroller's HTTP server directly from the "Live Chart" tab. The currently recorded sensor data are also displayed there. The major advantage here is that access is possible with any mobile device with an internet browser.

5 Components production

5.1 3D printing materials

5.1.1 Polylactic acid

The first 3D-printed eyeglass frame was produced using Polylactic Acid (PLA). PLA is very easy to process because of its low melting temperature. It consists of renewable raw materials such as corn starch or sugar cane, making it an environmentally friendly and biodegradable 3D printing filament.

However, this filament has a considerable disadvantage. It can easily break if the component is bent, twisted or dropped on the floor. PLA is also not suitable for components that are exposed to high temperatures as it melts from +60°C. It was for these two reasons, that the final version of the frame was printed with a different material.

Overview of the properties of PLA:

- Strength: high
- Flexibility: low
- Durability: average
- Level of difficulty: easy
- Print temperature: +180°C to +230°C
- Pressure bed temperature: +20°C to +60°C (not necessary)
- Shrinkage and distortion behavior: minimum
- Soluble: no

In this project, the filament ecoPLA with a diameter of 1.75 mm from the company 3DJAKE was used. The datasheet of this material is provided in the Appendix Appendix F.

5.1.2 Thermoplastic polyurethane

The final frame was constructed with thermoplastic polyurethane (= TPU). TPU is a stretchy material that resists shocks very well. Each type of TPU filament has its own shore hardness and flexibility (see Figure 41). The shore hardness is a measure for the hardness of plastics. It has two scales, Shore A and Shore D. Shore A is used for soft rubber types and Shore D is used for hard rubber types. Shore A ranges from extra soft to extra hard while Shore D consists of medium-hard to extra-hard plastics. The scales are divided into numbers: the higher the number, the greater the pressure resistance . The lower the number, the softer is the filament and the more difficult it is to print.
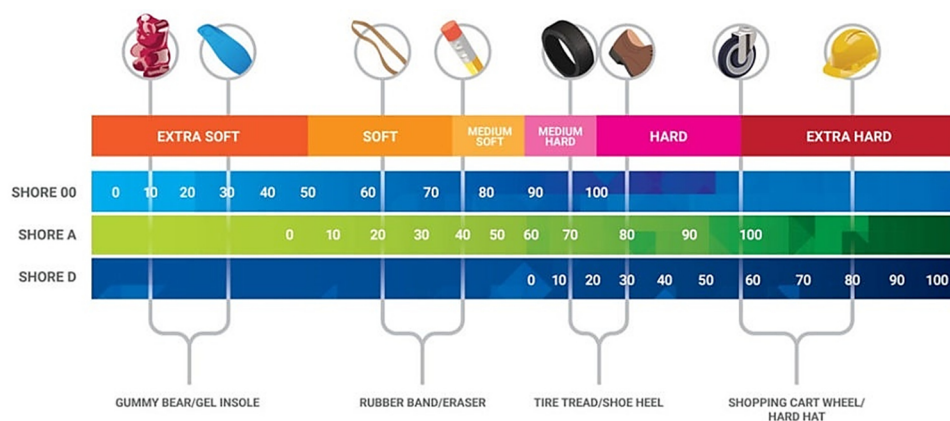

Figure 41: TPU – Shore hardness chart [39]

This property is particularly useful for eyeglass frames as they should provide a good fit on the head and be dimensionally stable at the same time. However, 3D printing with these materials is not easy because TPU is sticky and flexible during extrusion. Another important characteristic of this material is that processing more complex 3D models only works with a 3D printer that provides a full metal hot-end direct drive system. For further explanation on this topic, see chapter 5.2.

Overview of the properties of TPU:

- Strength: medium
- Flexibility: very High
- Durability: very high
- Level of difficulty: low
- Print temperature: +210°C to +230°C
- Pressure bed temperature: +30°C to +60°C (not necessary)
- Shrinking and distortion behavior: minimum
- Soluble: no

The selected material is the TPU A95 from the company 3DJAKE and the datasheet is available in the Appendix in chapter Appendix F.

5.1.3 ABSpro – Flame retardant

As for the control unit of this project where the data processing is performed, there are two LiPo batteries which can start burning in case of a short circuit. Therefore, a non-flammable filament was used for the housing of the control unit, which should protect the test person from burning for a short time. For this reason, the ABS DuraPro from the company Extrudr was used. This filament was developed especially for industrial applications and is characterized by its high process reliability. It has proven to be suitable for the production of mechanically highly stressed components. The material is fire-retardant according to UL94 HB and electrically insulating.

Overview of the properties of ABS DuraPro:

- for industrial applications,
- electrically insulating,
- high mechanical stability,
- low shrinking and warping,
- excellent layer and bed adhesion.

5.2 3D printer

To produce the 3D components, a CR-20 Pro 3D Printer from the company Creality was used. This printer was slightly modified for the project to be able to print the materials TPU and ABS. These materials are described in more detail in chapters 5.1.2 and 5.1.3. This particular printer was chosen because it has a good price-performance ratio despite the necessary major rebuilding .

Short key data of the Creality CR-20 Pro without modifications:

- automatic leveling ensures a high level of operating comfort,
- fast heating of the printing bed,
- resume function – printing can be resumed after a power failure,
- very high resolution and precision,

- magnetic building board ensures optimal adhesion of one's 3D prints to the building platform,
- high-quality power supply unit from Mean Well.

The 3D printer rebuilds included replacing the mainboard, extruder and hot end to convert the 3D printer from a Bowden system to a direct-drive system. This was necessary because otherwise it would not have been possible to print more complex TPU components.

5.2.1   Bowden vs. direct-drive system

All current 3D filament printers use either direct or Bowden extrusion. Both variants have an extruder that forces the filament through a heated nozzle. This can be done directly or through a Bowden tube, which is shown in Figure 42. These extruder versions differ greatly from each other.
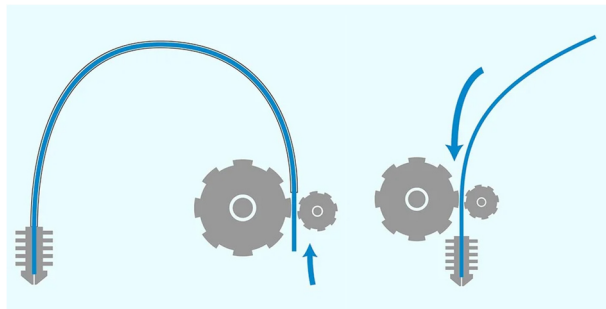
Figure 42: Bowden system (left) vs. direct-drive system (right) [40]

Direct-drive Systems:

The direct extrusion process presses the filament directly into the nozzle. There are several advantages and disadvantages, which are mapped in the following Table 2.

Table 2: Properties of direct drive

Advantages	+ Better extrusion The direct extruder is mounted directly onto the print head, allowing the motor to easily push the filament through the nozzle. This improves extrusion. + Faster retraction The direct extruder can pull the filament back quickly because it is close to the nozzle. + Less powerful motor The short distance between the extruder and nozzle allows for the reduction of torque from the motor to push the filament. + Greater choice of filaments A direct extruder is compatible with a wide range of filaments. Flexible and abrasive materials can also be extruded successfully.
Disadvantages	− Strained movements The mounting of the extruder on the print head results in increased weight on the head. This leads to additional speed restrictions, which can result in more wobbly movements and loss of accuracy in the x- and y-axes.

<u>Bowden extrusion System:</u>

The Bowden extruder is mounted onto the frame of the printer. Its task is to move the filament through a long PTFE tube to the nozzle. This method also comes with several advantages and disadvantages (see Table 3).

Table 3: Properties of Bowden extrusion

Advantages	+ Cleaner movements The mounting of the Bowden extruder on the frame of the printer reduces the weight on the x-axis. Less weight results in faster and quieter printing. + Larger construction volume A Bowden extruder allows for a smaller print head carriage, which in turn allows for a larger build volume. + Compact size Bowden extruders are generally more compact and take up less space than a normal direct extruder.
Disadvantages	− More powerful engine Transporting the filament through a long tube creates a certain friction between the material and the tube. This friction requires more torque to control the filament. − Slower response time The friction in the Bowden tube results in a slower response time, which means that the Bowden extruder needs a longer and faster filament retraction to avoid threading. − Smaller range of materials Some flexible and abrasive filaments can easily bind or wear out in Bowden tubes.

Since flexible and abrasive materials were to be processed in this project, a direct-drive system was chosen. Another influencing factor was the high wear of the Bowden hose, which increases with longer or higher processing temperatures of the filaments.

5.2.2   Modification of the 3D printer

In order to best process the created models and because a high-priced printer would have exceeded the private budget for this project, the CR-20 Pro 3D printer had to be modified in several ways. The modification included the control board and the conversion to a direct-drive system. All following features amount to approximately € 200, considerably improve the 3D printer and make it applicable for any material.

Control board of the 3D printer

The selected control board SKR1.3 was developed by the company BigTreeTech and allows the use of modular stepper motor drivers (see Figure 43). The replacement of the mainboard was necessary to increase the resolution of the printer to 32 bits, which in turn allows very high-quality prints. Another positive aspect is the integrated stealth mode using stepper motor drivers TMC2130, which lets the stepper motors of the x-, y- and z-axes move more smoothly and therefore reduces the noise level.
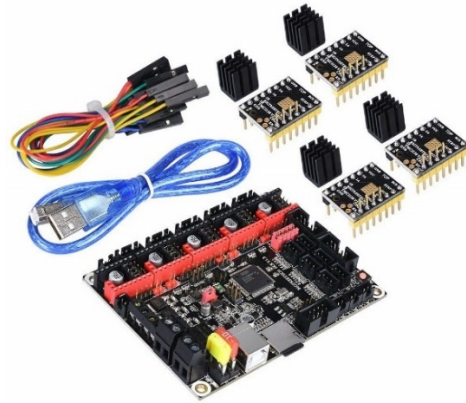
Figure 43: Control board SKR1.3 with TMC2130 [41]

Direct-drive system

The next modification was the extruder/hot-end system. The CR-20 Pro has a standard Bowden system, which can be converted into a direct-drive system. The old extruder and hot-end system were replaced by the Hemera Direct Kit from the British company E3D, as shown in Figure 44.

Figure 44: E3D Hemera Direct Kit   *Figure 45: E3D Hemera in detail*
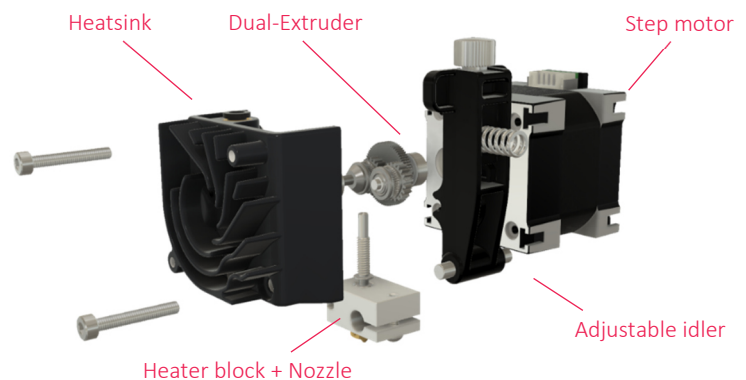
The system features a dual-drive arrangement of hardened stainless steel that provides enormous grip compared to single-drive systems. The secondary gear shaft is mounted onto a spring-loaded idler wheel, which allows to adjust the filament tension. All aforementioned features are shown in detail in

Figure 45. The system can be mounted to the 3D printer using T-slots on a previously self-printed adapter. In addition, a partial fan and a bed leveling probe (BL-Touch) were attached. For the nozzle, the E3D Nozzle X with diameter of 0.4 mm was used, which consists of special alloy of tool steel. The first alloy layer is composed of tool steel so that no deformation can occur at high temperatures. The following layer consists of nickel to achieve a higher wear resistance. The last layer is a WS2 polyphobic nanocoating, which ensures that no polymers stick to the nozzle.
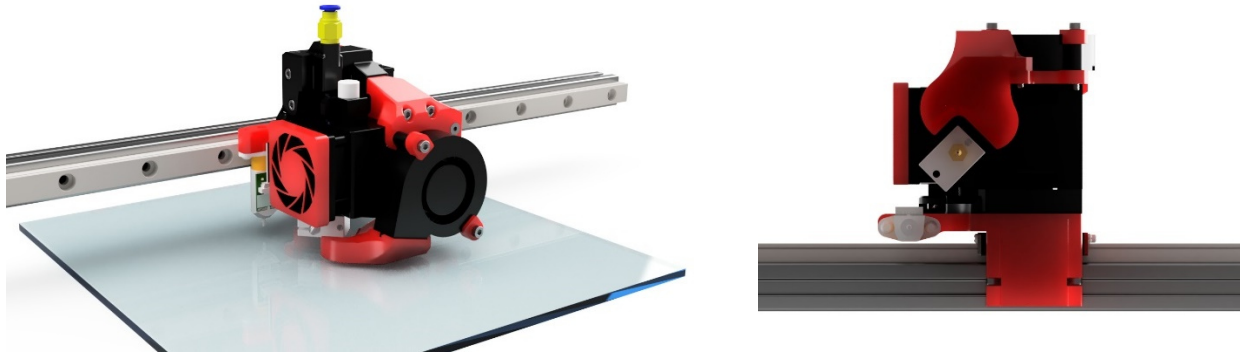
Figure 46: Fully assembled E3D Hemera with 3D-printed cooling components and cooling channel.

A separate 3D model was created for mounting and cooling the material during printing, as shown in Figure 46. A protective cover for the Noctua NF-A4x10 FLX fan was attached to the side as well as to the radial fan. Furthermore, an external cooling duct was mounted onto the radial fan. Particular attention was paid to the alignment of the cooling direction , as the nozzle must not cool down during the printing process. All components were printed with the same 3D printer before the rebuild.

Graphic smart display controller board

Finally, the LCD display, which is standard on the printer, was exchanged with a TFT display with touch function from BigTreeTech (see Figure 47). The new display has two working modes, the screen mode for the serial UART interface and the screen mode 12864, making the 3D printer easier to use.

Figure 47: BigTreeTech TFT35 V3.0 – Graphic smart display controller board

Further features

The following additional components are not included in the above mentioned costs and although they are not necessary, they are very useful. A Raspberry Pi 4 was equipped with several sensors (a gas, temperature and filament sensor) that improve printing safety and allow for remote control via mobile phone or other computer devices in the same network. The operating system used on the Raspberry Pi 4 is OctoPrint, which allows to remote-control the 3D printer via HTTP.

Structure

The entire implementation is shown in Figure 48 and Figure 49. In the upper section (section 2), the filament is stored in a dry box and enters the lower section (section 1) of the printer through an opening via a PTFE tube. From there, the filament is processed in the E3D Hemera. In the second area, there is a filament sensor where the filament is transported to the PTFE tube. A temperature sensor is also mounted on top of the second section to measure the temperature and control the airflow at the door. The fan is operated at maximum speed when the internal temperature exceeds 40°C.
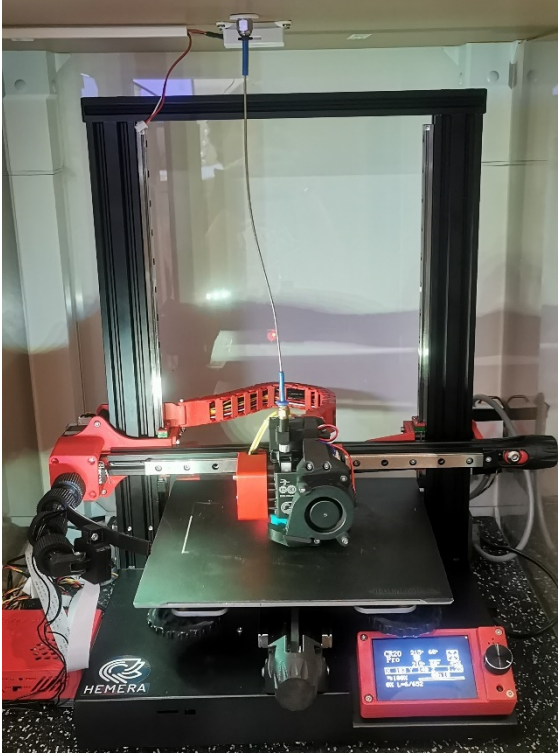
Figure 48:
Modified 3D printer

Figure 49:
3D printer housing with filament box and guide

6   Technical implementation

6.1   Flowchart of device design and construction

The steps for generating the project frame were performed as shown in Figure 50. These steps represent the basic procedures essential for the project.

AutoCAD Fusion

Create 3D eyeglass frame
Dimension of a housing

Autodesk Eagle
Design the circuit
Layout of the circuit
Making a 3D model of the circuit board

Autodesk Fusion

Assembly of housing and circuit

Complete

Complete eyeglass frame with biosensors
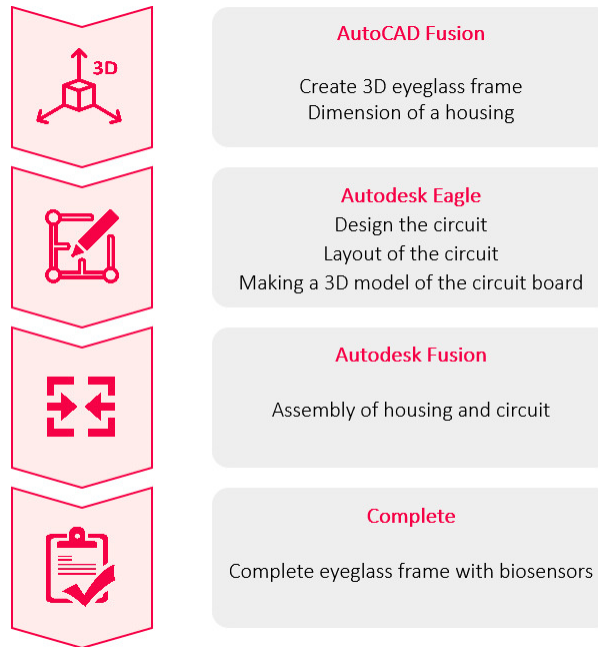
Figure 50: Flowchart of the construction

In the first step, a 3D model of the eyeglass frame was created. This model was required to fit and be adaptable to any head shape. The modelling was done in Autodesk Fusion, which can generate the necessary print file for the 3D printer. Next, the required components such as sensors and processors were combined in a circuit and positioned in one or more circuit boards. It was necessary to ensure that all safety measures were taken for the test person, such as protection from hazards, accumulators or batteries. In the last step, all components such as the eyeglass frame and circuit were combined.

6.2   Evolution steps of 3D eyeglasses (first idea to final design)

In the first design, an attempt was made to integrate all components directly into the eyeglass frame. A miniaturized CMOS camera called NanEye from the company *ams AG* should be used as camera, which was to be positioned on the inner side of the eyeglass frame. To obtain a frontal view of the eye, one lens per wing of the eyeglasses was to be attached to deflect the angle of view of the two cameras in such a way that a virtual image of both eyes would be created. This should ensure a frontal view of both eyes.
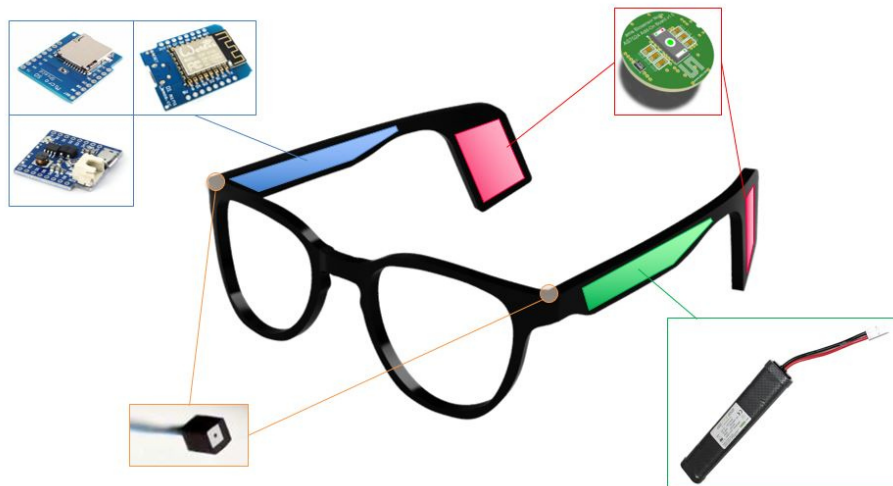
Figure 51: First version of the eyeglass frame

The microprocessor in this version, a Wemos D1 with ESP8266, was also a slightly weaker one, which had to be replaced in the following version due to performance reasons. The battery module for lithium batteries considered the battery connection because LiPo batteries were to be used. The data were to be stored on a microSD card module.

When creating the first version of the eyeglasses, it quickly became obvious that a different strategy had to be adopted since some ideas were very difficult to realize in the first test phase, for example the production of the lenses. Another aspect was the miniaturization of the components so that they would all fit on the frames. For this reason, the decision was made to focus on the feasibility of the individual functions in order to be able to test a possible operational capability.

These considerations resulted in a second version of the glasses consisting of two parts, the control unit and the frame, which are described in detail in chapters 3.2.1 and 3.2.2. The focus of the second version was on recording several biosignals and creating the conditions for a feasibility study. It should be noted, however, that the feasibility study is not part of this thesis. Another important aspect of the second version was the wearing comfort of the frame and other components. For producing the components (3D printing), the different materials described in chapter 5.1. were used.

6.3 Evaluation of signal

The measurement setup on the circuit board made it possible to check in advance whether the desired measurement results could be recorded and whether the signal quality was sufficient for further evaluation. The data transmission of the AS7024 Add-On Board (PPG, ECG, temperature) and the external signal sources (GSR) were tested on the ESP32 and mapped in corresponding signal curves, which are shown and analyzed in the following subchapters. These results should confirm the previously assumed measurement points from chapter 3.1 and show that measurement at the selected body regions is possible. The focus here is not on the evaluation of large data sets, but rather on whether the necessary signal quality can be achieved for further evaluation.

6.3.1 Photoplethysmogram measurement

Figure 52 shows the PPG signal recorded with the evaluation board and the add-on board. MP1, which is described in chapter 3.1, was chosen as a measuring point. The sensor used here is the AS7024, which is located on the add-on board. The x-axis shows the time and the y-axis shows the pulse amplitude. From this curve, the systole and diastole could be recorded in a weakened form behind the ear. For better visualization, the systole and diastole were marked accordingly in Figure 52 – green indicates the systole and orange indicates the diastole. The PPG history corresponds to the raw data and has no filtering. The data are in the range of ADC value between 6000 and 6500.
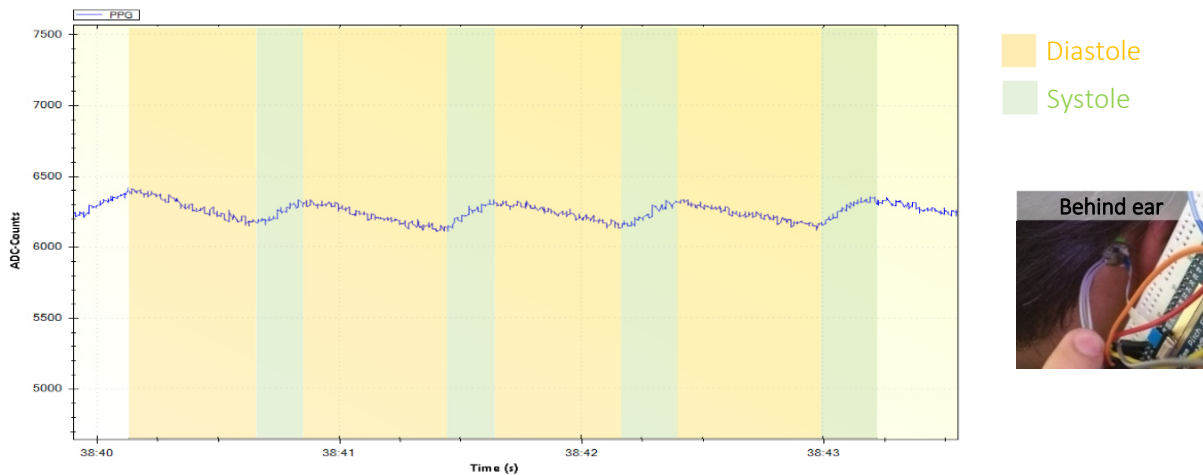
Figure 52: PPG signal behind the ear

Figure 53 shows the same measurement procedure as described in Figure 52, but here, the measurement was taken directly on a finger. The x-axis shows the time and the y-axis shows the pulse amplitude. Like in Figure 52, this PPG curve does not show any filtering. The curve is limited in the range of an ADC value between 5700 and 6400.
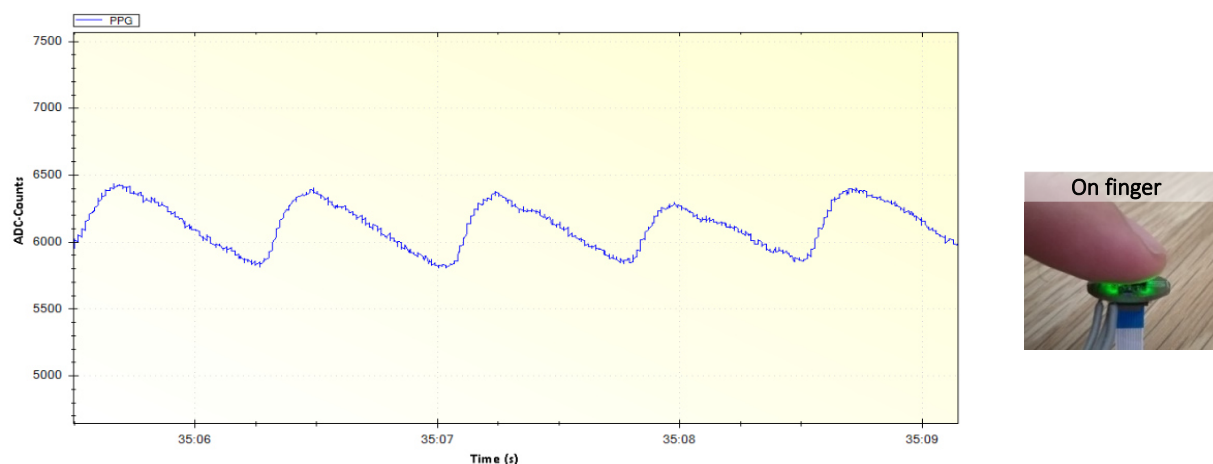
Figure 53: PPG signal on finger

Figure 54 represents the recording of PPG signal by the developed portable device. The blue curve represents the raw signal and the red curve the corresponding filtering (software low pass filtering of 8th order). A low pass IIR filter with a 3dB frequency of 0,05Hz was used as filter. The ADC counts of the PPG signal are between 5700 and 6600.
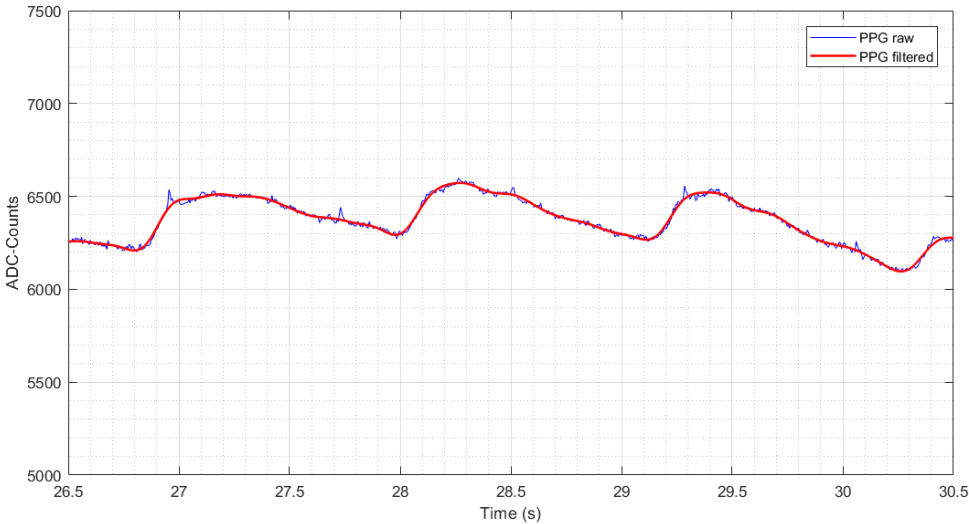

Figure 54: PPG signal behind the ear with mobile Device

6.3.2 Electrocardiogram measurement

The following figure shows the ECG course from measuring points MP1, MP2 and MP3, which are covered in chapter 4.1. The AS7024 chip with external electrodes (see chapter 4.2.2.4) was used as sensor. A strong noise can be detected in the signal path, which is affected by inductive and capacitive influences in the environment. Despite these influences, the QRS complex can still be clearly seen and is marked in red in Figure 55. The ECG course corresponds to the raw data and contains no filtering. The maximum ECG deflection is in the range of an ADC value of 5000 and 8000.
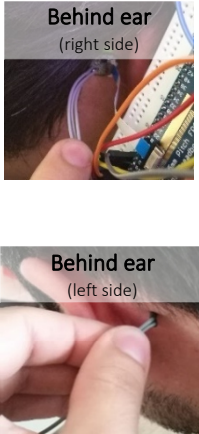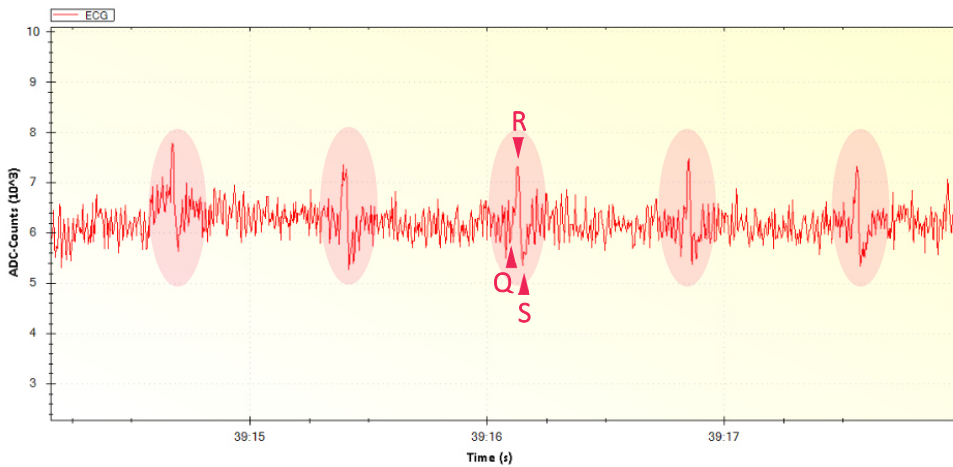

Figure 55: ECG signal behind the ear

In order to be able to compare the signal quality from Figure 55, the measurement was taken on the fingers of the same test person, as shown in Figure 56. The maximum ECG deflection is in the range of an ADC value between 4500 and 8000.
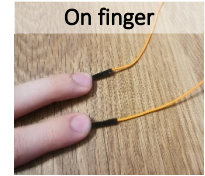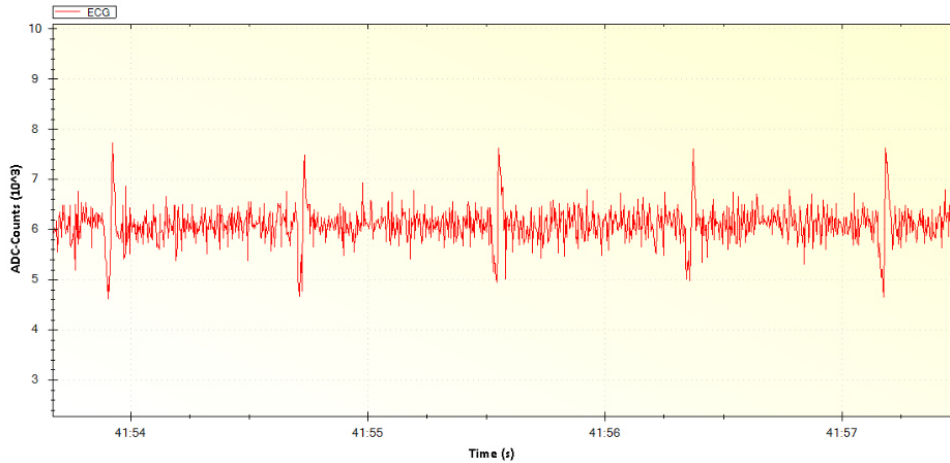

Figure 56: ECG signal on finger

Figure 57 shows the first test measurement of the ECG signal with the mobile device. The blue curve represents the raw data of the ECG signal, which ranges from 0 to 14000 ADC counts. The red curve represents the filtered ECG signal, which was realized with Matlab. A 4th order low pass IIR filter with a 3dB frequency of 0,3 Hz was used as filter. The samples are plotted on the x-axis and the ADC values of the ECG signal on the y-axis. The filtered R-wave is about 12000 ADC counts.
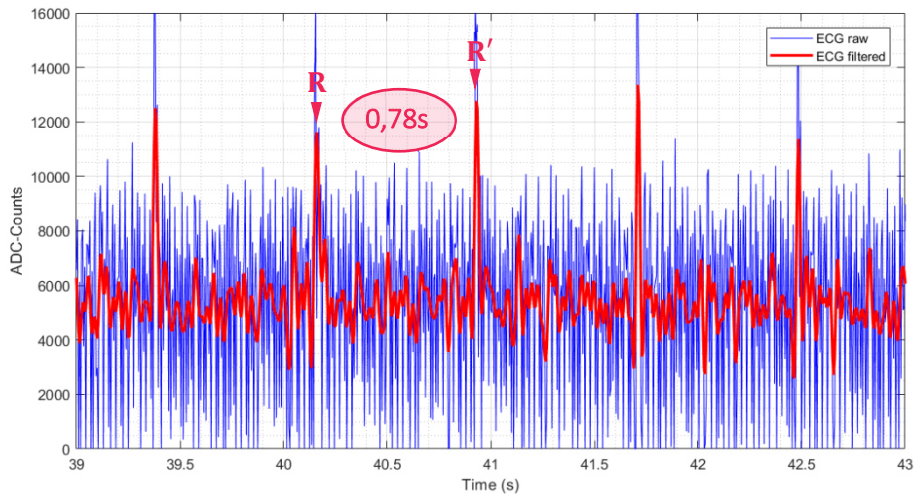

Figure 57: ECG signal behind the ear with mobile Device

From the data in Figure 57, the heart rate could be determined by detecting an RR-interval (see marker R and R'). In this case the RR distance is 0.78 s (see formula 5).

$$RR - Intervale = R' - R = 41,71 - 40.93 = 0,78s \qquad (5)$$

This RR distance marks the duration of an electrical heart action, whereby the heart rate (HF) can be derived mathematically:

$$HF\left[\frac{1}{min}\right] = \frac{60}{RR - Intervale[s]} \qquad (6)$$

The sampling rate of two RR-intervals in this case is 0,78 s, which results in a heart rate of 76.92 bpm (see following calculation in formula 7).

$$HF = \frac{60}{0.78s} = 76,92 \text{ min}^{-1} = 76,92 \; bpm \tag{7}$$

The RR-intervals are usually not of equal length, but subject to fluctuation. The quantification of these fluctuations then results in the **h**eart **r**ate **v**ariability (HRV). However, a more precise determination of HRV from the individual data sets is not performed in this thesis.

6.3.3 Galvanic skin response measurement

The GSR measurement was performed by applying 3.3 V to the corresponding measuring point and measuring the voltage drop with a second electrode. From this voltage drop, the corresponding skin conductance was then calculated, as described in chapter 2.1.4 and plotted in the following diagrams. Figure 58 shows the measured signal curve behind the ears and Figure 59 shows the signal curve on the fingers. The skin conductance was plotted on the x-axis in the unit siemens and on the y-axis in seconds. Both signal curves (Figure 58 and Figure 59) are in a range between 0 and 50 µS.
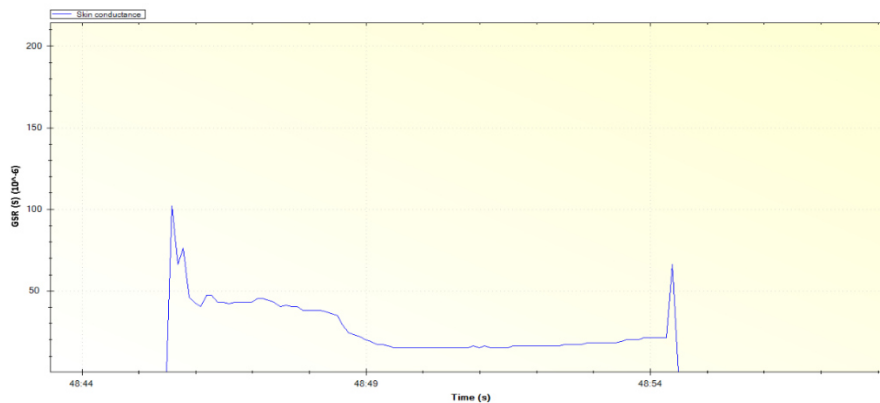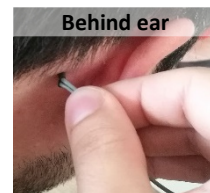

Figure 58: GSR signal behind the ear

The expression of the GSR signal of Figure 59 shows that the signal strength at the fingers is significantly higher than the signals at the head of Figure 58. The peaks at the beginning and at the end of both GSR waveforms were caused by attaching/detaching the electrodes.
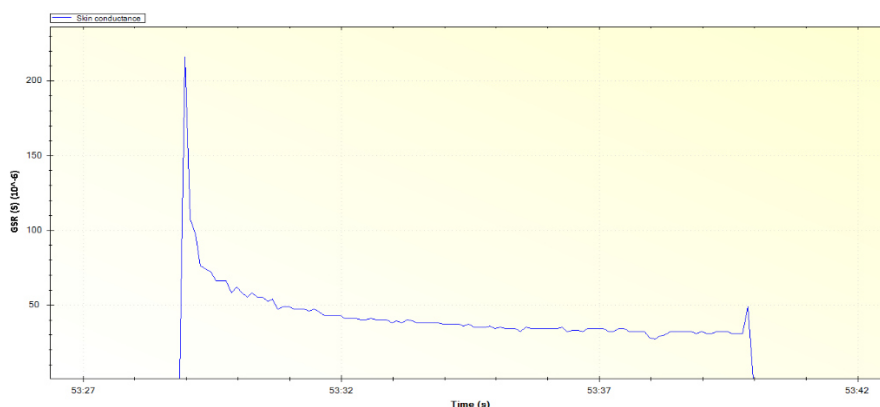

Figure 59: GSR signal on finger

Figure 60 shows the course of the GSR signal recorded with the mobile device. The blue signal curve represents the raw signal and the red curve shows the software-based filtering. As filter a low pass IIR

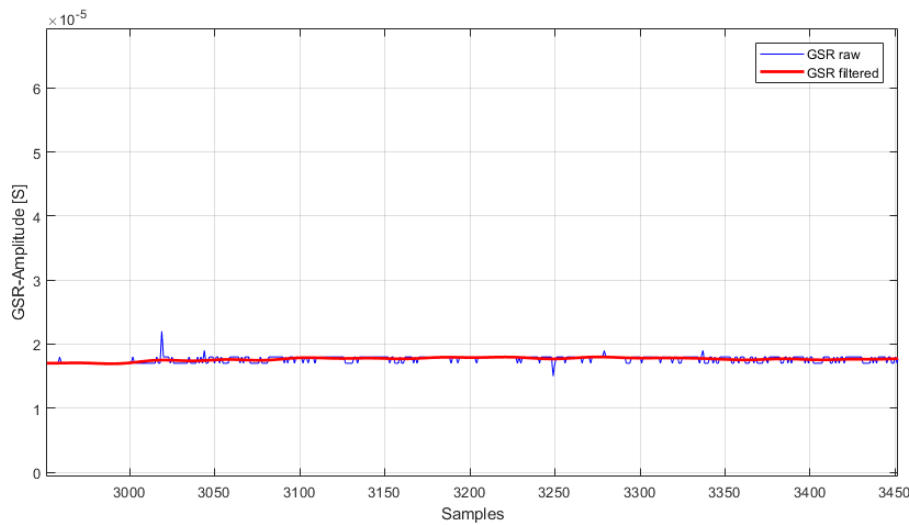filter with a 3dB frequency of 0,05 Hz was used. The figure shows that the recorded GSR value is about 18 µS.

Figure 60: GSR signal behind the ear with mobile Device

6.3.4 Body temperature

The AS6200 sensor, which is located on the add-on board (see chapter 4.2.2.1), was used for the temperature measurement. The first test measurement with this sensor is shown in Figure 61, where the temperature measurement was performed on the body by placing the finger on the sensor. The diagram shows the temperature change in relation to time. A small delay (approx. 1 min) is noted here, which the sensor needs to determine the actual temperature. This time was marked with a start and a stop marker to better illustrate the signal curve. The start marker shows the time from the first touch of the sensor and the stop marker shows the finger's distance from the sensor.
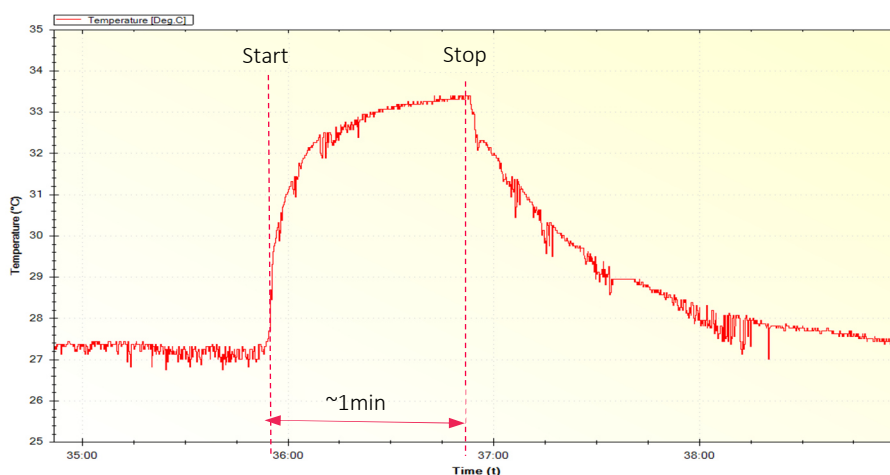

Figure 61: Temperature signal in the first test setup on the finger

In the second test, measuring point MP1 was used instead of the finger as explained in detail in chapter 3.1. Figure 62 shows no significant change compared to the previous measurement, which can be seen

in the signal curve. The start marker indicates the first contact of the skin with the sensor and the stop marker indicates the removal of the sensor from the skin.
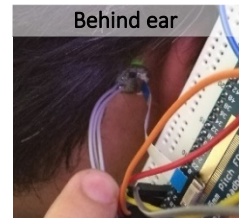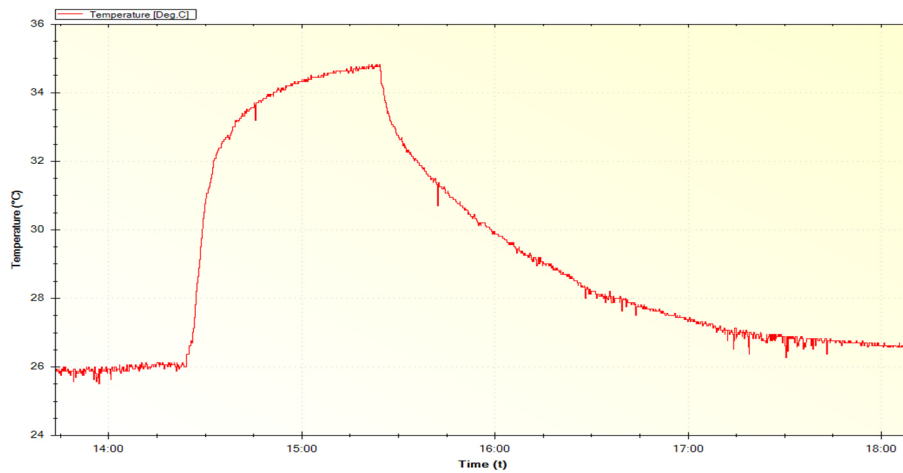

Figure 62: Body temperature signal in the first test setup behind the ear

The temperature curve in Figure 63 is the result of the first test measurement on a subject with the self-developed measuring device. The blue curve represents the raw data and the red curve represents the filtered signal. A low-pass IIR filter with a 3 dB frequency of 0.05 Hz was used to filter the raw data. The signal curve corresponds to a temperature of about 33°C.
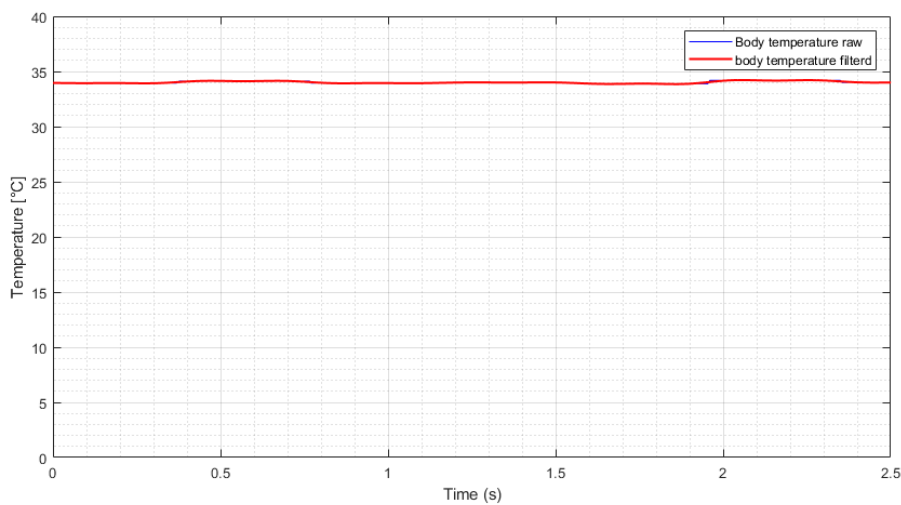

Figure 63: Body temperature behind the ear with mobile Device

6.3.5   Video (eye tracking)

The video function of microcontroller 2 (ESP32-CAM) provides a live video from the test person's pupil. A test image is shown in Figure 64. CIF (Common Intermediate Format), which has a resolution of 400x296, was chosen to keep the data transfer rate of the individual image sequences (in JPEG format) as low as possible. This can optionally be changed at any time using the code. The highest possible resolution would be UXGA with a resolution of 1600x1200.

Figure 64: Pupil recording of a test person with the ESP32-CAM (Resolution is 800x600).

Figure 65: ESP32-CAM – Face detection

This video function serves as the basis for the integration of an eye-pupil tracker, which is to be realized directly at microcontroller 2 (ESP32-CAM) but was not realized in this project. The implementation is most certainly feasible since there are already many examples of this microprocessor being used with software-based face recognition. An example of this implementation is shown in Figure 65, where a sample image of the corresponding person was loaded into the microprocessor and marked with "ID 0". When the person in the sample image appears in front of the camera, the microprocessor detects them and marks them (in this case with a yellow frame) with the words "Hello Subject <ID-Number>" (in this case with ID number 0). The complete detection takes place in real time.

The implementation of the eye-pupil tracker should be similar, but instead of detecting the complete face, the focus should be on the pupil of the eye. The size and position of the pupil should be determined and assigned to the corresponding coordinates. For this purpose, the complete image is provided with an x-y coordinate system at the beginning of the detection. A possible implementation could look like Figure 66. The reason for making this effort by choosing the coordinate system is to avoid large amounts of data and to avoid blocking the data line.
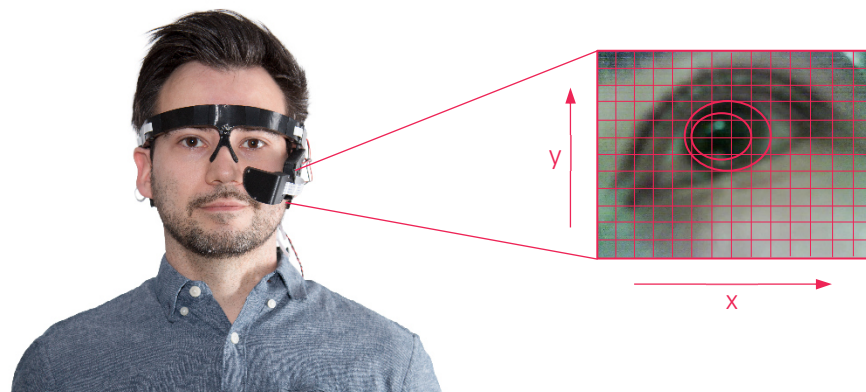

Figure 66: Example for the implementation of the eye-pupil tracker

6.4   Application examples of the multi-sensor glasses at rest vs. after physical stress

In this chapter, the recorded biosignals are compared in different situations by the developed recording device. The signals were measured once at rest and once under physical stress during a sporting activity (10 minutes on a rowing machine).
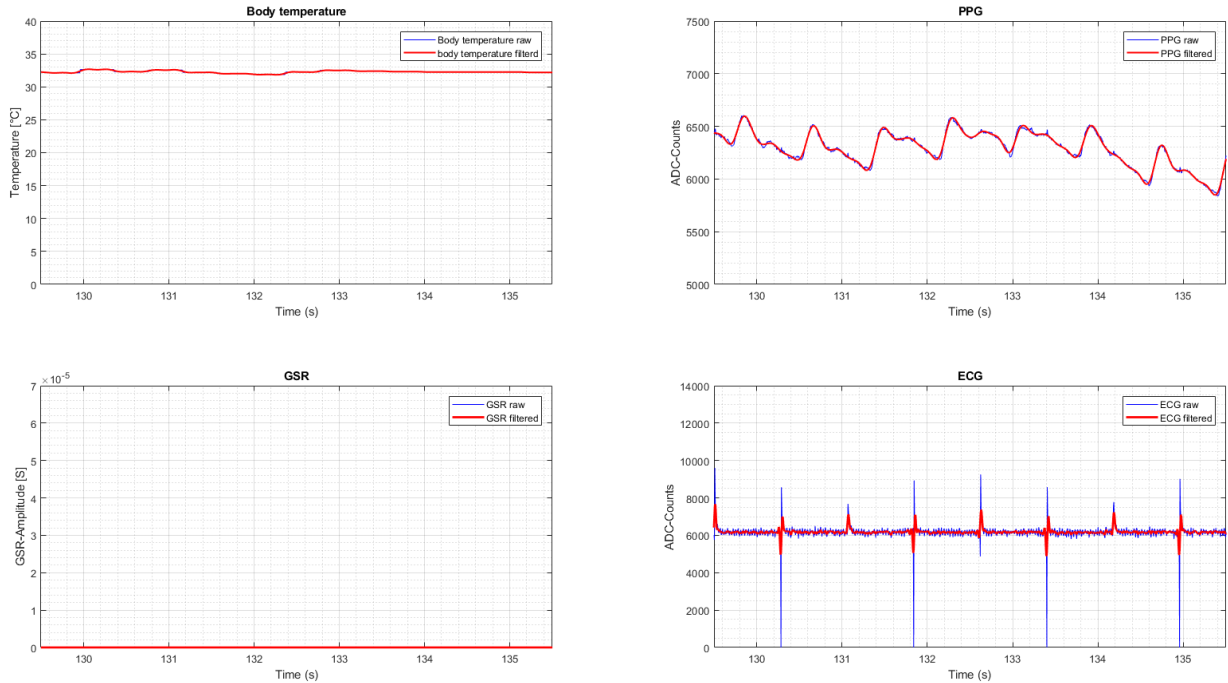

Figure 67: Biosignals at rest

Figure 67 shows the biosignals at rest. The body temperature is 33°C and the skin impedance is not significantly recognizable from the measurement signals. The pulse wave can be clearly identified, which in this case takes about 1s. The PPG signal lies between 6000 and 6600. The individual QRS complexes can be seen in the ECG curve. From a random sample of the ECG data sets, a heart rate of 75bpm was found, which would be typical for a resting pulse.
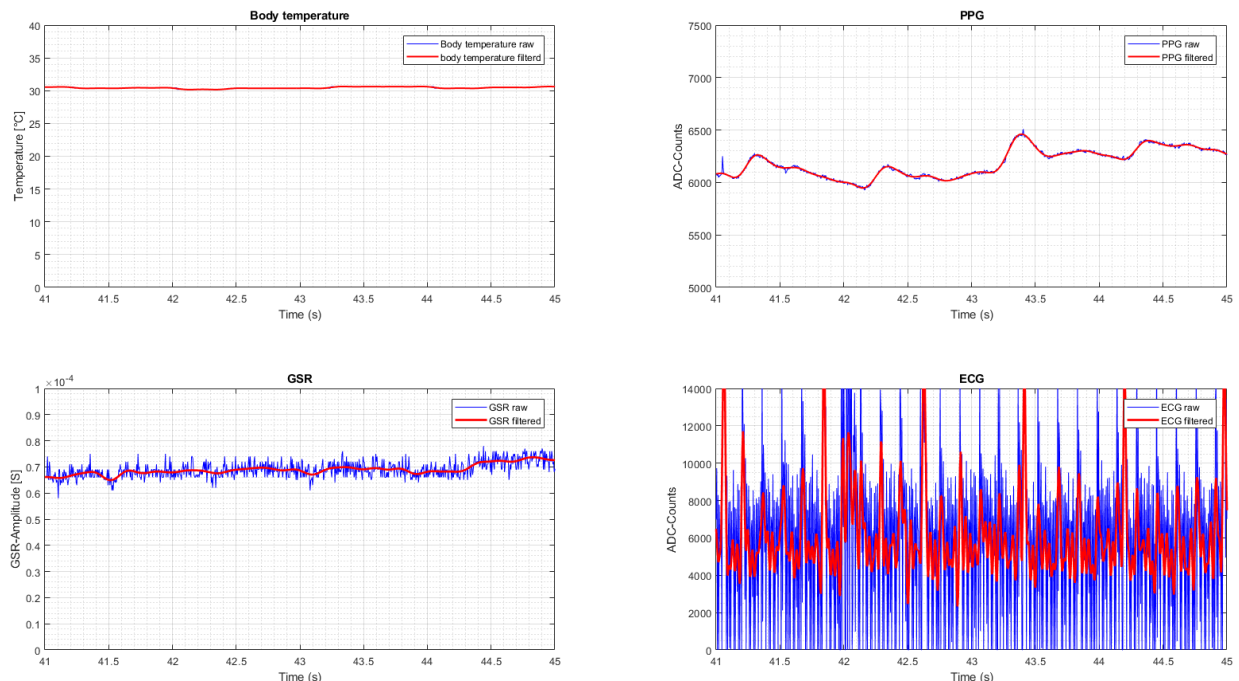

Figure 68: Biosignals at stress situation

Figure 68 shows the recording of biosignals under physical stress, which is interpreted by the test person as eustress. The recorded body temperature is approximately 31°C and skin impedance stabilises at about 65 μS. The PPG signal lies between 6000 and 6600. The ECG shows clear QRS complexes and the random sample of the ECG data set shows a heart rate of 127.65bpm which corresponds to an increased pulse rate due to physical activity.

6.5   Application examples of the multi-sensor glasses at rest vs. after physical stress Discussion and lessons learned

The evaluated signal curves in chapter 6.3 show all data clearly and can be evaluated without any problems. However, some signals are still affected by interference signals or the signal quality at their measuring points is a little lower, which is due to their measuring position.

The **PPG signal** (chapter 6.3.1) is weak, but still clearly visible, so that this position can be used when creating the eyeglass frame. The only issue to be noted is that the quality varies significantly since the contact pressure of the chip on the skin surface has a large influence on the PPG signal. For comparison, a second test measurement was taken on the finger. While a similar course as shown in Figure 52 can be seen, there is clearly a stronger signal due to better positioning of the sensor and measuring position. The measuring point on the head is measurable, but in a significantly weaker form. The measurement with the developed eyeglass frame on the head (see Figure 54) also shows a clear pulse progression, which is clearly visible even without filtering. There are also interfering signals in the raw data (blue curve), which can be eliminated with a software low-pass filter. This proved in any case that a measurement at the planned measuring point MP1 is possible.

The **ECG signal** (see chapter 6.3.2) is very noisy because the signal is relatively strongly affected by inductive and capacitive interference signals, most of which come from the environment. The comparison signal of Figure 56 was recorded on the finger and shows similar noisy measurement results as in Figure 55. The measurement with the self-developed mobile device (see Figure 57) shows similar results, but the signals are more pronounced, so that the R-wave can be seen in the raw data. However, a software-based low-pass filtering system was able to filter out most of the interference signals. A hardware-based low-pass filtering would probably be more recommendable to ensure a better signal quality from the start. Despite all this, the QRS complex can be seen in all signals, with the ECG trace on the fingers providing the best signal quality. The power supply unit of the PC or laptop has major influence on these interfering signals, because at this time, there was no galvanic isolation between the power supply and the measuring circuit, which, according to the manufacturer's information from the company *ams AG*, has a considerable influence on the ECG signal. In the final circuit, this problem was overcome by using a rechargeable battery so that galvanic isolation should no longer be necessary. Basically, it can also be said that a two-channel ECG measurement at the measuring points MP1, MP2 and MP3 is possible.

The **GSR signal** (see chapter 6.3.3) could be determined well in both the first test measurements and the prototype. The signal is clearly recognizable by the hardware low-pass filter and has little or no interference. In the beginning of the recording, the signal shows a higher amplitude, which is caused by the electrodes being placed on the head and being pressed on the skin. This is also shown by the first third of the signal curve. After that, the contact pressure of the electrodes balances out and results in an almost continuous curve. At the end of the signal, there is once again a short peak, which is also caused by the removal of the electrodes and the resulting change in contact pressure.

The **temperature signal** (see chapter 6.3.4) was recorded with the AS6200 chip and shows a relatively fast recording of about one minute of temperature. The test experiment was carried out on the finger as well as at measuring point MP1. The sensor requires this time to evaluate the signals, which must be classified

as calibration time. The signal quality at both measuring points shows that the signals can be recorded with relatively low noise by the sensor and can therefore be used for further evaluation.

The **camera image** for the eye-tracking function (see 6.3.5) provides sufficient quality for the further development of this function. The camera control is web-based, which allows the user to set several settings on one HTTP page without programming effort. This makes efficient first tests possible. The additional streaming function via web also supports integration via MATLAB. When developing the prototype, there was an unexpected complication in terms of runtime delay. In this project, all microcontrollers as well as the ESP32-CAM were placed in the control unit so that the camera was connected to the microcontroller via a long data line (approx. 500 mm). This caused an extreme transmission delay during the first test trials so that the microprocessor could no longer correctly combine the received data into an image. The solution to this problem was to position the microprocessor in the frame of the eyewear so as to shorten the data line to the camera.

The **application example** from chapter 6.4 allows the comparison of two data sets in two different situations – test person at rest and test person under physical stress. This enables an initial assessment of any significant difference in the signal characteristics. In this case, the comparison of the signal data is realized by the analysis of the diagrams because no paradigm has been defined for this test. The body temperature of the test person is in the normal temperature range during the resting phase (see Figure 67), which slightly fell during physical activity (see Figure 68) due to sweating. The GSR signal of the test person is practically not measurable in the resting phase, which also signals that the test person is in a relaxed condition. However, this value changes drastically under a physical stress situation, which is caused by sweat for the most part, enhancing the conductivity of the skin. The test measurement also showed a significant difference between rest and physical stress situations, which can also be determined from the heart rates. Physical exercise automatically increases the pulse rate because the muscles need more oxygen, which is transported by the blood. This causes the heart to beat faster and increase the pulse rate.

7   Conclusion and outlook

This master's thesis was carried out to investigate whether stress can be distinguished between eustress and distress by different biosignals. The thesis focused on the basic concept of a mobile measuring device which can record and store several biosignals at the same time to allow for a subsequent evaluation. The device was designed as an eyeglass-based sensing instrument.

The initial concept of positioning all electronic components in an eyeglass frame had to be discarded after a short time, as this concept would have made developing the prototype extremely complicated. For this reason, the approach was split into two components, a control unit and an eyeglass frame. This made it possible to use prefabricated component boards, such as the ESP32 Development Kit or the ESP32-CAM. However, this does not mean that miniaturization is not possible. For example, if a powerful microprocessor with sufficient RAM memory and low power consumption is available, it could process the currently assigned tasks (sensor signals and camera) in one, which would create more space for the other components on the frame. In addition, a custom-made battery would have to be produced, which would be best adapted to the entire surface of the eyeglass frame. Furthermore, it is possible to integrate the NanEye-CMOS camera from the company *ams AG* into the system instead of the previous OV2640 camera module, since its very small construction (1mm x 1mm) and the wide angle of the camera allow it to be very well integrated into the upper frame of the eyeglass, so that the test person's vision is no longer hindered.

During the implementation of the developed circuit, several complications occurred and impacted the measurement results that were discussed in detail in chapter 6.3. One solution to these complications would be to shield the complete device so that the circuit is protected from external capacitive and inductive influences. This solution is expected to minimize the main problem of the ECG signal quality. Such shielding was included in the design of the circuit boards, but not in the data lines between the eyeglass frame and the control unit. Instead of a flat band cable (FPC), a multicore cable (17-core) should be used, as it includes a shield.

The problem of the eye-tracking camera with the too long data line solution was adapted in the final version, as described in chapter 6.4. This made it possible to replace a 24-pole FPC cable with a two-pole cable between the control unit and the eyeglass frame. For further optimization and miniaturization, the CMOS camera NanEye from the company *ams AG* should be considered because its small dimensions of 1mm x 1mm x 1.6mm allow for easier positioning on the eyeglass frame.

Outlook and next steps for the realization of a significant stress indicator:

- Testing of the developed eyeglass frame in corresponding field studies with defined paradigms.
- Signal-Post-Processing to further improve the signal quality.
- Common interpretation of the biosignal and development of a stress index for evaluation with different probands.

Appendix A Circuit board diagrams – First version

Appendix A.1   Control Unit

Figure 69 shows the realized circuit of the control unit in which all used components are connected. Unfortunately, this version has a few errors that could be eliminated by cable bridges. An improved version (circuit and layout) is shown in chapter Appendix B.
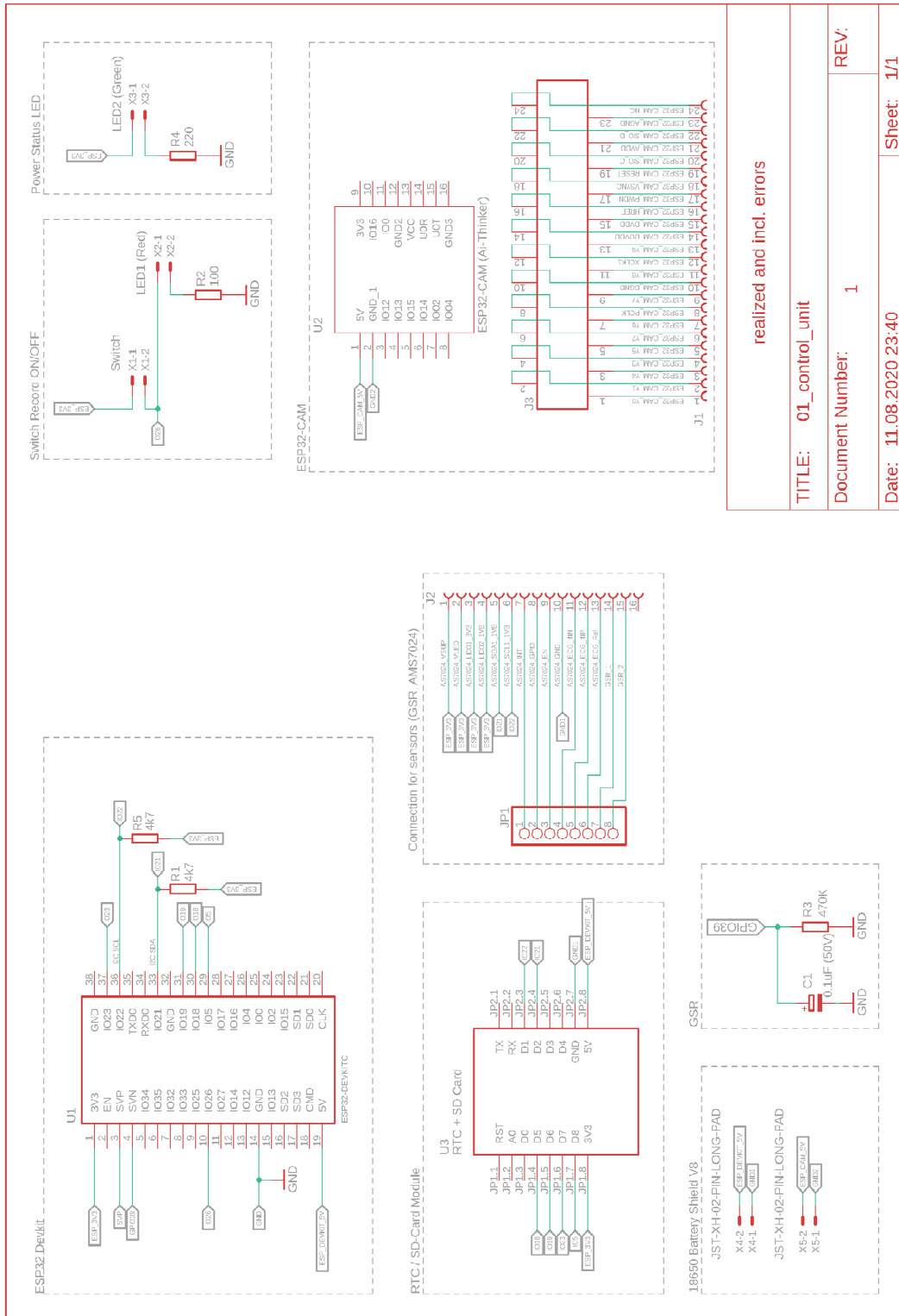

Figure 69: Circuit control unit v1 – realized version with errors.

The circuit board layout in Figure 70 shows the implemented circuit from Figure 69, which was realized for the first prototype. The red lines represent the conductors from the top view and the blue lines represent the conductors from the bottom view.
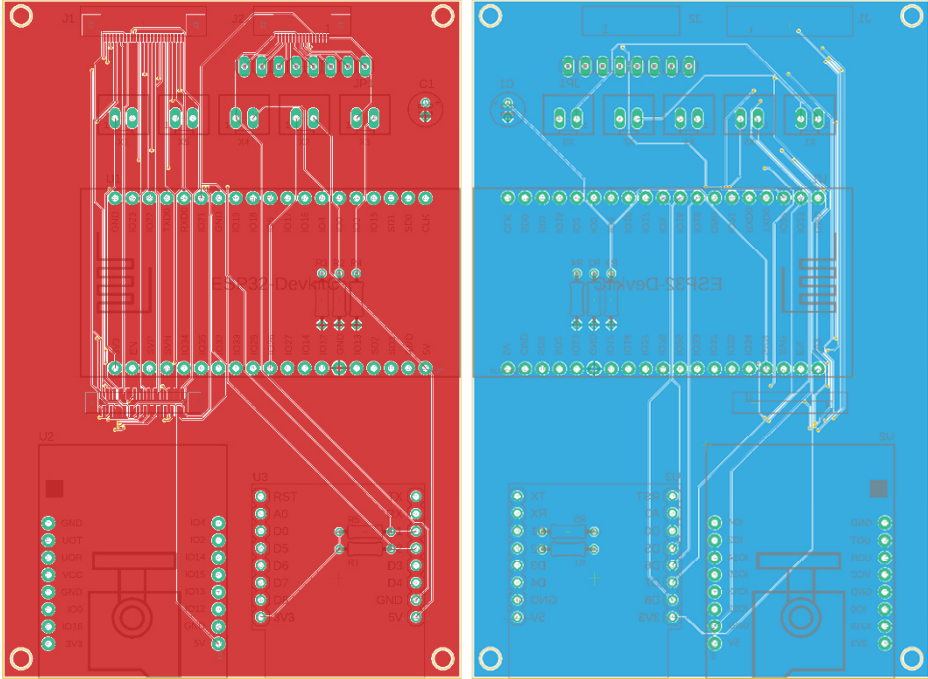
Figure 70: Control unit - layout v1
left – view from the top | right – view from the bottom

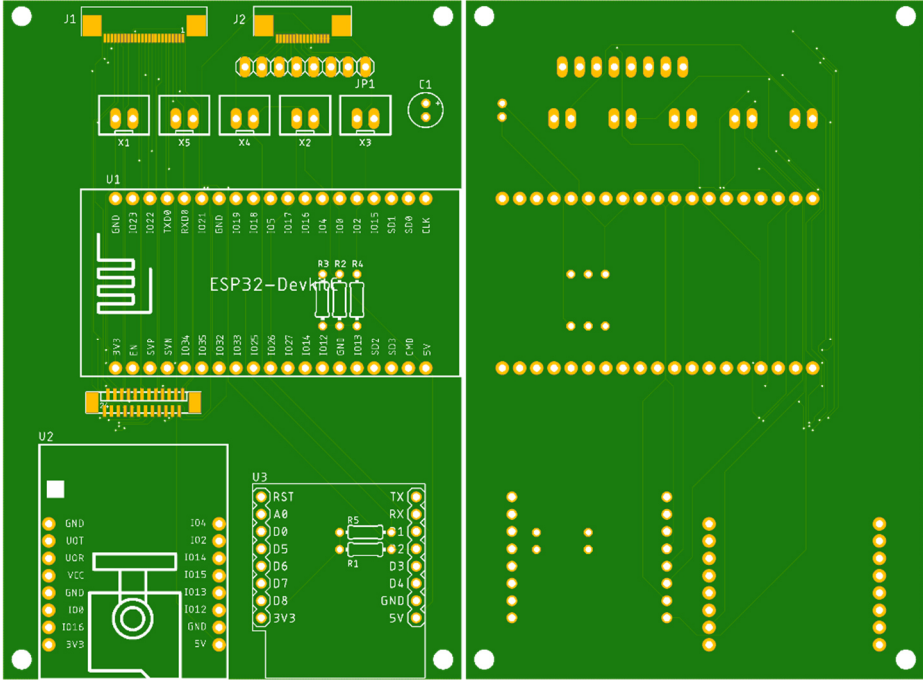The resulting circuit board is shown in Figure 71. The left figure shows the view from the top and the right figure the view from the bottom.

Figure 71: Realized printed circuit boards (v1)
left – view from the top | right – view from the bottom

Appendix A.2   Extension unit from the control unit

Figure 72 shows the extension unit from the control unit interfaces to the eyeglass frame. When routing the signals, it is important to note that when using these extensions, the signals on the FPC pins are swapped (for example, pin 1 becomes pin 24).

Figure 72: Circuit from the expansion interface of the control unit

Figure 73 shows the layout of the connector unit. The red conductors show the lines from the top view. As can be seen, it is a single-sided PCB with two FPC connectors of the same type.
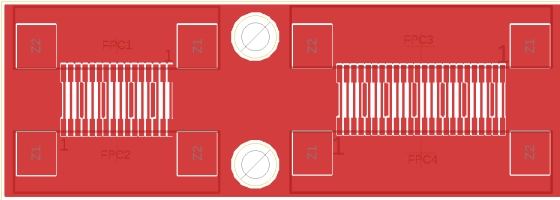

Figure 73: Layout from the expansion interface of the control unit

The realized circuit boards are shown in Figure 74. The left view represents the top PCB and the right view represents the PCB from below. This view is not true to the original scale.
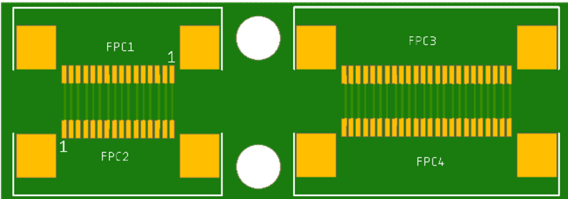

Figure 74: Realized printed circuit board from the connection unit of the control unit
left – view from the top | right – view from the bottom

Appendix A.3 Eyeglass frame – FPC connector left side

The circuit in Figure 75 shows the circuit design from the right side of the frame. As can be seen in the figure, here is the interface where the signals of ECG_INN and GSR_1 are recorded.
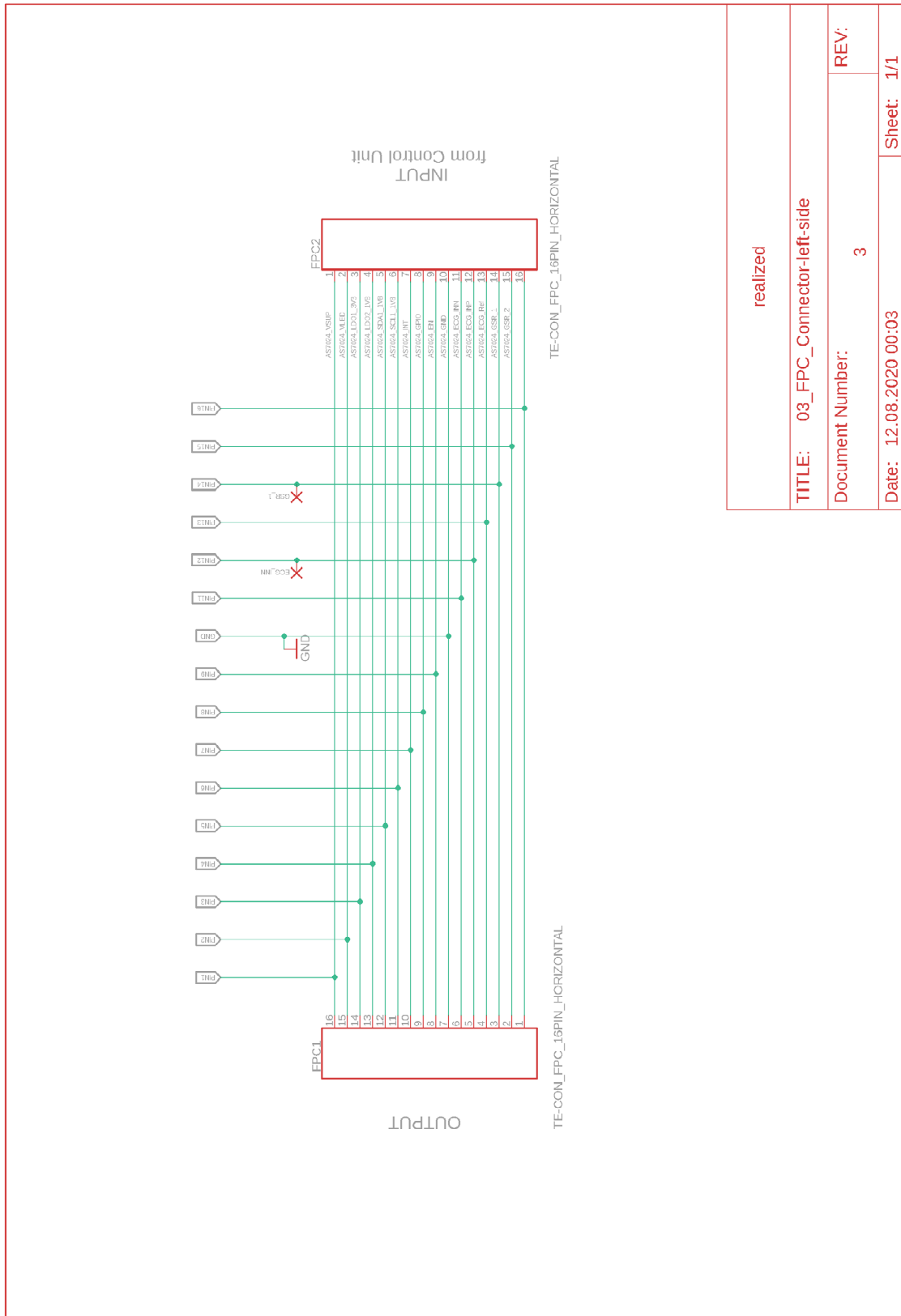

Figure 75: Circuit from the left side of the eyeglass frame

Figure 76 shows the layout from the previous circuit Figure 75. From the layout and finished PCB in Figure 77, one can see the connection pads on the top of the layout or PCB where the lead from ECG_INN and GSR_1 is soldered. The red conductors represent the lines on the top side and the blue conductors represent the lines on the bottom side.
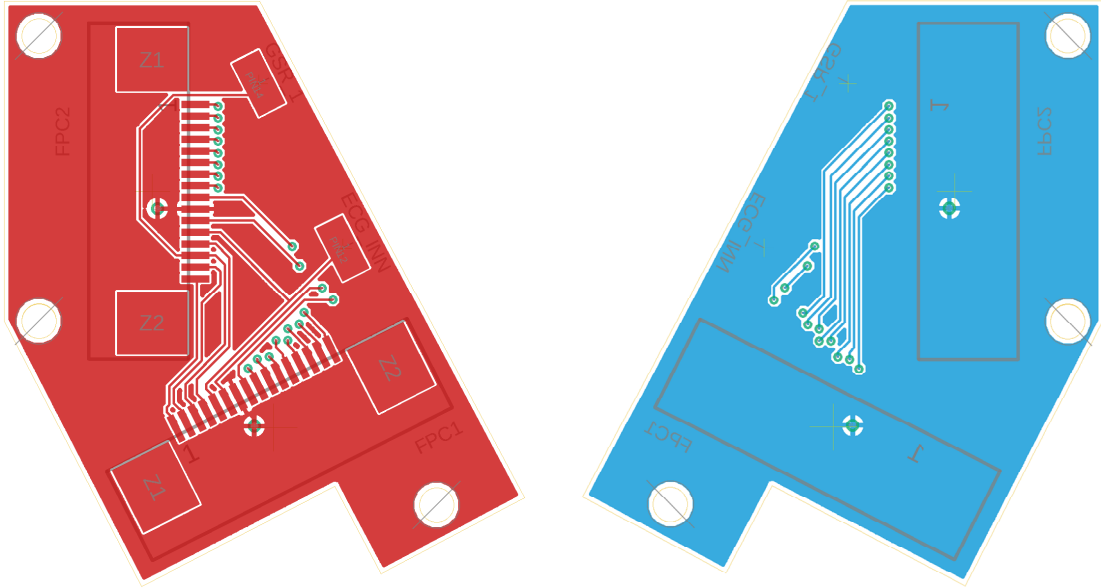

Figure 76: Layout from the left side of the eyeglass frame
left – view from the top | right – view from the bottom

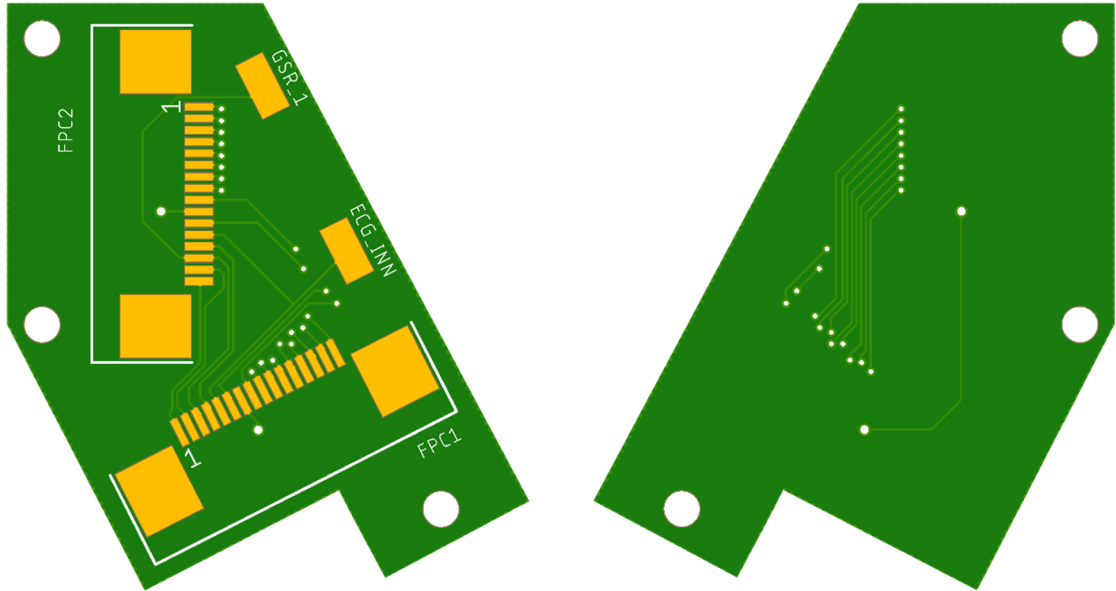The realized circuit boards shown in the figure are not true to the original scale.

Figure 77: Realized printed circuit board from the left side of the eyeglass frame
left – view from the top | right – view from the bottom

Appendix A.4   Eyeglass frame – FPC connector middle

The circuit in Figure 78 shows the circuit design from the middle of the eyeglass frame. The ECG_REF and the GSR_2 interfaces are designed as an additional pad to solder an external electrode.
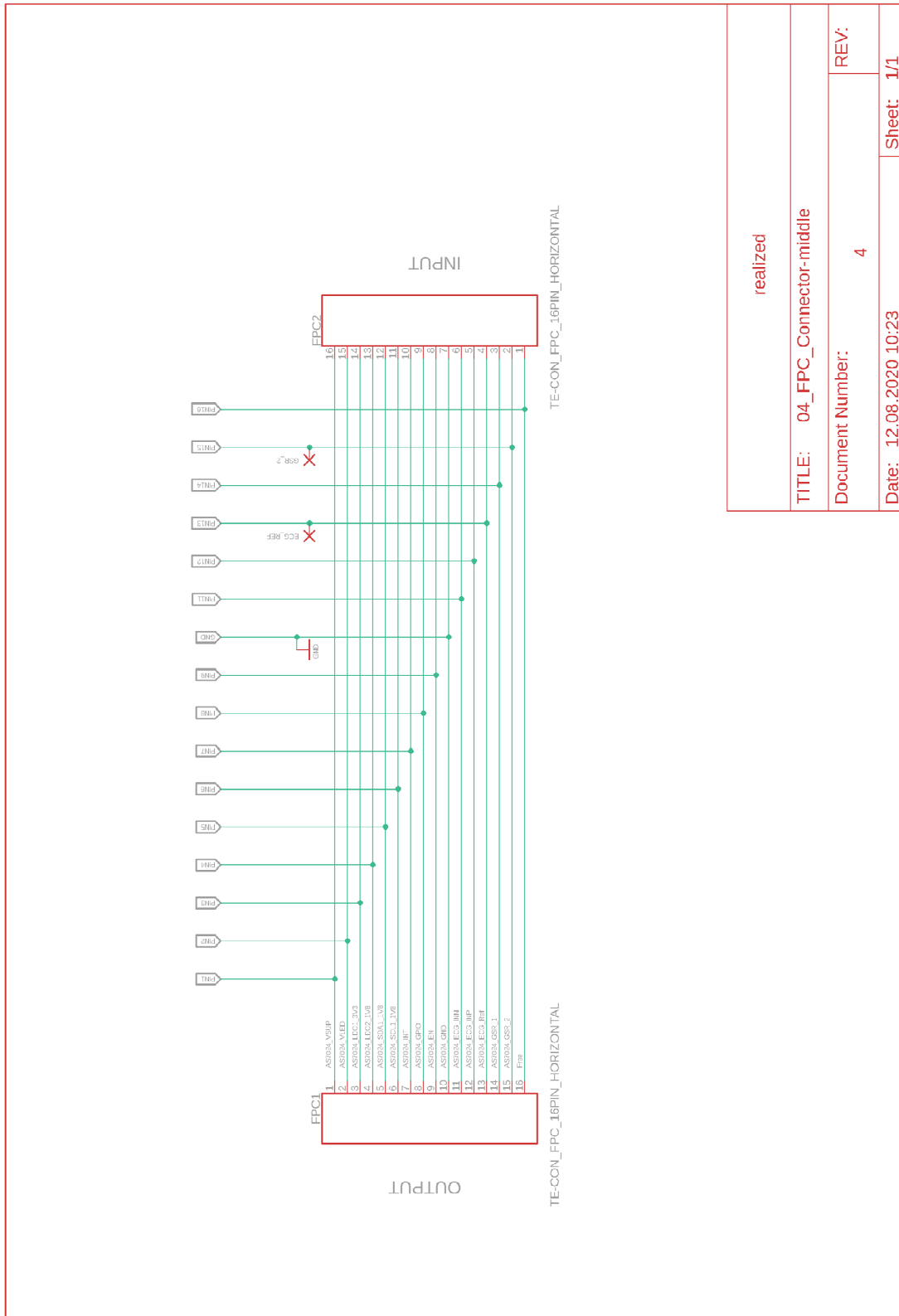
Figure 78: Circuit from the middle of the eyeglass frame – Version 1

The layout of the following circuit (Figure 79) represents the junction of interfaces ECG_Ref and GSR_2 and the connection of all signal lines. The pads of the two especially designed interfaces allow for the attachment of two external electrodes. The data line is continued via FPC cables using FPC connectors. The red lines represent the top conductors from the PCB and the blue lines from the bottom of the PCB.
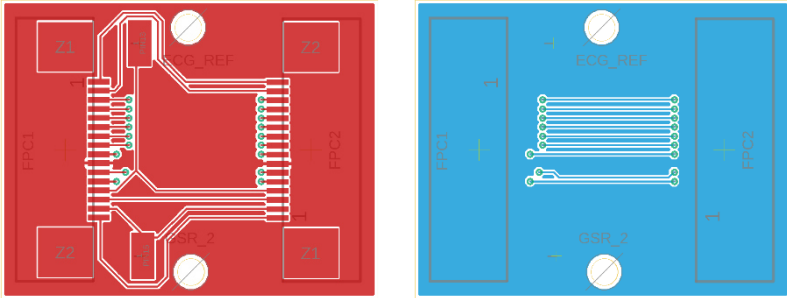

Figure 79: Layout from the middle of the eyeglass frame
left – view from the top | right – view from the bottom

Figure 80 shows the implemented circuit boards, with the top view on the left and the bottom view on the right.
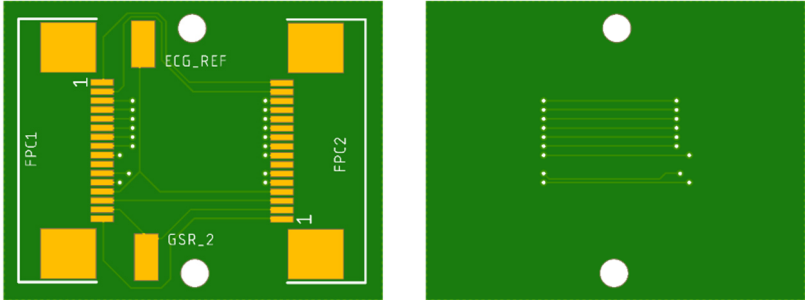

Figure 80: Realized printed circuit board from the left side of the eyeglass frame
left – view from the top | right – view from the bottom

Appendix A.5   Eyeglass frame – FPC connector right side

The circuit diagram in Figure 81 shows the right side of the frame. Interfaces ECG_INN, ECG_Ref and ECG_INP are here separately executed again and represent the ECG connection interfaces to the AS7024 board. The rest of the lines provide the power supply and communication with the control unit. These lines are connected via a 10-pin FPC cable, which is connected via FPC connectors.
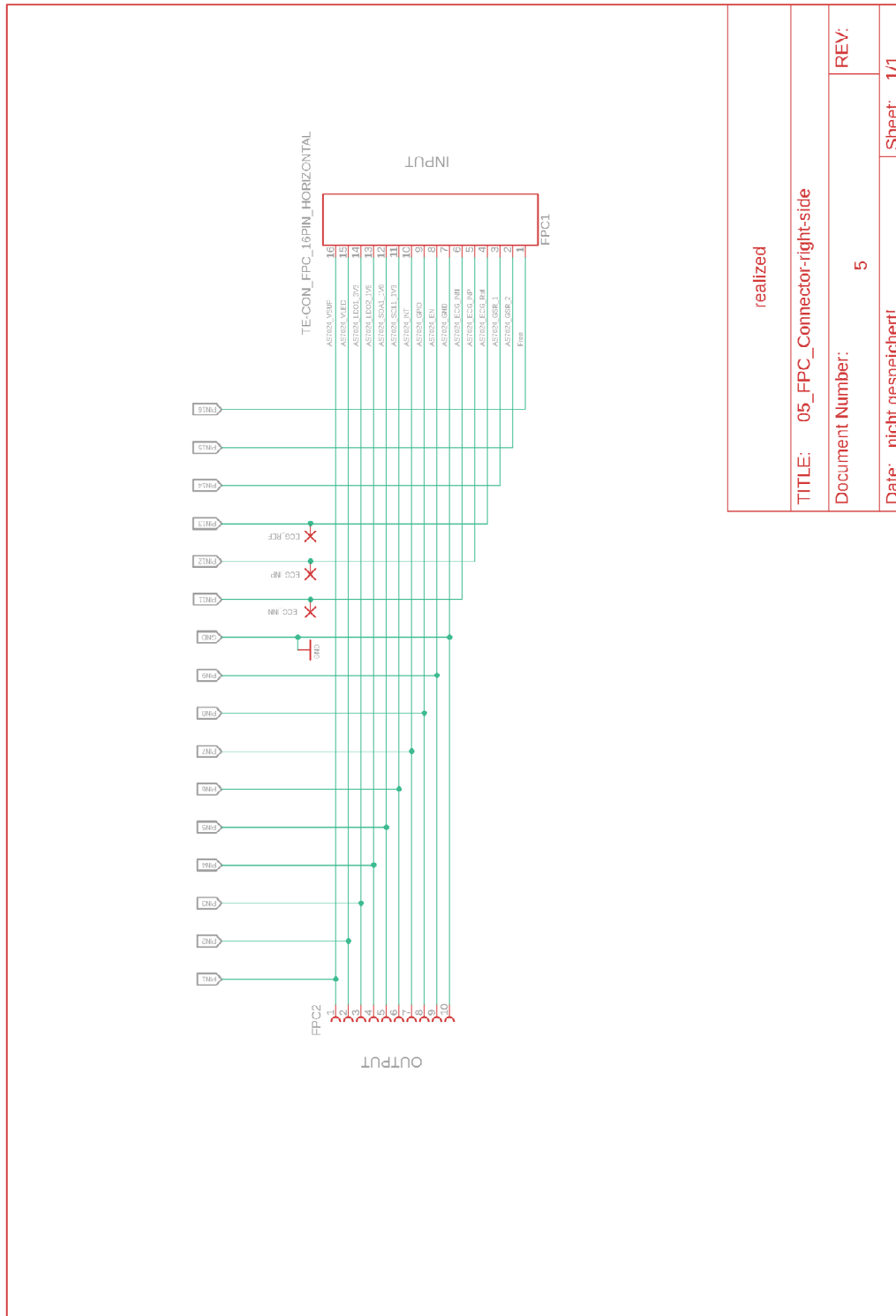

Figure 81: Circuit from the right side of the eyeglass frame

The layout in Figure 82 is a double-sided layout. The red traces represent the top view and the blue traces represent the bottom view. The external interfaces are designed as pads that are soldered to the AS7024 board.
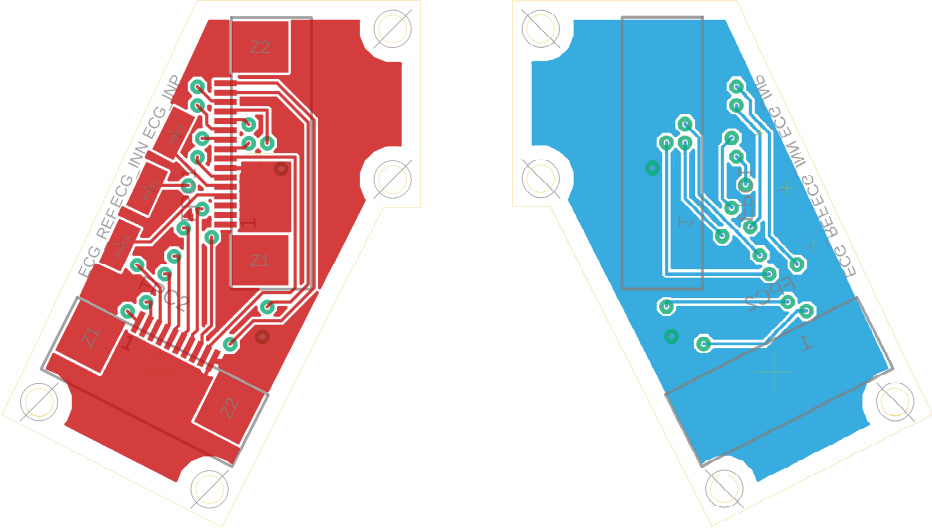

Figure 82: Layout from the right side of the eyeglass frame
left – view from the top | right – view from the bottom

The circuit boards in Figure 83 represent the manufactured circuit boards, which are not true to the original scale.
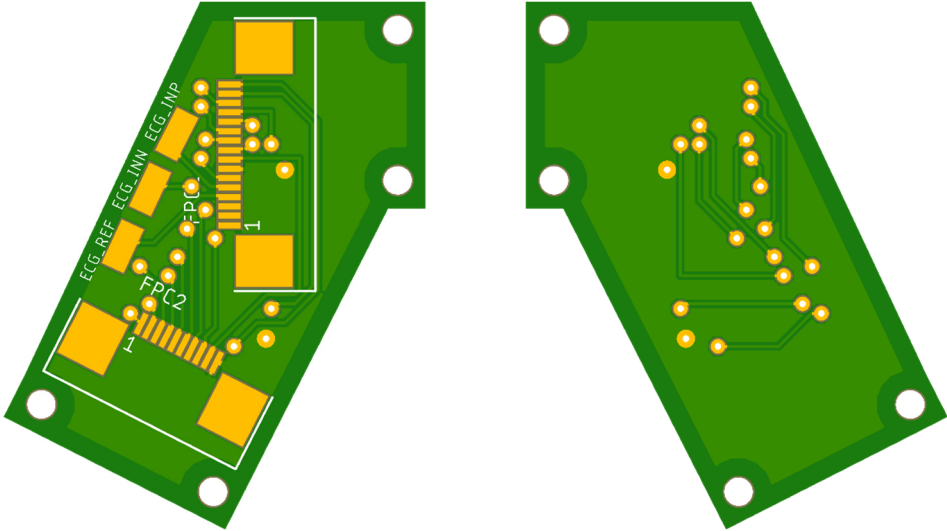
Figure 83: Realized printed circuit board from the right side of the eyeglass frame
left – view from the top | right – view from the bottom

Appendix A.6 Eyeglass frame – FPC connector cam part 1

The circuit shown in Figure 84 is the first connection element that establishes the data line between the camera and the ESP32-CAM module. However, this part became needless in the second version as the complete ESP32-CAM module is directly mounted on the eyeglass frame. For more details, see chapter 8.
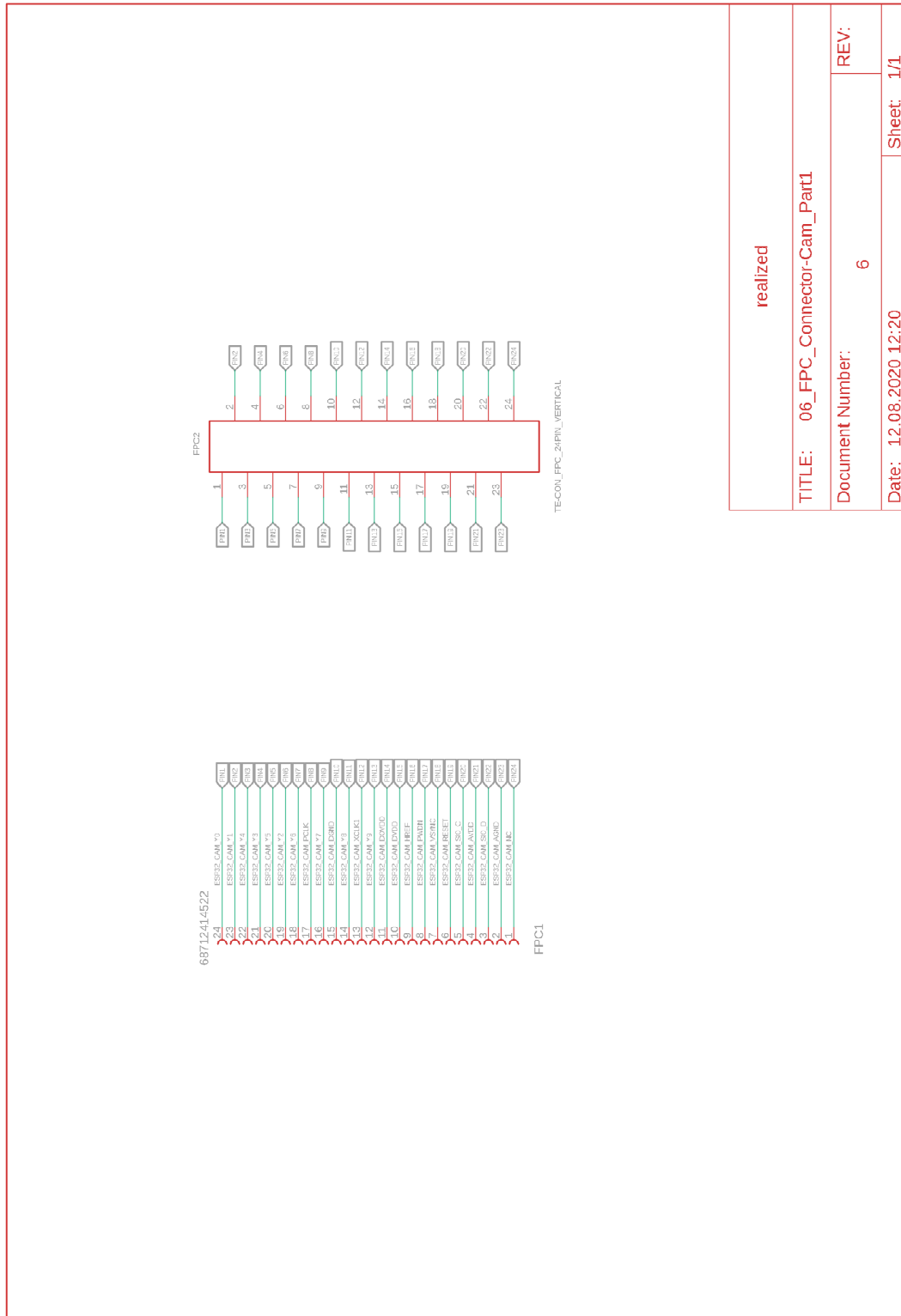
Figure 84: Circuit from the first connector of the ESP32-CAM module to the camera on the eyeglass frame

The layout represents the implementation of the previous circuit. As can be seen in Figure 85, this is a double-sided layout. The red lines represent the conductors from the top view and the blue lines from the bottom view. This layout is not true to scale.

Figure 85:
Layout from the first connector of the ESP32-CAM module to the camera on the eyeglass frame
left – view from the top | right – view from the bottom

The converted circuit board is shown in Figure 86. In this figure, one can see that the two FPC connectors have been placed on the upper side. In order to ensure the flexibility of the frame, a vertical and a horizontal FPC connector were used here.

Figure 86:
Realized printed circuit board from the first connector of the ESP32-CAM module to the camera on the eyeglass frame
*left – view from the top | right – view from the bottom*

Appendix A.7   Eyeglass frame – FPC connector cam part 2

The following circuit in Figure 87 is the second connection element between the camera and the ESP32-CAM module. On the output side, the corresponding camera is connected to the FPC connector. The input side leads to the first connection element in chapter Appendix A.6.

Figure 87: Circuit board from the second connector of the ESP32-CAM module to the camera on the eyeglass frame

The layout in Figure 88 shows the implementation of Figure 87. The conversion was carried out in the form of a double-sided layout. The red lines represent the conductors as seen from above and the blue lines represent the conductors as seen from below.
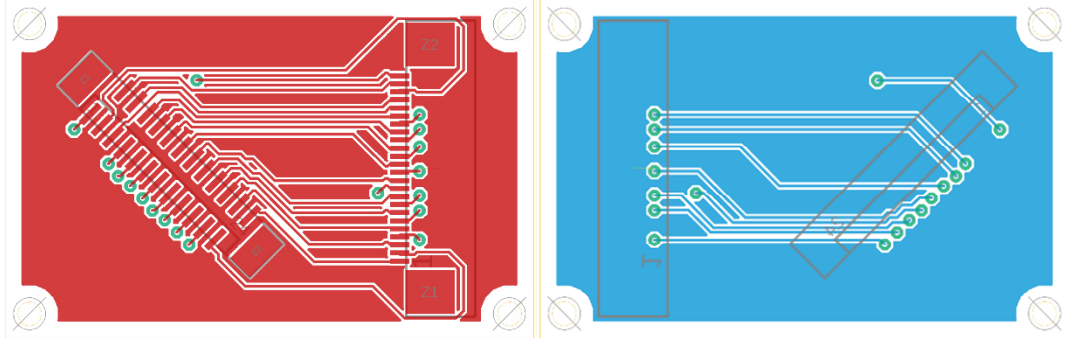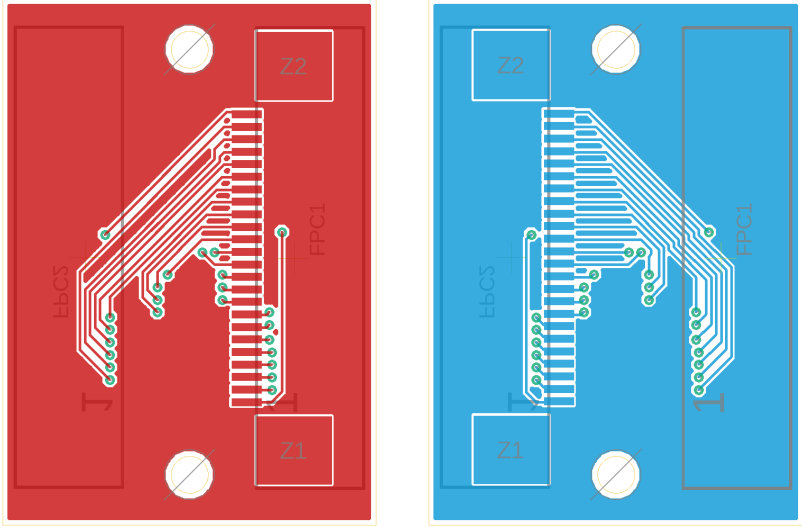

Figure 88:
Layout from the second connector of the ESP32-CAM module to the camera on the eyeglass frame
left – view from the top | right – view from the bottom

Figure 89 shows the implementation of the layout. As can be seen in the circuit board design, an FPC Connector has been placed on both sides so that the camera can be connected in the frame. The figure is not true to scale.
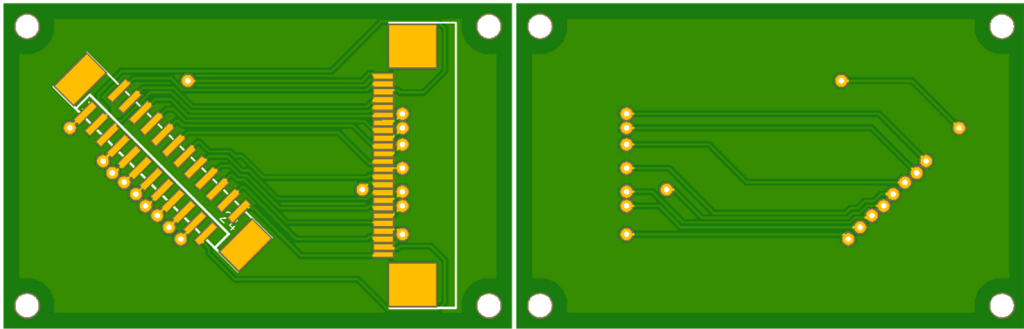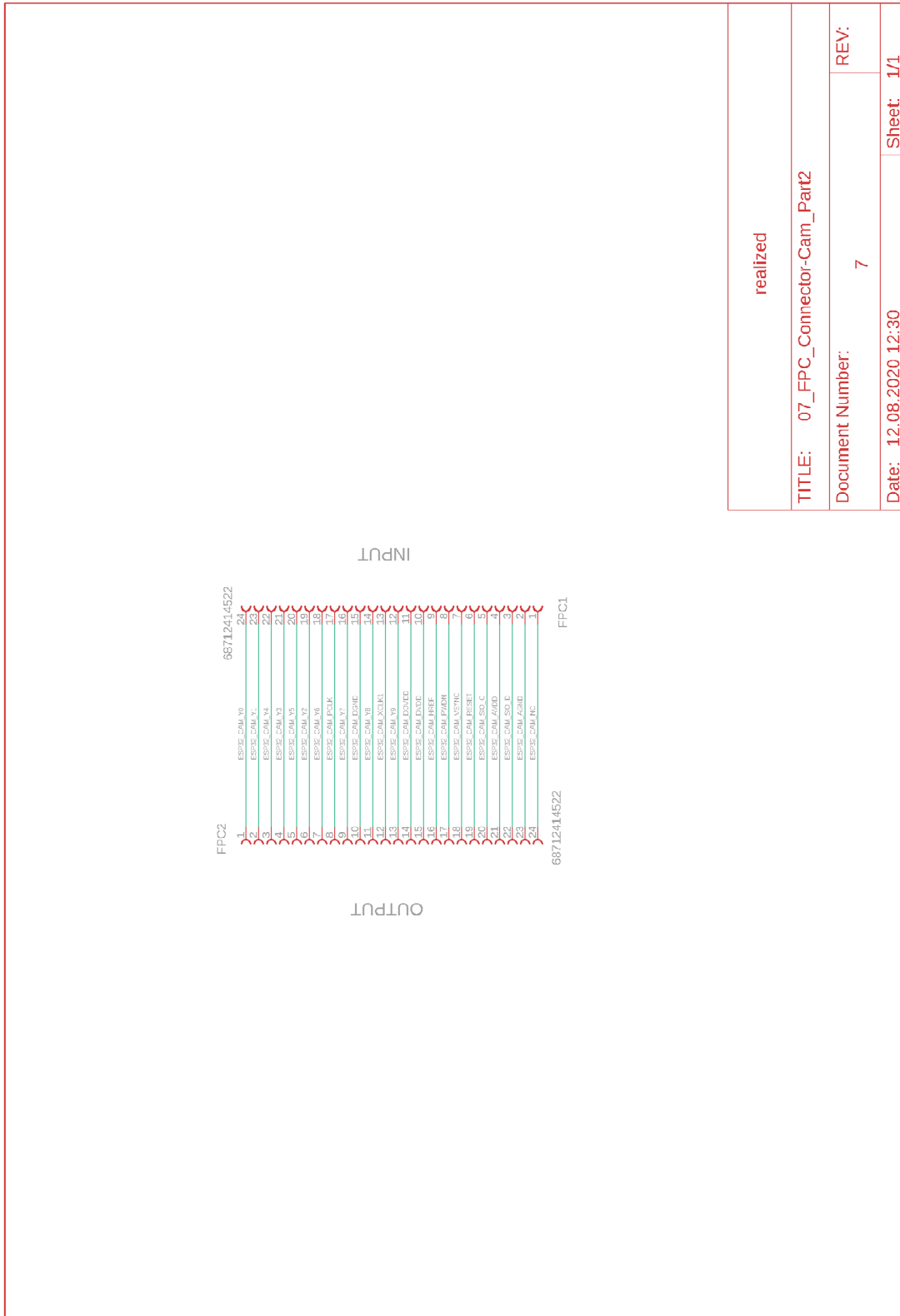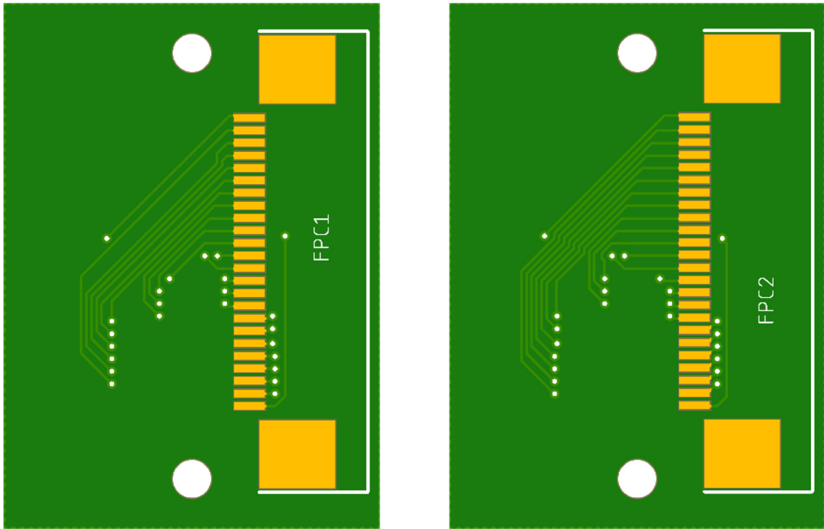

Figure 89:
Realized printed circuit board from the second connector of the ESP32-CAM module to the camera on the eyeglass frame
left – view from the top | right – view from the bottom

Appendix B   Circuit board diagrams – Second version

Appendix B.1   Control unit – Version 2

The following circuit diagram shows the second version of the v2 control unit (Figure 90). This version uses only the first two pins of the 24-pin FPC connector to provide power to the ESP32-CAM module on the eyeglass frame. The reason for this change is that the whole ESP32-CAM module will be integrated into the frame to avoid runtime errors of the camera which were described in chapter 0.
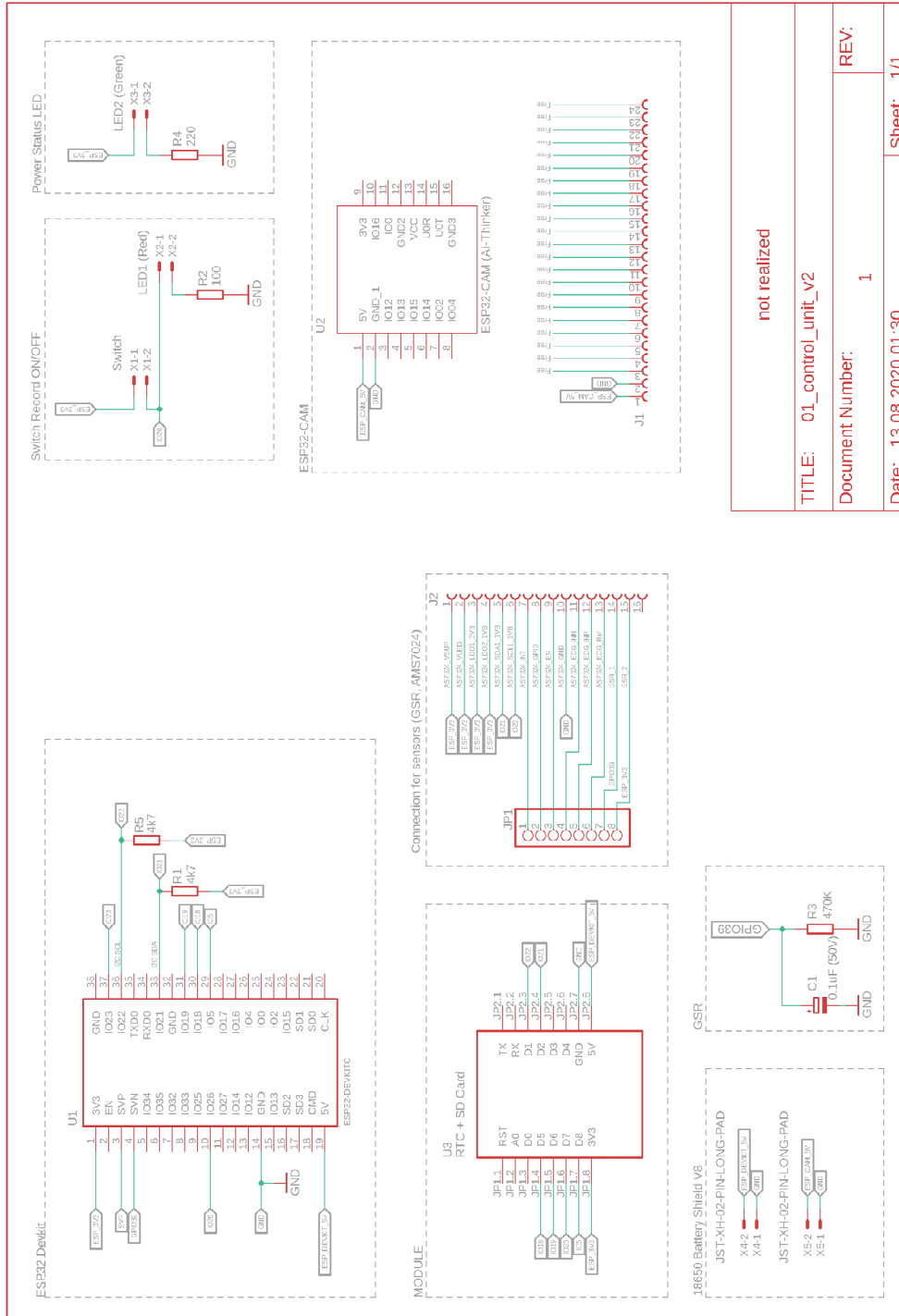
Figure 90: Circuit control unit v2 – not realized version

The layout in Figure 91 is the result of the previous circuit (Figure 90). The blue lines represent the conductors from the top view and the red lines represent the conductors from the bottom view. The existing 3D-printed case was taken into account when creating the layout, which means that no changes to the case are necessary.
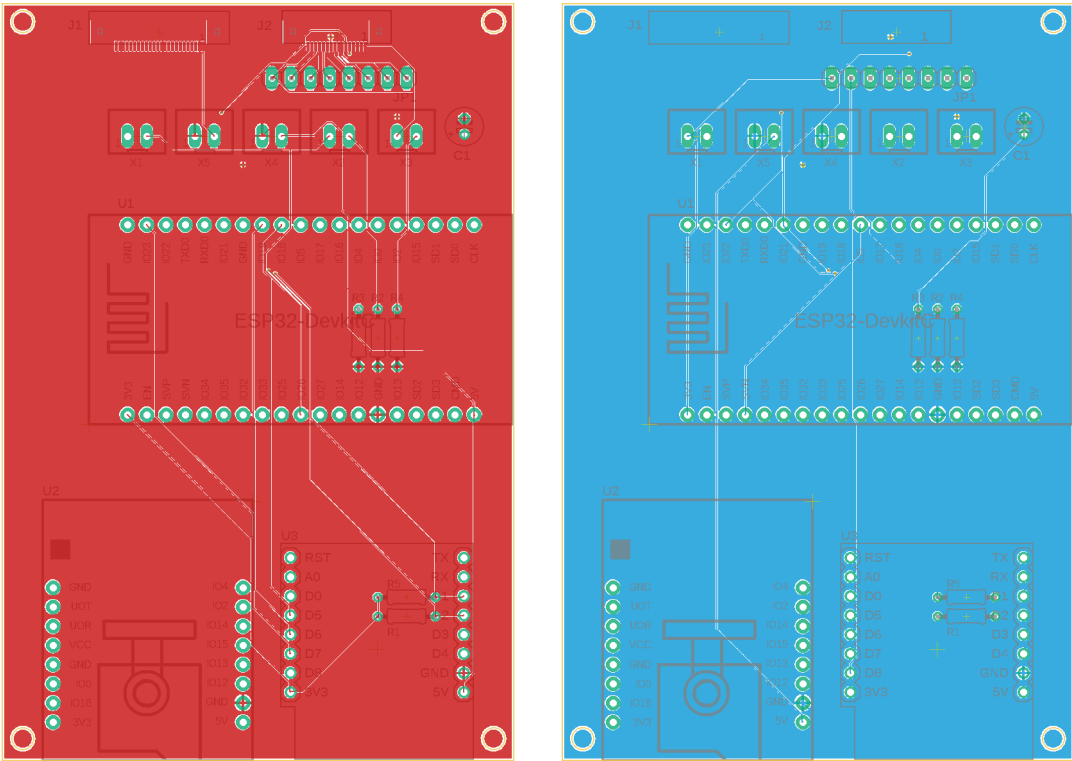
Figure 91: Control unit – layout v2 – final version

Appendix B.2   Extension unit from the control unit – Version 2

The circuit in Figure 92 shows the correction of the error in Figure 72. The difference to the first version is that the 24-pin FPC connector uses only 2 pins to supply power to the ESP32-CAM module. The layout is the same as in Figure 73, so the same PCBs (Figure 74) can be used.
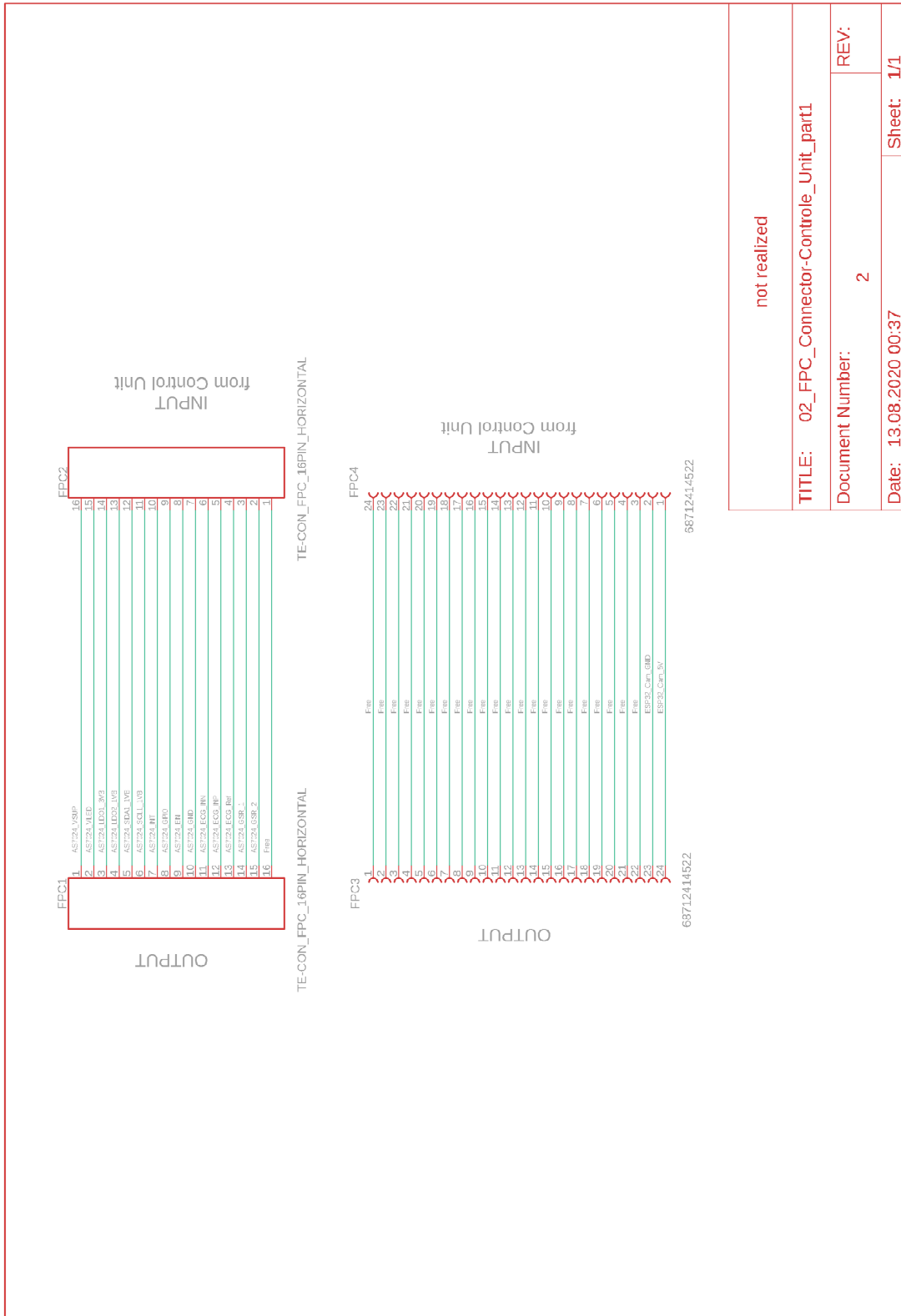
Figure 92: Circuit from the middle of the eyeglass frame – Version 2

Appendix B.3   Eyeglass frame – FPC connector left side – Version 2

In the second version, no changes were made to the circuit or layout, so both can be taken over completely from chapter Appendix A.3.

Appendix B.4   Eyeglass frame – FPC connector middle – Version 2

In the second version, no changes were made to the circuit or layout, so both can be taken over completely from chapter Appendix A.4.

Appendix B.5   Eyeglass frame – FPC connector right side – Version 2

In the second version, no changes were made to the circuit or layout, so both can be taken over completely from chapter Appendix A.5.

Appendix B.6   Eyeglass frame – FPC connector cam part 1 – Version 2

The first connection element to the ESP32-CAM module was reduced from 24 pins to two pins, which is realized via a JST-XH (B2B-XH-2) socket. These two pins are soldered directly to the ESP32-CAM module via a 2-pin JST connector. The advantage of doing so is that the module can be removed again without further desoldering.
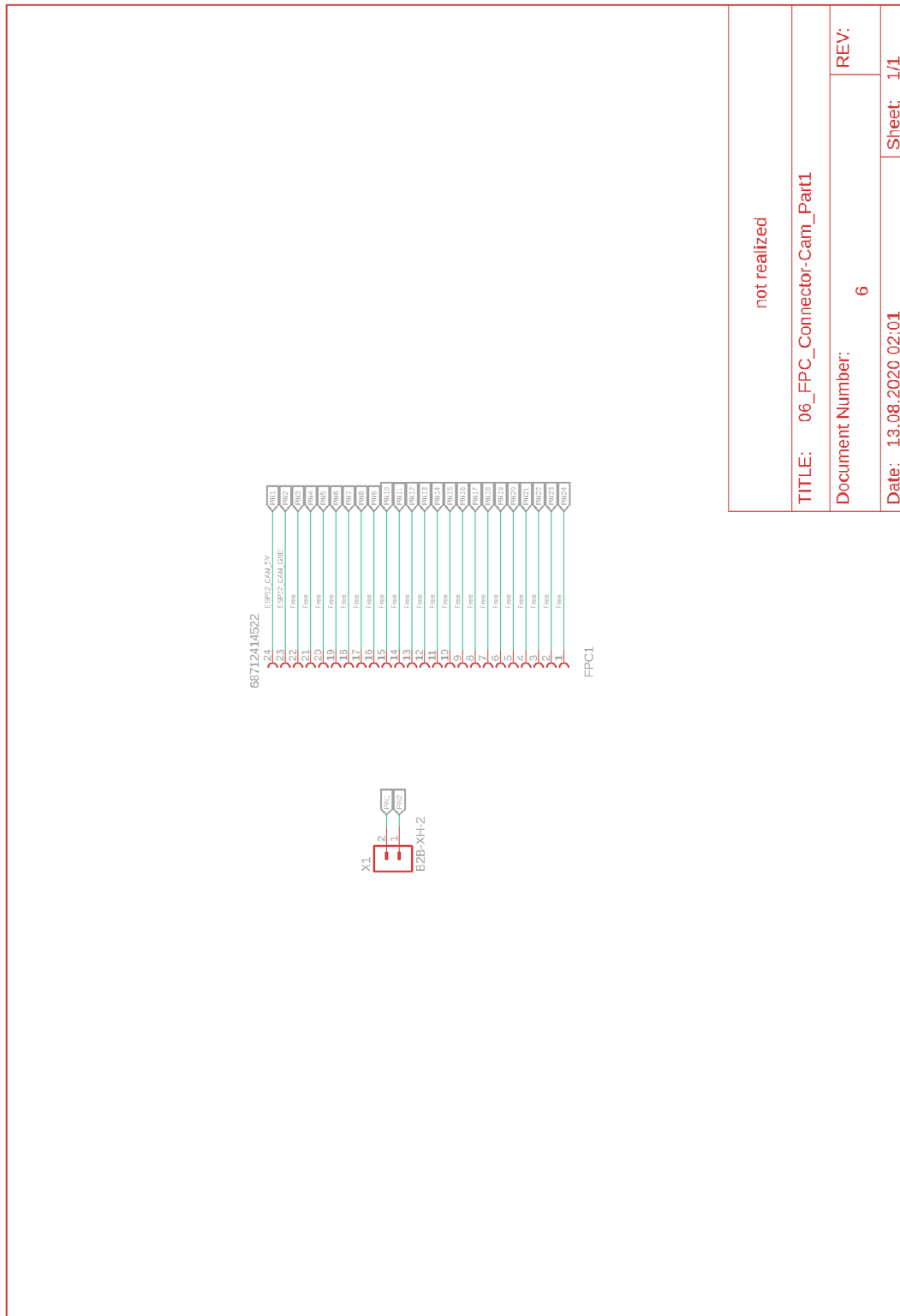
Figure 93:
Circuit from the first connector of the ESP32-CAM module to the camera on the eyeglass frame – Version 2

The following layout in Figure 94 shows the realization of the circuit. This implementation is a one-sided layout, which is not illustrated true to scale.
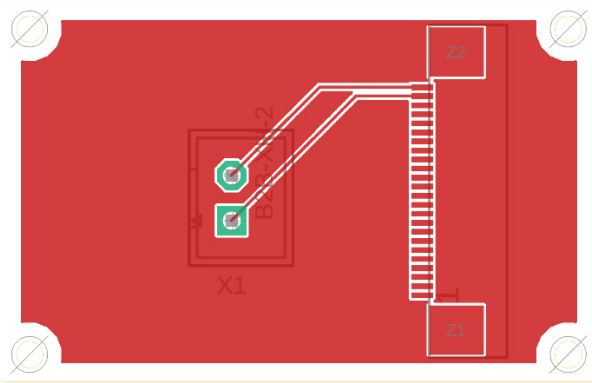

Figure 94:
Layout from the first connector of the ESP32-CAM module to the camera on the eyeglass frame – Version 2

Appendix B.7   Eyeglass frame – FPC connector cam part 2 – Version 2

In the second version, no changes were made to the circuit or layout, so both can be taken over completely from chapter Appendix A.7.

Appendix C   Programming code

The following flowcharts will give an overview of the individual program sequences of the components. The flowchart in Figure 95 shows the functional sequence of the ESP32-DevKit and ESP32-CAM microprocessors. After shortly pressing the ON/OFF button, the power supply from the battery module is released and supplies the entire prototype with power. The ON/OFF button has two additional functions. Shortly pressing the button again displays the battery status, which is represented by 4 LEDs. If all 4 LEDs are on, this means that the battery is fully charged. By pressing the ON/OFF button for approximately three seconds or longer, the power supply to the prototype is interrupted, causing a complete shutdown.
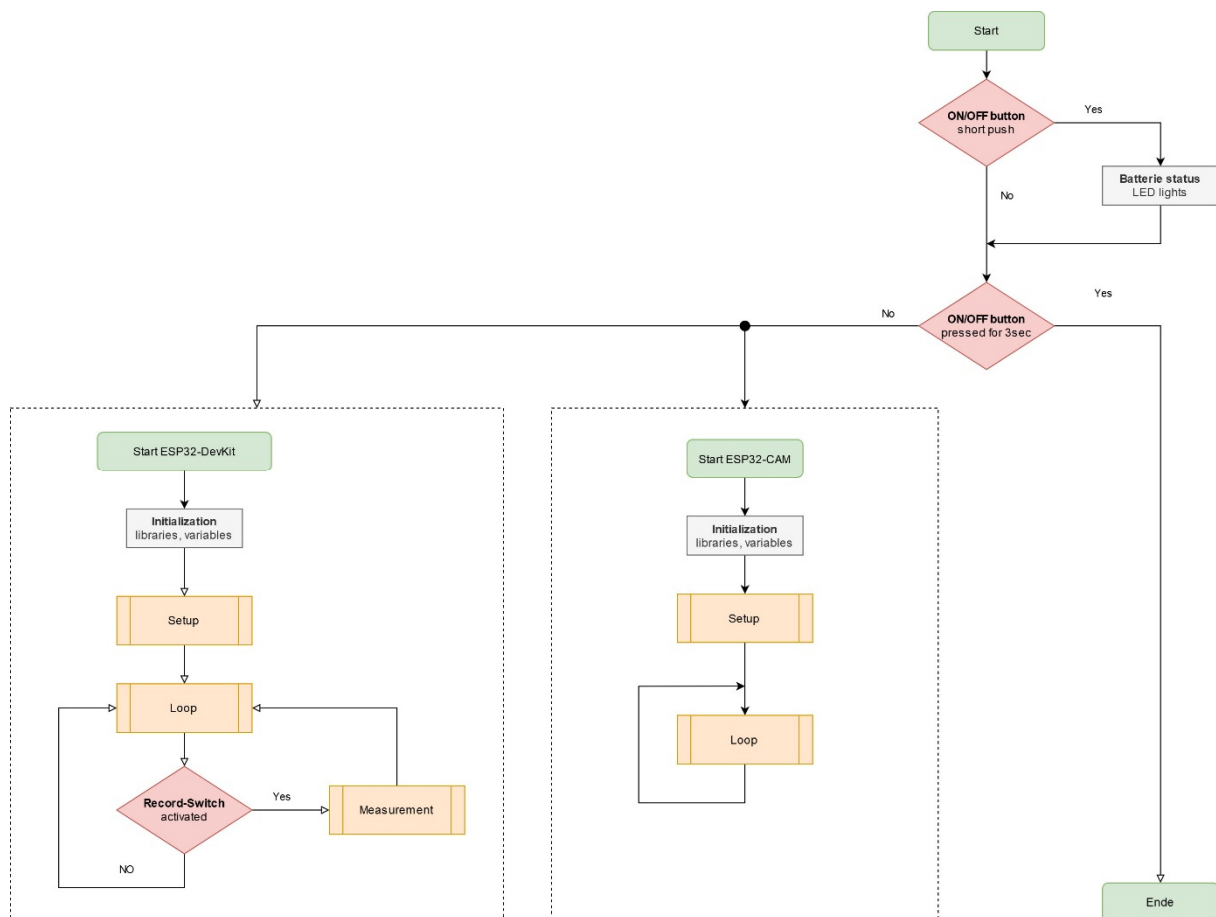
Figure 95: Flowchart from ESP32-DevKit and ESP32-CAM

After activating the power supply, the individual libraries and variables are loaded or created by the ESP32-DevKit and ESP32-CAM. Afterwards, the execution of the individual "Setup" methods takes place. The ESP32-DevKit will start to set up the access point and activate the required interfaces. The ESP32-CAM starts to activate the necessary interfaces for the camera function and establishes the WLAN connection to the ESP32-DevKit. When the "Setup" methods have been successfully completed by the two microprocessors, the microprocessors begin the "Loop" method. This is when the actual routine work of the processors begins.

The first step of the ESP32-DevKit is to then check the status of the "Record" switch. If the switch is deactivated, the microprocessor remains in a waiting loop. If the switch is enabled, the registration file for the AS7024 sensor is loaded and the "Measure" method is executed. This method activates all sensors, records sensor data and stores it on a microSD card. This process will continue until the "Record" switch is deactivated or the power supply is cut off by pressing the ON/OFF button for 3 seconds.

With the ESP32-CAM, the "Loop" function starts building a web page where the user can adjust the camera settings and activate live video transmission from the connected camera. The video transmission is sent directly to the website.

Programming the individual microcontrollers was done by C++ classes, which are normally split into two files. The header file had the extension .h, which contains the class definition and functions. The class is implemented in the .cpp file. The advantage here is that the implementation needs to be compiled only once if it does not change.

For a better overview of the file structures, an organization chart was created for each microcontroller, as shown in Figure 96 und Figure 97. The files were divided into pre-installed libraries and self-programmed files.
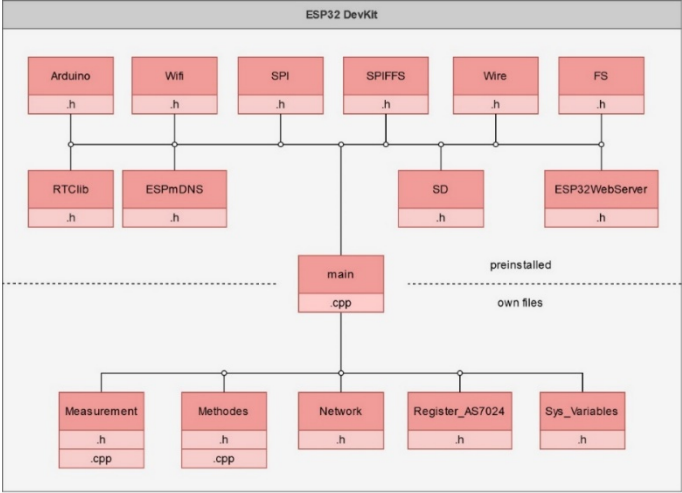
Figure 96: Overview of all files in ESP32-DevKit

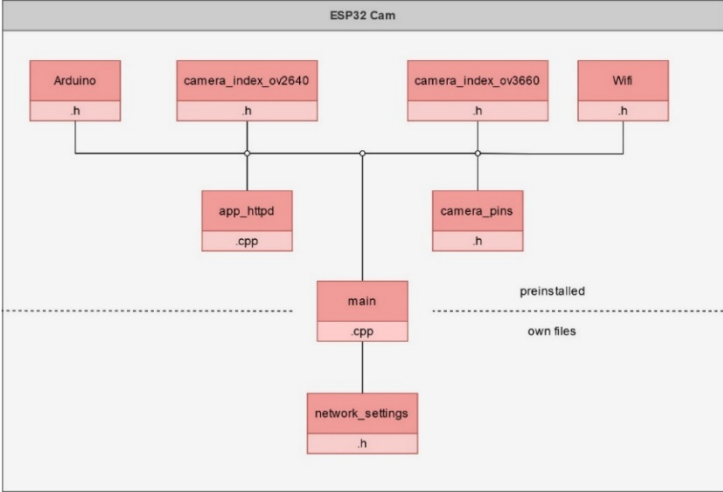Figure 97: Overview of all files in ESP32-CAM

The first set of files to be addressed are the individual pre-installed libraries that were used for programming. The following list is only a short list of functions of the individual libraries. The individual methods are not described in detail because the developers of these libraries provide a more elaborate description in the download package of the libraries.

ESP32-DevKit – pre-installed libraries:

- **Arduino.h** establishes the connection to the Arduino framework, which allows for Arduino-specific commands to be included in the program.
- The **wifi.h** library provides the wireless network connection so that an access point can be established on the ESP32-DevKit and clients like the ESP32-CAM or the user can connect it.
- The **SPI.h** (SPI = Serial Peripheral Interface) enables the use of the serial data protocol, which establishes the communication between one or more peripheral devices over short distances as well as between two microcontrollers.
- The **SPIFFS.h** (SPI Flash File System) offers the methods needed to read and write from a file of the ESP32. With the included **FS.h** library, one has access to the SPIFFS external variable, which will be used to interact with the file system.
- The **Wire.h** library makes the communication with I^2C-capable devices possible through the data lines SDA (data line) and SCL (clock line). There are both 7- and 8-bit versions of I^2C addresses. 7-bits identify the device and the 8-bit determines if the device is written or read.
- The **RTClib.h** library provides software access to the DS1307 chip, which supplies the time and date.
- The **ESPmDNS.h** library offers access to the mDNS-related functionalities that provide a local network service and host discovery.
- The **SD.h** library gives the SD card module access to store and read data and directories on it.
- The **ESP32WebServer** library is used to create a web server where the user can perform different settings directly on a browser. These settings were described in chapter 4.6.2.

ESP32-CAM – pre-installed libraries:

- **Arduino.h** establishes the connection to the Arduino framework, which allows for Arduino-specific commands to be included in the program.
- The **wifi.h** library provides the wireless network connection so that an access point can be established on the ESP32-DevKit and clients like the ESP32-CAM or the user can connect it.
- The **camera_index_ov2640** contains the possible settings of the camera in relation to the lens OV2640.
- The **camera_index_ov3660** contains the possible settings of the camera in relation to the lens OV3660.
- The **app_http** library generates the web-based structure when the IP address is called from the ESP32-CAM.
- In the **camera_pins** library the corresponding interface assignments for the different ESP32-CAM versions are defined.

In the following, the self-programmed files (.h and .cpp) are listed and their contents are described in detail. The resulting methods have been structured in a way that ensures easy further use.

<u>ESP32-DevKit – self-programmed files:</u>

- The "**Measurement**" library provides the methods necessary to record and save the measurements of the individual signals.

void RecordingAS7024(RTC_DS1307 rtc)	
Return value:	None
Parameter:	rtc → values of date and time
Description	In this method, the pulse and ECG signals are recorded and displayed simultaneously with date, time, GSR and body temperature. The output is collected in this method by the serial interface due to runtime performance.

float getTemperature48()	
Return value:	float → value of the measured body temperature
Parameter:	None
Description	The 0x48 address is used to address the AS6200 sensor via the I^{2}C bus. For each measurement, two bytes are recorded by the sensor and then processed further. A negative two's complement is formed from 12-bit integers by appropriate bit shifting and the temperature is determined with the reference value 0.0625. This value is then transferred as return value.

float getGSR()	
Return value:	float → value of the measured skin conductance
Parameter:	None
Description	The method measures the measured voltage drop through the skin via the GSR_PIN of the ESP32-DevKit. This voltage value is used to determine the skin conductance value as described in Chapter 2.1.4. However, this process is only carried out when the measured voltage value is greater than zero.

- The library "**Methods**" contains multiple processes configured as single methods, which are called in different classes.

Void i2cWrite(byte addr, byte *data, byte len)			
Return value:	None		
Parameter:	byte addr	→	is the hex address of the respective device
	byte *data	→	is an array in which bytes contain records
	byte len	→	contains the number of data records
Description	Start a transmission to the I^{2}C slave device with the specified address. Then set the bytes for transmission with the write() function in a queue and transfer them by calling endTransmission().		

Void i2cRead(byte addr, byte reg, byte *rec, byte readLen)			
Return value:	None		
Parameter:	byte addr	→	is the hex address of the respective device
	byte reg	→	is a register address for controlling the AS7024
	byte *reg	→	is an array containing the byte records read from the bus
	Byte readLen	→	contains the number of data to be read
Description	Start a transmission to the AS7024 I²C slave device with the specified address. Then set the bytes for the transmission with the write() function in a queue and transfer them by calling endTransmission(). Depending on how many records are read, this process is repeated.		

void i2cScanner()	
Return value:	None
Parameter:	None
Description	The method scans the I²C bus for all possible addresses and outputs them to the serial interface. The connected devices for which the address is known are then assigned to the corresponding hex address.

void currentTime(RTC_DS1307 rtc)			
Return value:	None		
Parameter:	RTC_DS1307 rtc	→	Object from the library RTClib.h
Description	This method determines the date and time from the DS1307 RTC module and outputs it via the serial interface.		

void saveData(RTC_DS1307 rtc, float tempData, float gsrData, int ppgData, int ecgData)			
Return value:	None		
Parameter:	RTC_DS1307 rtc	→	Object from the library RTClib.h
	float tempData	→	Temperature signal with decimal places
	float gsrData	→	GSR signal with decimal places
	int ppgData	→	Integer number of the recorded pulse signal
	int ecgData	→	Integer number of the recorded ECG signal
Description	This method stores the recorded data in the text file recordFile.txt. The file is stored in the root directory of the SD card. Newly recorded data are stored at the end of the file.		

- The **"Network"** library stores the necessary variables for the establishment of a network or integration into a network. Depending on the configuration in the main section (main.cpp), an access point is configured on the ESP32-DevKit or the connection to an existing WLAN network is established.

ESP32-Cam – self-programmed files:

- The "**network_settings**" library contains the necessary variables for connecting to the WLAN network of the ESP32-DevKit so that the ESP32-CAM can connect to the ESP32-DevKit.

Appendix D 3D model

This chapter focuses on the structure of the 3D-printed components so that they can be manufactured again if necessary or defective components can be replaced. The components shown in the following refer to the first prototype, which was completely manufactured for this master's thesis.

Appendix D.1 Control unit – Version 1

Figure 98 shows the control unit with the individual labelled components from the top view.
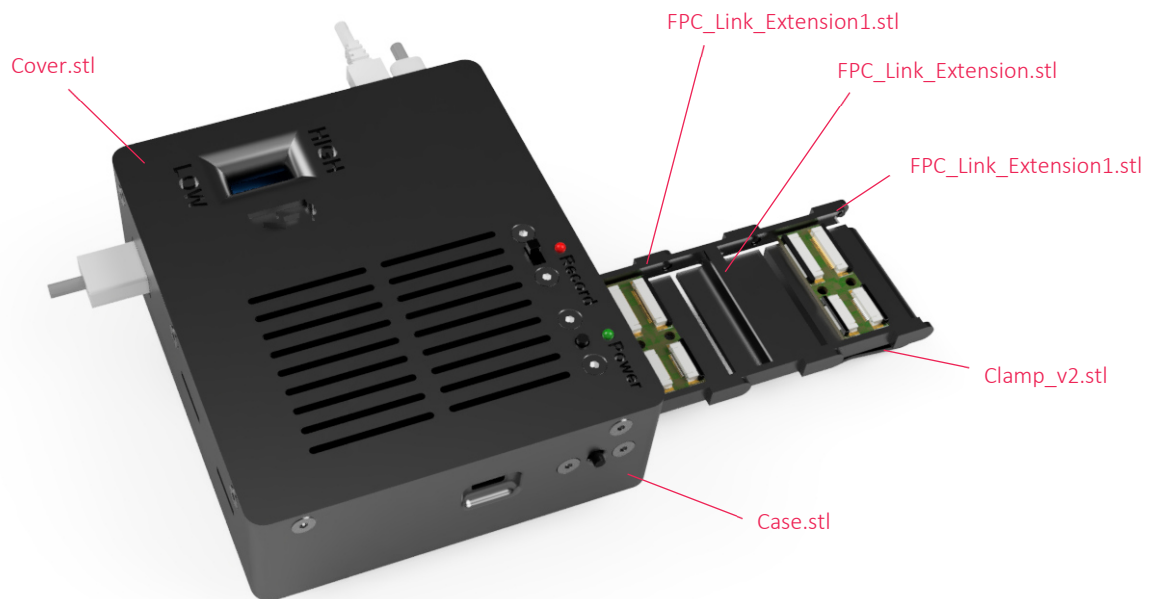

Figure 98: Control unit with cover from the top view

Figure 99 shows the control unit with the individual labelled components from the bottom view.
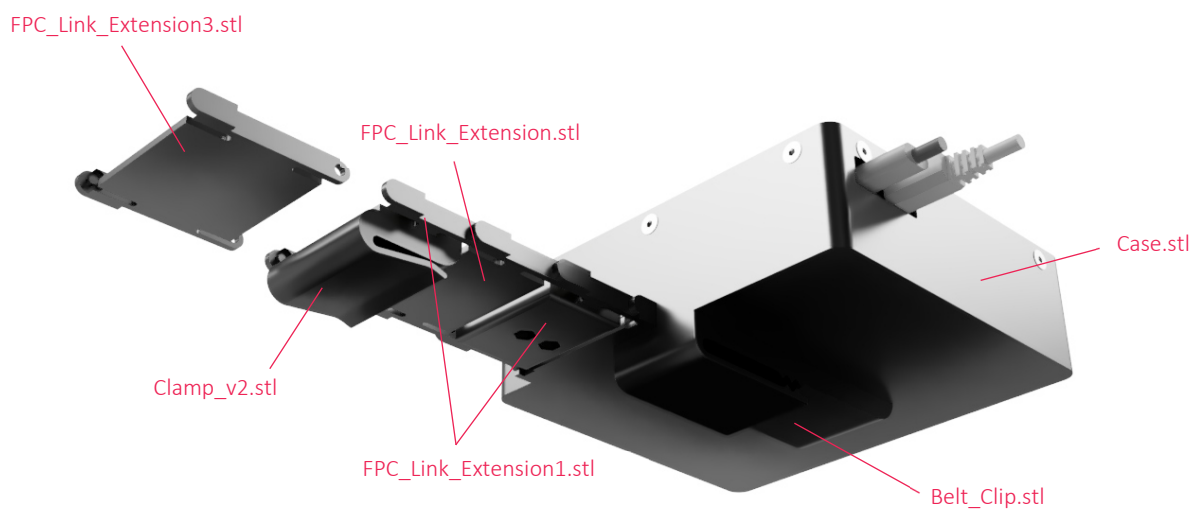
Figure 99: Control unit with cover from the bottom view

Appendix D.2   Eyeglass frame – Version 1

Figure 100 gives the individual designations of all covers of the eyeglass frame shown from the left side.

Eyeglass_Frame_Front_Part1_Cover.stl

Temples_Left_Part2_Cover.stl

Cam_Holder_Part3_Cover.stl

COVER_CamHolder_Part2.stl

Figure 100: Eyeglass frame – labelling of all covers (left view)

Figure 101 gives the individual designations of all covers of the eyeglass frame shown from the right side.

Temples_Right_Part1_Cover.stl

Eyeglass_Frame_Front_Part1_Cover.stl

Temples_Right_Part2_Cover.stl

Figure 101: Eyeglass frame – labelling of all covers (right view)

Figure 102 shows the individual designations of all components of the eyeglass frame as viewed from the left.

Figure 102: Eyeglass frame – labelling of all components (left view)

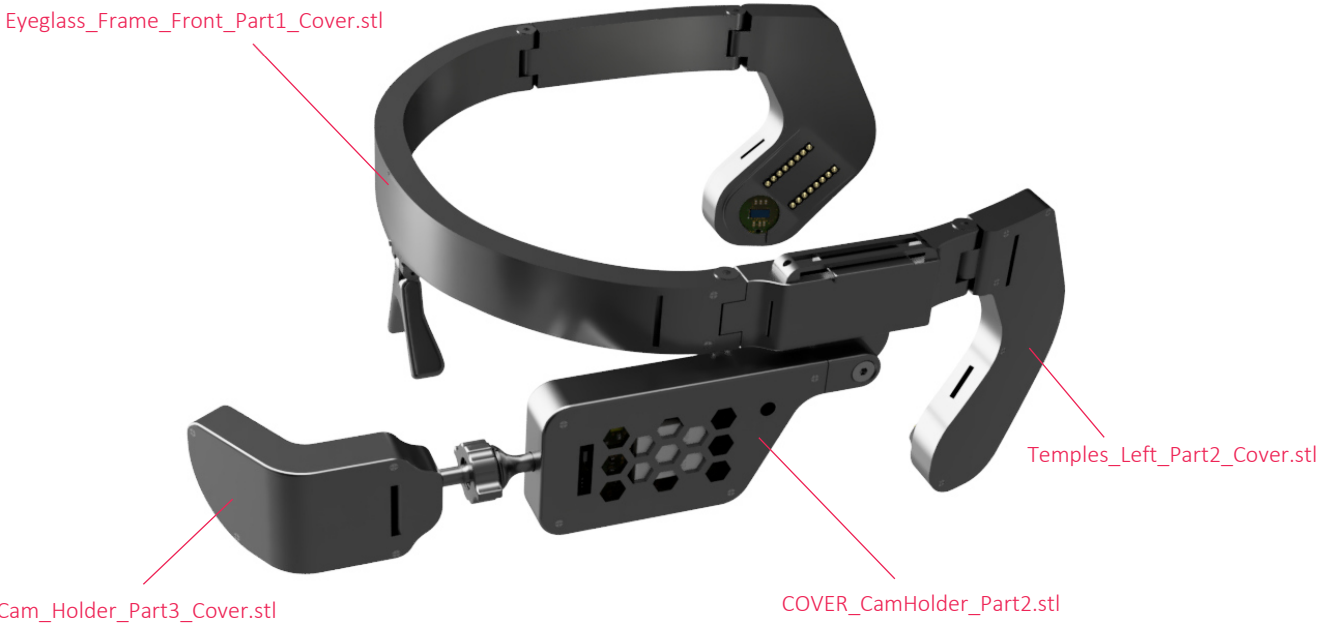Figure 103 shows the individual designations of all components of the eyeglass frame as viewed from the right side.
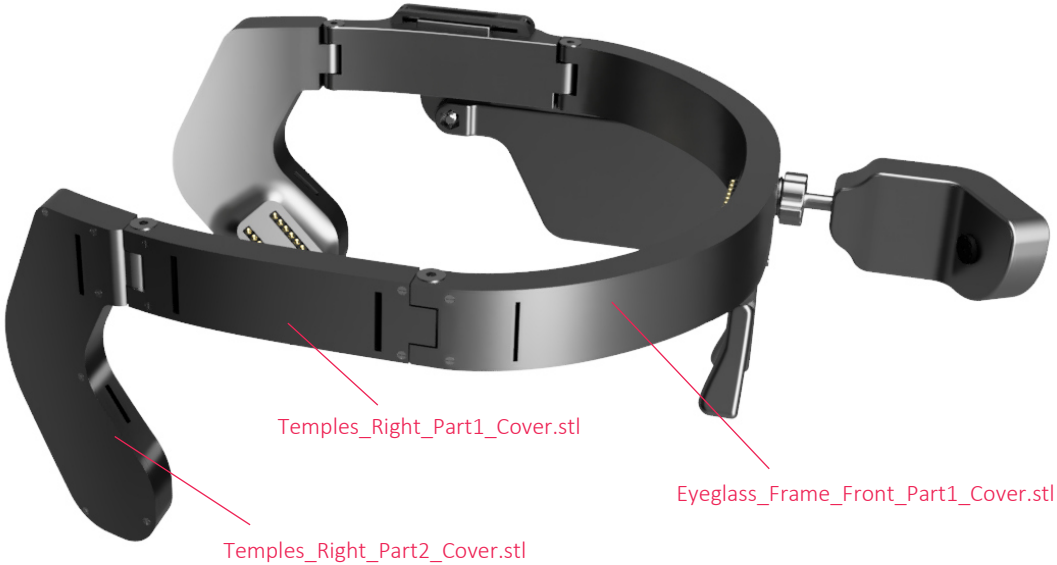

Figure 103: Eyeglass frame – labelling of all components (right view)

Appendix E   Filament box

For storing the different filaments and controlling their humidity and temperature, a dry box was developed. This was necessary because these two factors (humidity and temperature) determine the printing properties of almost all types of filaments and therefore also their further processing and properties.

Figure 104: Dry box

The filament box contains a spool holder with ball bearing, a PTFE connector, a roll unwind brake, a sensor clip and a holder for a silica gel. Most of these components were slightly modified or completely redesigned by other designers. The construction consists of several individual parts so that anyone can equip the filament box according to their own wishes.

Appendix E.1   Component assignment

In this chapter, the individual 3D components are assigned to a corresponding category. The assignments correspond to the folder structure in which the individual 3D components can be found.
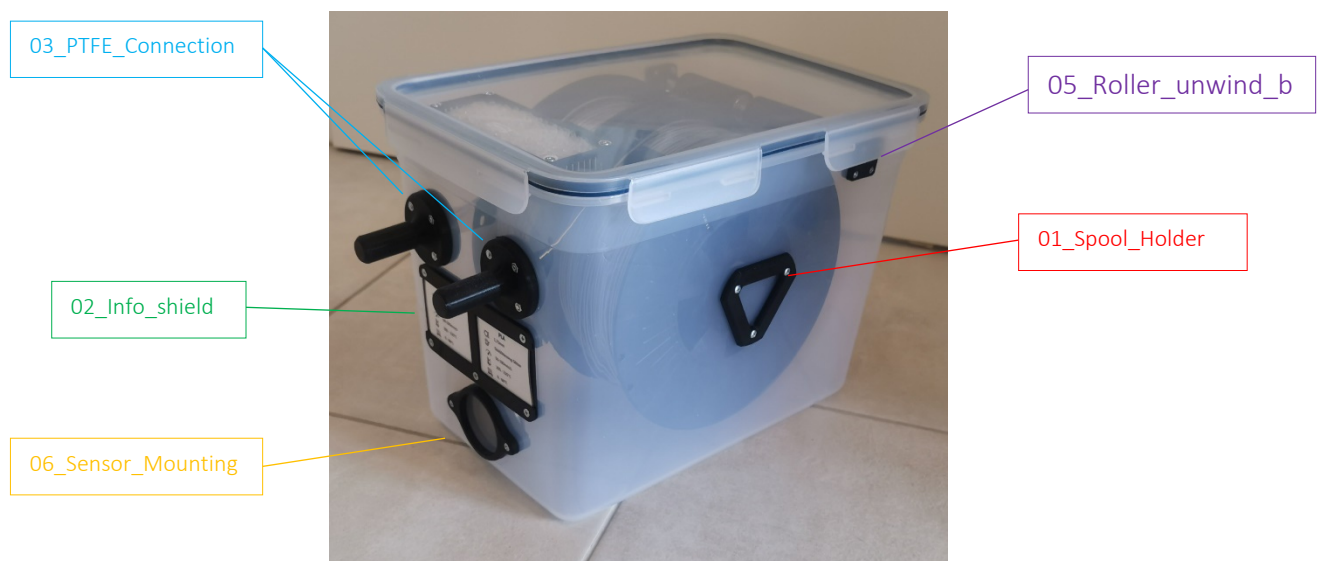
Figure 105: Components assignments – Part 1

07_Silica_box

05_Roller_unwind_brake
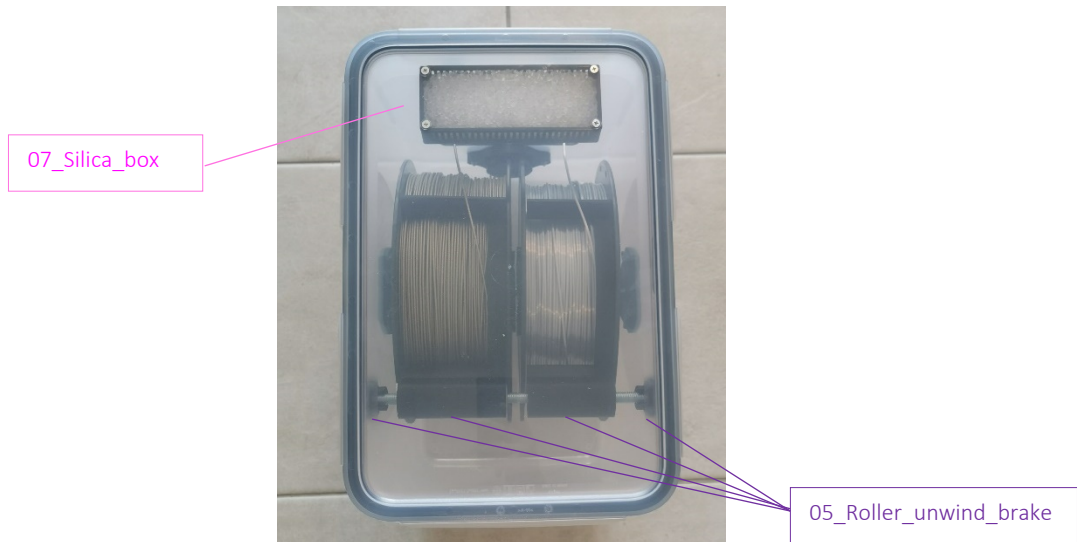
Figure 106: Components assignments – Part 2

04_Roller_suspension

Figure 107: Components assignments – Part 3

Appendix E.2   Component – 01_Spool_Holder

In the construction group **01_Spool_Holder**, there are two 3D models that must be printed twice for each filament box. The structure is shown in Figure 108. Six M3x10 cylinder head screws and three M3 lock nuts are used for mounting.

1_2_RodSlotBacking.stl

1_1_RodSlot_v1.stl

Figure 108: Spool holder

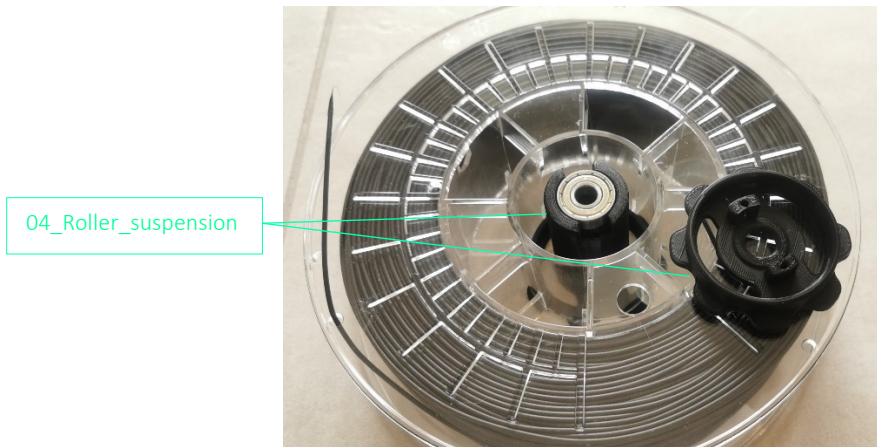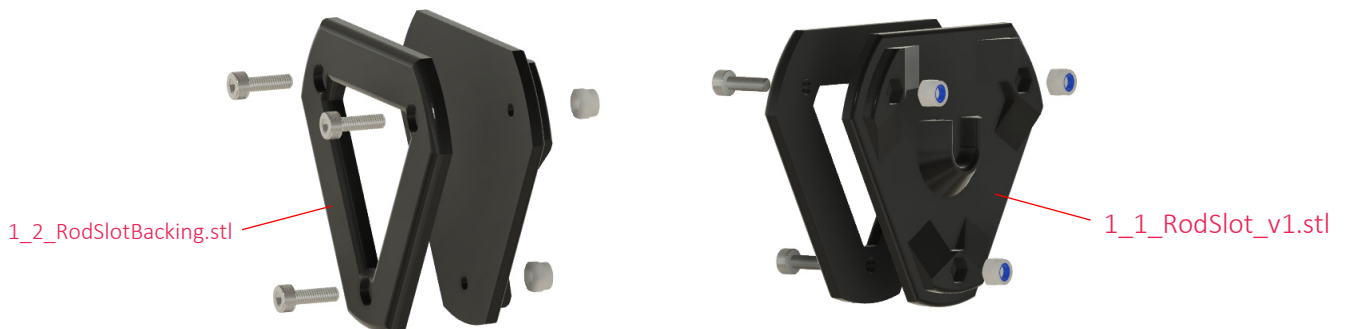The following tables list the required 3D parts, bolts and nuts.

Table 4: 01_Spool_Holder – 3D Parts

Quantity	3D parts
6	1_1_RodSlot_v1.stl
2	1_2_Rod

Table 5: 01_Spool_Holder – Bolts and Nuts

Quantity	Parts
6	M3x10 cylinder head screws (hexagon)
6	M3 lock nuts

Appendix E.3   Component – 02_Info_shield

The assembly group **02_Info_shield** shows the information label on which the filament content in the box can be labelled. When installing them on the box, the screws should only be screwed hand-tight, otherwise the thin components may break. The construction of this component group is shown in Figure 109. The holes of the M3 nuts were chosen so that they fit into the opening with a little pressure. This makes mounting easier.
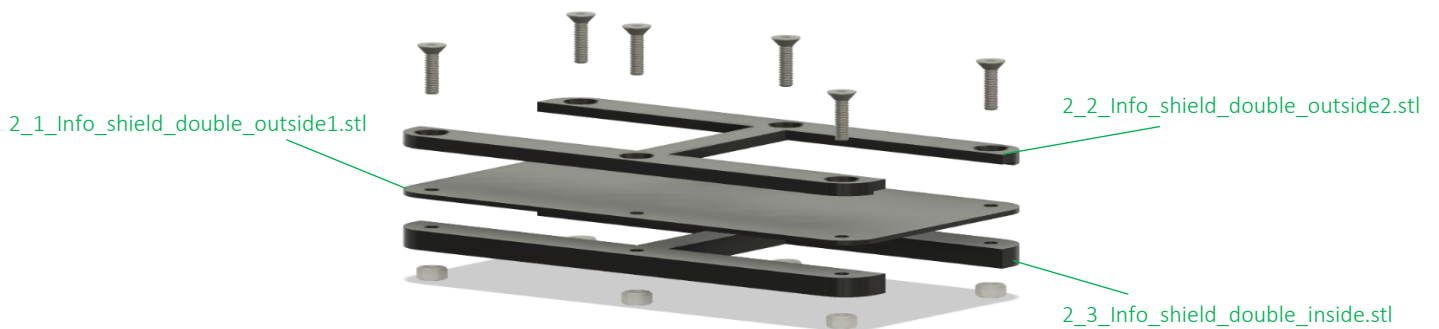
Figure 109: Info shield

The following tables list the required 3D parts, Screws and Nuts.

Table 6: 02_Info_shield – 3D Parts

Quantity	3D parts
1	2_1_Info_shield_double_outside1.stl
1	2_2_Info_shield_double_outside2.stl
1	2_3_Info_shield_double_inside.stl

Table 7: 02_Info_shield – Screws and Nuts

Quantity	Parts
6	M3x10 cylinder head screws (hexagon)
6	M3 nuts

Appendix E.4   Component – 03_PTFE_Connection

This assembly is put together as shown in Figure 110 and the lock nuts are positioned in the opening with little pressure. The pneumatic connection PC4 is screwed into the printed thread. Again, all connections and screws must be hand-tightened.
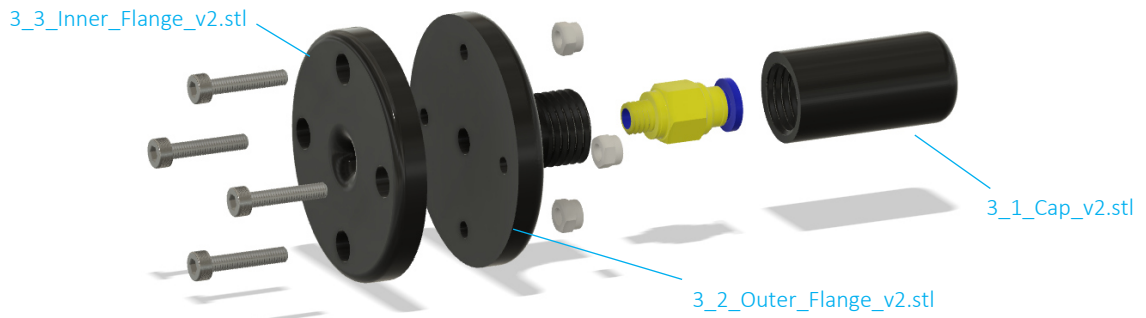

3_3_Inner_Flange_v2.stl

3_1_Cap_v2.stl

3_2_Outer_Flange_v2.stl

Figure 110: 03_PTFE_Connection

The following tables list the required 3D parts, Screws and Nuts.

Table 8: 03_PTFE_Connection – 3D Parts

Quantity	3D parts
2	3_1_Cap _v2.stl
2	3_2_Outer_Flange_v2.stl
2	3_3_Inner_Flange_v2.stl

Table 9: 03_PTFE_Connection – Screws and Nuts

Quantity	Parts
8	M3x16 cylinder head screws (hexagon)
8	M3 nuts

Appendix E.5   Component – 04_Roller_suspension

This unit is used to reduce the filament roll diameter so that the roll can be positioned on an M8 threaded rod. To obtain a smooth roller movement, the 3D model includes holes for ball bearings. The model was designed so that the ball bearings are positioned in the recess by pressure. This assembly consists of three components that are connected by M3 countersunk screws. Several 3D models were designed to get the largest possible number of different filament role models. Figure 111 shows how the three components are joined together.
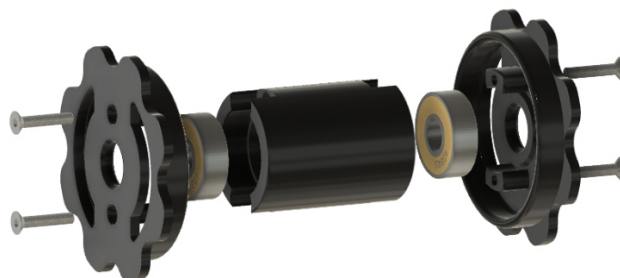

Figure 111: Suspension for filament rolls

The following tables list the required 3D parts, Screws and Nuts. The <XX> in the 3D component list indicates the different sizes of the filament rolls. For example, if a filament roll has a diameter of 52 mm, then the model should be printed with 52 mm.

Table 10: 04_Roller_suspension – 3D Parts

Quantity	3D parts
2	4_1_<X>_<X>mmSpoolFaces.stl
4	4_2_<X>_RollerCore_<X>mm.stl

Table 11: 4_Roller_suspension – Screws and Nuts

Quantity	Parts
8	M3x16 countersunk screws (hexagon)
4	Ball bearing 608 ZZ
1	Threaded rod M8 (length: 176 mm)

Appendix E.6   Component – 05_Roller_unwind_brake

The component in Figure 112 was designed to prevent the filament from unwanted rolling during the print retraction process. The component gives a small force to the filament roll so that it does not unwind as easily. A good average size was chosen so as not to make it too difficult for the extruder to pick up the filament.
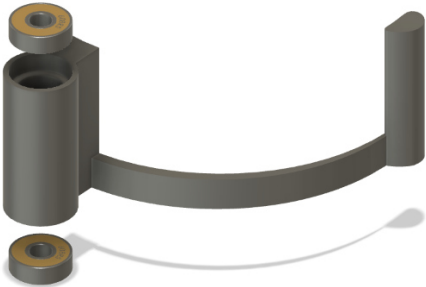
Figure 112: Filament unwinding brake

The second component of this unit is the suspension of the previous component in the filament box. For this purpose, one component is attached to each side of the box so that they face each other. The filament roller brake is suspended by an M8 threaded rod.
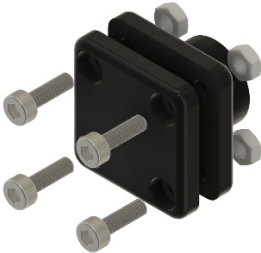
Figure 113: Rod hanger for filament unwinding brake

The following tables list the required 3D parts, Screws and Nuts. The designations <X> and <Y> again refer to the filament roll width. Depending on how wide the roll is, the appropriate roll size must be selected.

Quantity	3D parts
2	5_0_1_Rod_Hanger_8mm_inner.stl
2	5_0_2_Rod_Hanger_8mm_outer.stl
1	5_<X>_Spool_Guard_v3_<Y>mm.stl

Table 13: 05_Roller_unwind_brake – Screws and Nuts

Quantity	Parts
8	M3x10 cylinder head screws (hexagon)
4	Ball bearing 608 ZZ
1	Threaded rod M8 (length: 180 mm)

Appendix E.7   Component – 06_Sensor_Mounting

For monitoring the temperature and humidity inside the filament box, a hygrometer and thermometer are mounted inside the box. The 3D model in Figure 114 was designed for this reason. Two M3x16 cylinder head screws with M3 nuts are used for mounting.
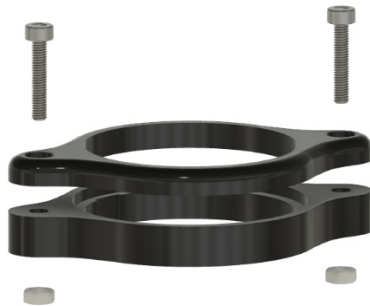
Figure 114: Sensor mount

Figure 115: Digital hygrometer / thermometer

The following tables list the required 3D parts, Screws and Nuts.

Table 14: 06_Sensor_Mounting – 3D Parts

Quantity	3D parts
1	6_1_Sensor_mount_part_inside.stl
1	6_2_Sensor_mount_part_outside.stl

Table 15: 06_Sensor_Mounting – Screws and Nuts

Quantity	Parts
2	M3x16 cylinder head screws (hexagon)
2	M3 nuts

Appendix E.8   Component – 07_Silica_box

Most filaments should be stored at a humidity between 15 – 25 %, which is created with silica gel. For storing the small silica spheres, the following 3D model in Figure 116 was created. The silica box is attached to the lid of the filament box.
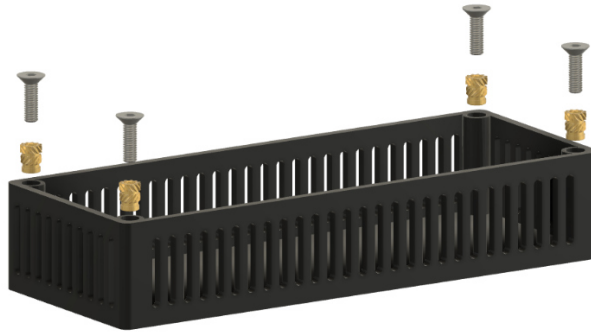

Figure 116: Silica box

The following tables list the required 3D parts, Screws and Nuts.

Table 16: 07_Silica_box – 3D Parts

Quantity	3D parts
1	7_1_Bottom_mm.stl

Table 17: 07_Silica_box – Screws and Insert Nuts

Quantity	Parts
4	M3x10 countersunk screws (hexagon)
4	M3 insert nut

Appendix F   Datasheets of components

The datasheets used are annexed to this chapter. For a short overview, all datasheets used are listed here.

- ams Add-On Board
    - AS7026GG_AddOn_1v0.PDF
    - AS7026GG_Evalboard_1V1.PDF

- ams AS6200
    - AS6200_DS000449_2-00.pdf

- ams AS7024
    - Application_Note_-_AS702x_DOC_UserGuide_EVK_v2.0.0.pdf
    - Application_Note_-_AS7024_Galvanic_Skin.pdf
    - AS702x_DOC_DesignGuide_v2.0.0.pdf
    - AS702x_DOC_UserGuide_EVK_v2.0.0.pdf
    - AS7024_DS000469_4-00-1531731.pdf
    - AS7024_QG000124_1-00.pdf

- ESP32-CAM
    - ESP32_CAM_XC6206.pdf
    - ESP32_Cam_Schematic.pdf
    - esp-psram32_datasheet_en.pdf

- ESP32-DevKit
    - ESP-32 NodeMCU Development Board Schematics.pdf
    - ESP-32 NodeMCU Developmentboard Datenblatt.pdf
    - ESP-32 NodeMCU Developmentboard Pinout Diagram.pdf

- Filament
    - Datasheet_3DJake_ecoPLA.pdf
    - Datasheet_3DJake_TPU_A95.pdf
    - Datasheet_Extrudr_ABS_DuaPro.pdf

- Surface mount spring contacts
    - Spring_Loaded_Connectors.pdf

- Wemos RTC DS1307 + Battery + SD
    - Wemos_D1_mini_-_MicroSD_card_shield.pdf
    - Wemos_D1_mini_-_Real_Time_Clock.pdf
    - PINOUT==0G-00005816==D1mini-SHLD-DATALOG.pdf
    - Schematic==0G-00005816==D1mini-SHLD-DATALOG.pdf

References

[1]   Schelle A., Stress - erhöhte Anforderungen an die Gesellschaftsmitglieder - was erhält den Menschen gesund?, 1st ed.: Grin Verlag 2013.

[2]   Lieb K., Frauenknecht S., Brunnhuber S., Wewetzer C., Intensivkurs Psychiatrie und Psychotherapie, 7th ed. München: Elsevier Urban & Fischer 2012.

[3]   Kollak I., Burnout und Stress. Berlin: Springer 2008.

[4]   Kramme R, editor, Medizintechnik: Verfahren - Systeme - Informationsverarbeitung, 5th ed. Berlin: Springer 2017.

[5]   Conveyor_belt_worker, Web, URL <https://ak2.picdn.net/shutterstock/videos/6675872/thumb/1.jpg>, 05.01.2020.

[6]   Testdriver; 2020, Web, URL <https://i1.wp.com/die-testfahrer.com/wp-content/uploads/2019/01/SeAT-SICHER.jpg?fit=1772%2C1181&ssl=1>, 05.01.2020.

[7]   Sergeon; 2019, Web, URL <https://enorm-magazin.de/sites/enorm-magazin.de/files/operation_im_krankenhaus_header.jpg>, 05.06.2019.

[8]   Strobel I., Stressbewältigung und Burnoutprävention, 2nd ed. Stuttgart: Georg Thieme Verlag 2018.

[9]   Wehrlin U., Stressmanagement, 1st ed. Göttingen: Optimus 2016.

[10]   Schneiderman N., Ironson G., Siegel S. D., STRESS AND HEALTH: Psychological, Behavioral, and Biological Determinants. Annual review of clinical psychology 2005; 1: 607–628.

[11]   Dietrich R., Stressbewältigung und berufliche Identität in der Bankenbranche. Wiesbaden: Springer Fachmedien Wiesbaden 2017.

[12]   Müller R, Weninger S, Wenzel RR, Psyche, Stress und hoher Blutdruck. Journal für Hypertonie - Austrian: 148–151.

[13]   3-Channel-ECG derivation system according to Einthofen (edit), Web, URL <https://www.cardiosecur.com/fileadmin/content/Fachartikel/3_ECG.png>, 05.01.2020.

[14]   Kochs E, editor, Anästhesievorbereitung und perioperatives Monitoring. Stuttgart, New York: Thieme 2015.

[15]   Pulsoximeter; 2016, Web, URL <https://sportuhrenguru.net/wp-content/uploads/2016/08/Epson-optische-Pulsmessung.jpg>, 07.01.2020.

[16]   Lambert beer's law; 2017, Web, URL <http://www.chemgapedia.de/vsengine/media/vsc/de/ch/13/pc/praktikum1/saeurebase/images/cell1a.gif>, 08.01.2020.

[17]   Boucsein W., Electrodermal activity, 2nd ed. New York, NY: Springer 2012.

[18]   Tobii Pro Glasses 2; 2015, Web, URL <https://www.tobiipro.com/imagevault/publishedmedia/wlw5s0lm8hyixw98rd0m/TobiiPro_Glasses_2_Eye_Tracker_side_3_1.jpg>, 09.01.2020.

[19]   Pupil Labs - pupil core, Web, URL <https://www.researchgate.net/profile/Hongwei_Wang7/publication/333447038/figure/fig1/AS:76379

9439171586@1559115385374/Pupil-Labs-wearable-eye-tracker-and-its-components-55.jpg>, 09.01.2020.

[20]   Pupil Core Packages, Web, URL <https://pupil-labs.com/products/core/>, 09.01.2020.

[21]   Dikablis Glasses 3, Web, URL <https://www.meditech.de/web/image/product.product/11228/image?unique=53b0221>, 09.01.2020.

[22]   Arterien von Kopf und Hals im Überblick (edit); 2017, Web, URL <https://eref.thieme.de/images/l/868141_25.jpg>, 05.01.2020.

[23]   ams_evaluation_boart_kit.jpg, Web, URL <https://ams.com/documents/20143/36005/AS7024_QG000124_1-00.pdf>, 21.03.2020.

[24]   ams_evaluation_boart_kit2.jpg, Web, URL <https://ams.com/documents/20143/36005/AS7024_QG000124_1-00.pdf>, 21.03.2020.

[25]   ams_AS7024_Add-on_board.jpg, Web, URL <https://ams.com/documents/20143/36005/AS7024_QG000124_1-00.pdf>, 21.03.2020.

[26]   ams_AS7024_Add-on_board2.jpg, Web, URL <www.ams.com>, 26.03.2020.

[27]   ams_AS7024_Add-on_board3.jpg, Web, URL <www.ams.com>, 26.03.2020.

[28]   esp32-wroom-32.jpg, Web, URL <https://dl.espressif.com/dl/schematics/pictures/esp32-wroom-32-front-back.jpg>, 27.03.2020.

[29]   esp32-devkit.jpg, Web, URL <https://cdn-reichelt.de/bilder/web/artikel_ws/A300/SBC-NODEMCU-ESP32-01.jpg>, 27.03.2020.

[30]   ESP32-CAM_1.jpg, Web, URL <https://www.berrybase.de/media/image/a2/b7/d8/ID_74706_orig_600x600.jpg>, 27.03.2020.

[31]   camera_OV2640.jpg, Web, URL <https://ae01.alicdn.com/kf/He8ac6639e3e44930955c6caef259aeb7H.jpg>, 27.03.2020.

[32]   spring_electrodes, Web, URL <https://www.all-electronics.de/wp-content/uploads/migrated/img/artikel/32134_3-620x349.jpg>, 27.03.2020.

[33]   power_supply_module.jpg, Web, URL <https://images-na.ssl-images-amazon.com/images/I/61l8MaidOjL._AC_SL1000_.jpg>, 27.03.2020.

[34]   power_supply_2.jpg, Web, URL <https://images-na.ssl-images-amazon.com/images/I/61aCOuQ93yL._AC_SL1000_.jpg>, 27.0.2020.

[35]   Datenlogger_Module_1.jpg, Web, URL <https://images-na.ssl-images-amazon.com/images/I/61%2BmZxhZ%2B9L._AC_SL1024_.jpg>, 29.03.2020.

[36]   Datenlogger_Module_2jpg, Web, URL <https://images-na.ssl-images-amazon.com/images/I/611v2RULsCL._AC_SL1024_.jpg>, 29.03.2020.

[37]   MegunoLink, Web, URL <https://www.megunolink.com/wp-content/uploads/2017/05/filteringsetup.png>, 17.04.2020.

[38]   ESP32 DevKit (Fritzing), Web, URL <https://i0.wp.com/www.bizkit.ru/wp-content/uploads/2019/03/MH-ET_LIVE_ESP32_DEVKIT_38_pins.jpg?resize=768%2C380>, 17.04.2020.

[39]   TPU Shore category, Web, URL <https://makeshaper.com/wp-content/uploads/2018/08/WE55931_Durometer-Chart_web-1024x473.jpg>, 19.04.2020.

[40]   Bowden vs. Direct Drive, Web, URL <https://i.all3dp.com/cdn-cgi/image/fit=cover,w=1000,gravity=0.5x0.5,format=auto/wp-content/uploads/2018/10/29154851/direct-vs-bowden-extrusion-craftunique-181026.jpg>, 20.04.2020.

[41]   Control_board_SKR1.3, Web, URL <https://images-na.ssl-images-amazon.com/images/I/71c%2ByJj-PmL._SL1000_.jpg>, 24.04.2020.